AN ABSTRACT OF THE THESIS OF

Dana L. Desonie for the degree of Doctor of Philosophy in Oceanography presented on September 11, 1990

Title: Geochemical Expression of Volcanism in an On-Axis and Intraplate Hotspot: Cobb and Marquesas

Redacted for Privacy

Abstract approved: Robert A. Duncan

The Pacific Ocean basin is home to a set of hotspots diverse in their eruption rate, duration of volcanism, and basalt chemistry. Pacific hotspots are found in a spectrum of distinct plate tectonic settings, from near a spreading ridge to intraplate. Cobb hotspot, which resulted in formation of the Cobb-Eickelberg seamount (CES) chain, is currently located beneath Axial seamount, on the Juan de Fuca ridge. The Marquesas hotspot, which formed the Marquesas archipelago and, perhaps, older seamounts to the west, is a member of the cluster of hotspots found within French Polynesia, located well away from the nearest spreading ridge. Geochemical and geochronological studies of volcanism at these two hotspots contribute to an understanding of the effect of plate tectonic environment on hotspot volcanism.

Cobb hotspot has the temporal but not the isotopic characteristics usually attributed to a mantle plume. The earlier volcanic products of the hotspot show a westward age progression away from the hotspot and a westward increase in the age difference between the seamounts and the crust on which they formed. These results are consistent with movement of the Pacific plate over a fixed Cobb hotspot and

encroachment by the westwardly migrating Juan de Fuca ridge. CES lavas are slightly enriched in alkali and incompatible elements relative to those of the Juan de Fuca ridge but they have Sr, Nd, and Pb isotopic compositions virtually identical to those found along the ridge. Cobb hotspot is a stationary upper mantle melting anomaly whose volcanic products have strong mid-ocean ridge basalt affinity.

Basaltic lavas from dredge hauls in the Marquesas archipelago decrease in age from northwest to southeast, with the youngest volcanism at a group of seamounts southeast of the island of Fatu Hiva. Tholeiitic and transitional basalts compose the shield of a typical Marquesan volcano; alkalic lavas form a later phase. Tholeiitic and transitional basalts result from variable degrees of melting of a relatively depleted mantle source with pods of incorporated radiogenic-Pb enriched material. Alkalic lavas represent smaller degrees of melting of a radiogenic Sr and Pb enriched mantle source. Volcanism at both hotspots can be explained by variable amounts of entrainment of a heterogeneous upper mantle into a mantle plume of isotopically depleted (Cobb) or enriched (Marquesas) composition.

Geochemical Expression of Volcanism in an On-Axis and Intraplate Hotspot: Cobb and Marquesas

by

Dana L. Desonie

A THESIS

submitted to

Oregon State University

in partial fulfillment of
the requirements for the
degree of

Doctor of Philosophy

Completed September 11, 1990

Commencement June 1991

APPROVED:

Redacted for Privacy

Professor of Oceanography in charge of major

Redacted for Privacy

Head of College of Oceanography

Redacted for Privacy

Dean of Graduate School

Date thesis is presented September 11, 1990

Typed by the author for Dana L. Desonie

ACKNOWLEDGEMENTS

Without a doubt, the person who deserves most of the credit for guiding and supporting me throughout my stay at OSU is my thesis advisor, Robert Duncan, who always seemed to know when I needed a helping hand or was best left to muddle through alone. From conception of the thesis topic through submission of the manuscripts, I always felt that Bob was at least two steps ahead of me. Like a good parent, though, he let me learn for myself and empathized with my difficulties. Bob made many opportunities available to me: a research cruise in the Marquesas and one in the Galapagos, a chance to learn isotope geochemistry at Cornell. And he rarely said no to the opportunities I found for myself, even if it meant putting off work for a while. Because of his understanding my tenure here has been extremely enjoyable.

My committee was always available to me for advice and guidance. Anita Grunder set standards high; whenever I thought about pleasing my committee it was Anita who came to mind first. The model of her as woman scientist was extremely valuable. Through Bob Embley came some important opportunities. With Bob and NOAA, I had the chance to visit the Juan de Fuca ridge region from aboard the Atlantis II. He also served as co-editor for the special volume on Axial volcano in which the Cobb-Eickelberg manuscript appears. His encouragement and comraderie helped me to persevere in preparing my first manscript. Martin Fisk served as counsel on a number of petrological problems. In his absence, Dave Christie kept me on my "petrologic toes". Wojciech Kolodziej served well as graduate school representative; his was a face I could turn to for relief in the tougher moments of oral exams.

Many other faculty contributed to the quality of my education and experience in the past years. Roger Nielsen was invaluable in his capacity as petrologic modeller, *par*

excellence. William White was generous with his laboratory and his time at Cornell University. Mark Richards introduced me to geodynamics and guided me as I tried to relate plume dynamics and geochemistry. Mike Perfit was extremely valuable as petrologist and friend. Beth Wright assisted with the concept of South Pacific ambient mantle and helped with generation of a unified theory of Pacific volcanism.

One of the real advantages to working in the College of Oceanography has been the excellent technical support available. Lew Hogan spent many hours assisting with K-Ar analyses. Andy Ungerer, Bobbie Conard, and Chi Meredith helped with analytical techniques and general procedures. Their positive and helpful attitudes could always make a lab day better. At Cornell, Michael Cheatham was invaluable at teaching me trace element separations and heavy isotope mass spectrometry. Sue Pullen has always been a great assistant and friend.

Samples from the Cobb-Eickelberg seamounts were supplied by Drs. Delaney and Johnson of the University of Washington. Marquesas samples were dredged from the R/V Thomas Washington of Scripps Institution of Oceanography, a more fun and cooperative crew have never set foot aboard a research vessel. Special thanks to the Capt. Tom Desjardins, Res. Tech. John Boas, and the scientific party for recovering rocks that clearly preferred to remain *in situ*. XRF analyses were provided by Peter Hooper of Washington State University and Mike Perfit of University of Florida.

Throughout these long graduate school days there have been friends to talk science and climb mountains with, at OSU and Cornell. Although they are too numerous to be mentioned (you know who you are), all made time at and away from work very special.

I thank Miles Orchinik for his patience and support. Instead of this last year being one of the worst of my life, as I hear it often is for people finishing their dissertations, it has been one of the best.

This work was supported by NSF grants OCE-8710905 and OCE-8610250.

TABLE OF CONTENTS

LIST OF FIGURES

LIST OF TABLES

LIST OF APPENDIX FIGURES

PREFACE

This thesis is composed primarily of two manuscripts with introductory and concluding chapters concerning volcanism at one intraplate and one near-ridge hotspot within the Pacific ocean basin. Chapter II, "The Cobb-Eickelberg Seamount Chain: Hotspot Volcanism with Mid-Ocean Ridge Basalt Affinity", appeared in the *Journal of Geophysical Research* in August 1990. Authors are D. L. Desonie and R. A. Duncan. Dr. Duncan acquired funding for the project, supervised the research and was initial editor of the manuscript. Chapter III, "Temporal and Geochemical Variability over the Marquesas Hotspot", will be submitted to a journal sometime after the final oral defense of the thesis. D. L. Desonie, R. A. Duncan and R. N. Nielsen are currently listed as co-authors. Again, Dr. Duncan attained funding for the project, supervised much of the research and served as editor. Dr. Nielsen supervised the differentiation modelling and reviewed the geochemistry portion of the manuscript. Chapter I is an introduction to the chemistry and dynamics of mantle plumes, particularly those which are found in the Pacific basin. It is primarily a review of the literature. Chapter IV summarizes major results of Chapters II and III and attempts to unite these results with what is known about oceanic volcanism in the Pacific.

GEOCHEMICAL EXPRESSION OF VOLCANISM IN AN ON-AXIS AND INTRAPLATE HOTSPOT: COBB AND MARQUESAS

INTRODUCTION

Volcanism on Earth is largely explained in plate tectonic theory [Hess, 1962]. In the ocean basins basaltic melts are formed by decompression of the upper mantle (asthenosphere) as lithospheric plates separate at spreading ridges, while plate subduction causes upper mantle hydration and melting, yielding volcanic arcs along collisional plate boundaries [Ringwood, 1975]. A volumetrically minor but significant class of basaltic volcanism occurs within plates or crosses plate boundaries, and is characterized by linear chains of volcanoes that grow older in the direction of plate motions [Morgan, 1971, 1972]. Classic examples of this volcanic phenomenon are the Hawaiian Islands, the Yellowstone-Snake River Plain province, and the platform and ridge system centered on Iceland. Due to their geometry and age distributions these volcanic provinces are proposed to result from focused zones of upper mantle melting called hotspots [Wilson, 1963; 1965] that remain stationary as the Earth's outer shell of lithospheric plates move across them. The present locations of hotspot volcanism are shown in Figure I.1.

Characteristically, a stable pattern is observed in the geometrical configuration of hotspot volcanic chains on single plates. For example, Duncan and Clague [1985] demonstrated that, for most hotspots on the Pacific plate, volcano migration rate is consistent with rotation of the plate about a single pole. They also demonstrated that Pacific hotspots have been fixed relative to each other for at least 43 Ma [Duncan and Clague, 1985]. Studies of inter-hotspot motion of Atlantic and Indian Ocean hotspots

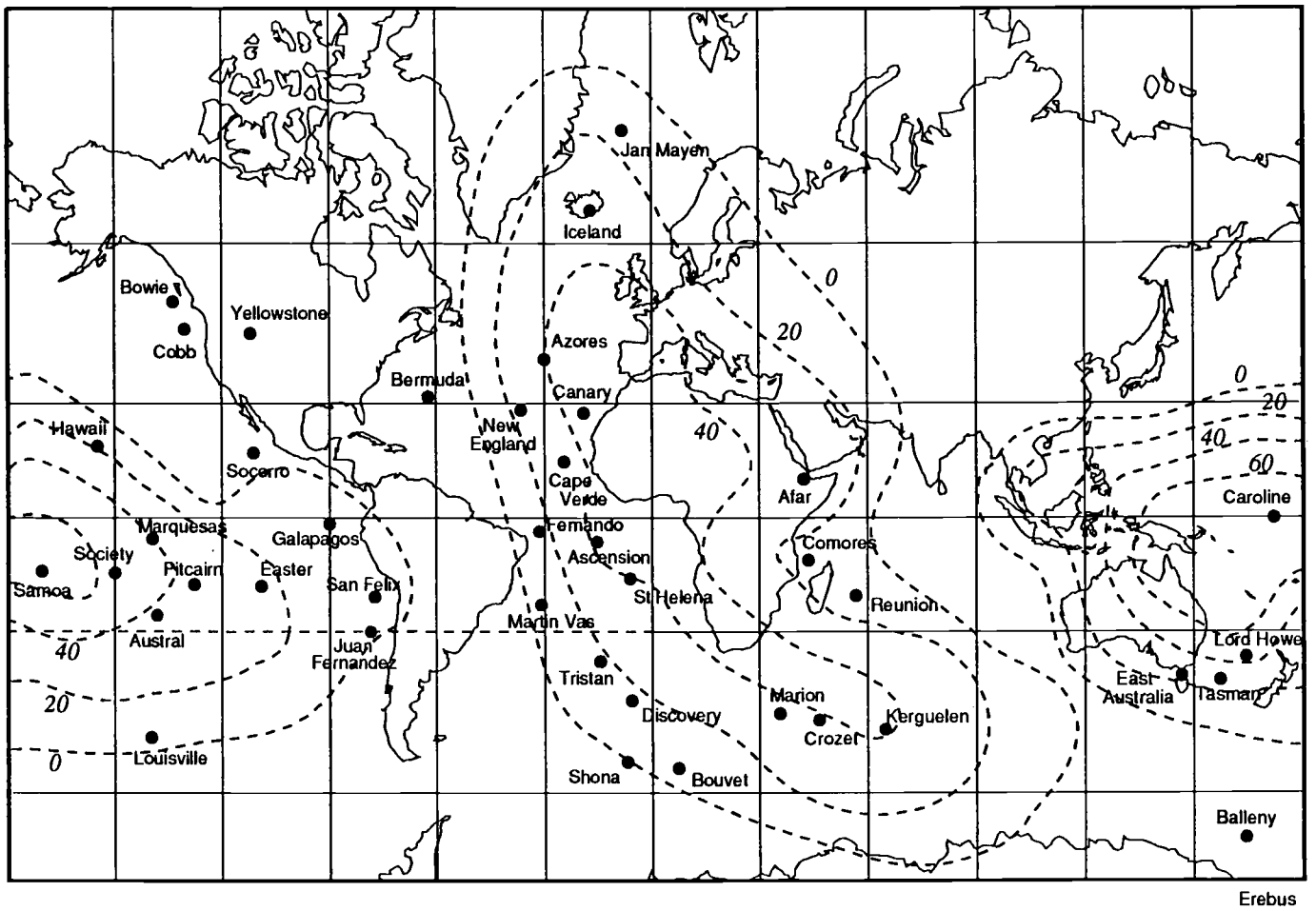

Figure I.1. Locations of hotspots over the Earth. Dotted lines indicate contouring of the geoid. Geoid values are in meters; after Duncan and Richards [1990].

through time have determined that hotspots have remained stationary relative to each other for at least 100 Ma [Duncan, 1981; Morgan, 1981].

The uppermost mantle is convecting at a velocity virtually equal to that of lithospheric plate motion; convection velocity decreases with depth in the mantle [Gurnis and Davies, 1986]. Because hotspots remain fixed with respect to each other, it is likely that they are supplied by plumes of material which originate below the more rapidly convecting upper mantle, perhaps at the core-mantle boundary (CMB). Although the lower mantle almost certainly convects also, convection deep within the mantle is probably much less vigorous than in the upper mantle [Gurnis and Davies, 1986; Richards, 1990]. Hotspots are thought to be the surface expressions of deeply rooted mantle plumes located in areas of lower mantle upwelling [Morgan, 1972]. Their long term stability requires that the convective pattern of the lower mantle is stable on a long time scale [Okal and Batiza, 1987]. Hotspots, supplied by mantle plumes that are rooted deep within the mantle, give the most abundant samples of the lower mantle available at the Earth's surface.

Deviations in the Earth's hypothetical surface of equal gravity (the geoid) represent large scale gravity anomalies. Statistical studies of the global distribution of hotspots have determined that these features are concentrated on the half of the Earth's surface that corresponds to geoid highs [Stefanick and Jurdy, 1984]. Geoid highs are found in regions that may have been the former sites of large continental masses [Anderson, 1982]. Corresponding geoid lows may represent the sites of ancient subduction from 125 to 200 Ma [Chase, 1979]. The present geoid pattern may reflect deep mantle convection patterns with sites of material upwelling from lower to upper mantle leading to plume formation [Chase, 1979].

Seismic experiments can be used to determine the structure of the mantle and core beneath the Pacific basin. Global imaging by seismic tomography has revealed 3-

dimensional views of the Earth's interior based on P-wave and S-wave velocities [Dziewonski and Woodhouse, 1987]. Seismic heterogeneities must reflect thermal or compositional heterogeneity. P-waves are fast moving beneath continental shield areas but are relatively slow in warm tectonically active regions, such as at mid-ocean ridges. Subduction zones are cold and thus exhibit a high seismic velocity. Regions of concentrated hotspot volcanism, such as the south-central Pacific, are seismically slow and may indicate mantle upwelling. Velocity contrasts reveal the level of heterogeneity within different regions of the mantle. For example, the upper mantle is seismically heterogeneous; velocity contrasts are also high near the core mantle boundary (CMB) [Dziewonski and Woodhouse, 1987]. Seismically slow regions near the CMB match with geoid highs at the Earth's surface supporting the concept of whole mantle convection [Castillo, 1988].

Volcanic rocks formed at hotspots are usually compositionally distinct from those formed at mid-ocean ridges and subduction-related volcanic arcs. Basaltic rocks that result from hotspot volcanism are characterized by more highly radiogenic Sr, Nd, and Pb ratios and higher concentrations of incompatible elements, relative to basalts erupted at spreading ridges. Differences between volcanic arc and hotspot basalts are more subtle but are clear in concentrations of such elements as Ti, Nb, Ba and sometimes volatile elements such as K and Rb.

The variation in chemistry of the products of oceanic volcanism can be explained in several ways. Melts extracted from a portion of the mantle composed of a variety of minerals will have compositions determined by the composition of minerals melted, volatile content, the degree of melting that takes place before the melt is extracted, the depth (pressure) of melting, and the extent to which the region has been partially melted previously. Although melts originating in different melting regimes of this portion of mantle will differ in their major and trace element compositions, isotopically they will be

identical. The diversity of isotopic compositions of basalts found in the ocean basins can only have developed if regions of the mantle have been chemically isolated for billions of years. The compositional diversity of mantle source regions and the scale of the heterogeneities is a field of study for which the integration of chemical analyses from spreading ridges, near-ridge seamounts, volcanic arcs, and hotspot volcanoes within the ocean basins is necessary.

Chemical heterogeneity within oceanic mantle exists on several scales. Mid-ocean ridge basalts (MORB) erupted at spreading ridges are generally depleted in trace elements and radiogenic isotopes relative to ocean island basalts (OIB) erupted over most hotspots; along-ridge variations in basalt composition reflect lateral heterogeneity of the upper mantle beneath spreading ridges [Langmuir et al., 1986; Liias, 1986; Karsten, 1988]. Compilations of analyses from MORB and OIB have led to the recognition of 4 to 6 mantle components which can be visualized as endmember compositions in oceanic volcanism [Zindler and Hart, 1986]. Volcanism resulting from depleted MORB-mantle (DMM), with low $^{87}Sr/^{86}Sr$, $^{206}Pb/^{204}Pb$ and high $^{143}Nd/^{144}Nd$, is observed at spreading ridge segments that are geographically separate from all hotspot activity. DMM is the geochemical complement of continental crust and is thought to be the residue left behind when continental crust was extracted from the upper mantle. HIMU component, named for its inferred high μ (=U/Pb), exhibits high $^{206}Pb/^{204}Pb$ and $^{208}Pb/^{204}Pb$ but low $^{87}Sr/^{86}Sr$ values, is ubiquitously present in the convective mantle [Zindler and Hart, 1986]. At some ocean islands, including Mangaia in the Cook Islands and Tubuai in the Austral Islands, HIMU is the dominant melt component. Smaller enrichments of radiogenic Pb, without equivalent increases in radiogenic Sr, are found along some ridge segments or within some volcanic phases at ocean islands, suggesting that HIMU may be present as a dispersed component in DMM or elsewhere in the convective mantle. These unusual isotopic compositions may have

resulted from melting of subducted oceanic crust that was altered by seawater or mantle metasomatism or that was preferentially stripped of some alteration phases as it subducted [Hart and Zindler, 1989].

Enriched mantle components, with relatively low (EM I), or relatively high (EM II), radiogenic Sr and high radiogenic Pb, are tapped primarily in the Southern Hemisphere between 0 and 45° S [Hart and Zindler, 1989]. Chemical characteristics of EM I suggest it is derived from recycled lower continental crust or metasomatized mantle, both associated with subduction processes. Based on its elevated $^{207}Pb/^{204}Pb$ values, EM II is thought to represent ancient continental material that was reinjected into the mantle more than 3 billion years ago [Hart and Zindler, 1989]. One isotopic composition, with moderately radiogenic Sr, Nd, and Pb isotopic values, is frequently found in basalts of ocean islands, continental regions and island arcs. Although mixing of mantle components such as EM I, EM II, HIMU and DMM could produce melt of this isotopic composition, the wide-spread occurrence of this composition is evidence that it may represent the prevalent composition of the mantle, PREMA. Like DMM, PREMA may also be the geochemical complement of continental crust and may be the residue of separation of crustal material from the mantle over time; alternatively, PREMA may represent differentiation of the silicate fraction of Earth material at the time of core formation [Zindler and Hart, 1986].

This study focuses on the volcanic products of two hotspots in the Pacific basin, the Cobb-Eickelberg seamount chain, a volcanic lineament located near the Juan de Fuca Ridge, and the Marquesas Islands, an intraplate volcanic chain. Volcanism at these two lineaments has occurred in different tectonic settings, each with very different physical properties of the mantle and lithosphere. Compositionally, the Cobb-Eickelberg and Marquesas volcanic edifices are extraordinarily different. The Cobb-Eickelberg seamounts are characterized by spreading ridge-like trace element and isotopic

compositions while the Marquesas contain a variety of unenriched and enriched compositions. The Cobb-Eickelberg seamount chain and the Marquesas volcanic lineament are representative of two very distinct types of hotspot volcanism found in the Pacific basin.

PLUME AND UPPER MANTLE CONTRIBUTIONS IN PACIFIC VOLCANISM

Volcanism within the Pacific Ocean basin occurs in tectonically diverse settings. In the northeastern Pacific, basaltic volcanism has occurred at the Juan de Fuca (JDFR) and Gorda (GR) Spreading Ridges, at several small near-ridge seamount chains, and two hotspot lineaments, the Cobb-Eickelberg and the Pratt-Welker (Figure I.2). The hotspots that led to volcanism at these lineaments, Cobb and Bowie respectively, are currently located near the JDFR. In the central and south Pacific, the East Pacific Rise (EPR) and numerous near-ridge seamount chains have been the focus of many recent studies. The Galapagos Archipelago and Easter Island are the results of volcanism that occur at hotspots located near a spreading ridge.

Several intraplate hotspots are also found in the Pacific. The cluster of hotspot volcanic lineaments found the south-central Pacific (the Marquesas, Society, Cook-Austral, Pitcairn and Samoa Island chains) are noteworthy for their higher $^{87}Sr/^{86}Sr$, and $^{207}Pb/^{204}Pb$ and $^{208}Pb/^{204}Pb$ at a given $^{206}Pb/^{204}$ Pb than Pacific hotspots outside the region [Hart, 1984]. This broad-scale geochemical feature of the mantle has been termed the Dupal anomaly, which circles the globe at 0-45° S. Other intraplate hotspots, including Hawaii and Louisville, have resulted in large volumes of basaltic volcanism that are less highly radiogenic than hotspots within the Dupal region.

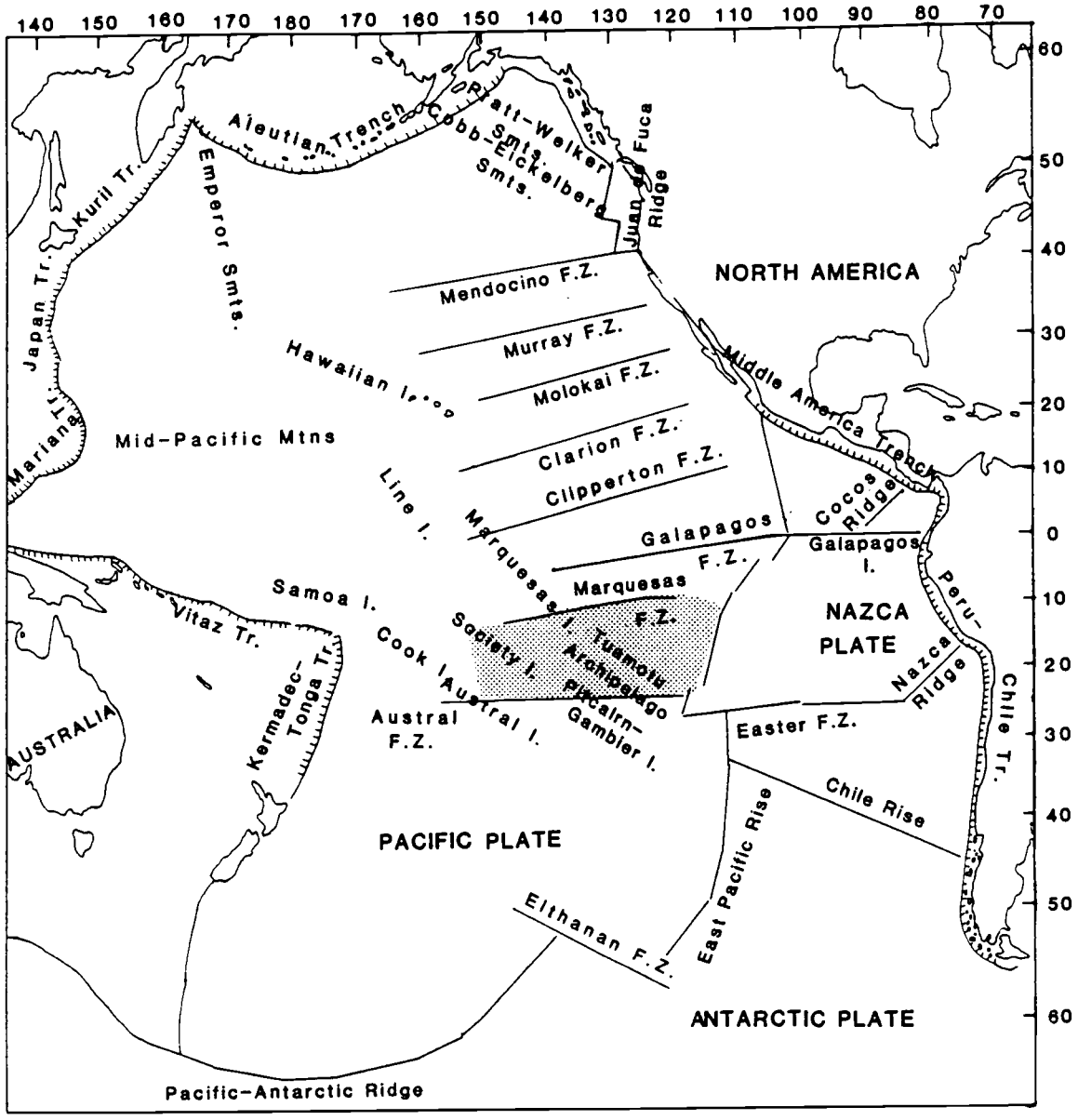

Figure I.2. Map of the Pacific Ocean basin showing major spreading ridges, fracture zones, and hotspot volcanic lineaments. The region of the South Pacific Superswell is in a dotted pattern.

Geophysical characteristics of the Pacific basin

In the Pacific, hotspots are clustered within the geoid highs but some, most notably the northeast Pacific hotspots (Cobb and Bowie), lie within geoid lows. Contouring of the flux values of Sleep [1990] for each of the Pacific hotspots shows that hotspots with a high flux are clustered in the south-central Pacific at the location of a geoid high and that the flux decreases outward from that high, with Cobb and Bowie having among the lowest flux values for hotspots globally. High flux may indicate the existence of intense mantle upwelling in the south-central Pacific. The Hawaiian hotspot, with a flux equal to more than twice that of any other single hotspot, is located well outside the zone of flux maxima, however, this hotspot has no near neighbors so its flux should be distributed over a broad area [Sleep, 1990].

Geophysically, north Pacific seafloor is "normal". Depths and thermal structure of north Pacific lithosphere follow the thermal evolution curve of Parsons and Sclater [1977]. With the exception of the Hawaiian hotspot, only two hotspots are found in the north Pacific, Cobb, which formed the Cobb-Eickelberg seamount chain [Desonie and Duncan, 1990], and Bowie, which resulted in the formation of some of the volcanoes of the Pratt-Welker chain [Dalrymple et al., 1987]. Both hotspots are currently located near the JDFR. There is a noticeable lack of recent plume volcanism in the northwestern Pacific which may be due to interference by cold lithospheric slabs at subduction zones currently around the region.

Several recent studies have characterized the geophysically anomalous south-central Pacific region. Unusual features include a widespread depth anomaly [McNutt and Fischer, 1987]; small scale convection [Haxby and Weissel, 1986]; low elastic strength of the lithosphere [Calmant and Cazenave, 1987]; slow seismic velocities at deep

[Dziewonski and Woodhouse, 1987] and shallow [Nishimura and Forsythe, 1985] levels; a large number of active volcanoes [Menard, 1984]; and radiogenic isotope anomalies in the volcanic products [Dupre and Allegre, 1983; Hart, 1984]. McNutt and Fischer [1987] termed the anomalous region the South Pacific Superswell, based primarily on the characteristic depth anomaly. Because the Marquesas Islands do not show anomalous depth they were not included in the superswell [McNutt and Fischer, 1987]. However, the Marquesas exhibit the anomalous isotopic ratios and elastic plate thicknesses characteristic of the region and therefore were included in SOPITA (the South Pacific Isotopic and Thermal Anomaly) by Smith et al. [1989]. They argue that although many hotspots, including Hawaii, Bermuda, and Cape Verde have underlying swells, the anomalous elastic plate thickness is the definitive feature in the South Pacific. Clearly, the Marquesas are unusual in their isotopic compositions and the term SOPITA, which includes the Marquesas, will be used here. A further discussion of some of the anomalous geophysical features of the region follows.

Within SOPITA, seafloor depths are 250-750 m shallower than seafloor of the same age in the north Pacific [McNutt and Fischer, 1987]. Lithosphere in this region follows a thermal subsidence curve appropriate for a 75 km thick plate, whereas to the north and south of this anomalous zone the lithosphere behaves as a 125 km thick plate [McNutt and Menard, 1978; Calmant and Cazenave, 1987; McNutt and Judge, 1990]. Evidence from heat flow and thermal load modelling suggests that the lithosphere was anomalously thin before it reached the region of high hotspot density [McNutt and Fischer, 1987; McNutt and Judge, 1990]. Growth of a stable lithospheric thermal boundary layer to a thickness greater than 75 km may have been prevented as a consequence of enhanced heat flux from the convecting mantle and lowered viscosity beneath the plate. Small scale convective instabilities within the low viscosity zone may have further thinned the base of the lithosphere [McNutt and Judge, 1990].

Beneath SOPITA, seismic tomography indicates a high temperature region, interpreted as broad scale upwelling from the deep mantle which has thinned the lithosphere and allowed its penetration by hotspots [Dziewonski and Woodhouse, 1987]. The South Pacific Superswell also has unusually low seismic velocities in the upper mantle, as well [Nishimura and Forsyth, 1985]. A relatively large amount of intraplate seismicity, more diffuse than expected at epicenters related to active volcanoes, such as are found beneath the active volcanoes in the Hawaiian Islands, occurs in the region [Wysession et al., 1990].

Heat flow data described by Stein and Abbott [1990] have shown that regional reheating of the lithosphere is not sufficient to explain the anomalously shallow elastic plate thickness in SOPITA. In Hawaii, heat flow and other data have been used to develop a model of uplift of the Hawaiian swell based on a 100-200°C temperature increase at the base of the plate but with a significant dynamic component [Von Herzen et al, 1989]. Surface wave velocities which are similar to values expected for unperturbed 100 Ma lithosphere are significantly faster than if the Hawaiian swell originated by large scale reheating [Woods et al., 1990]. A mechanical component of uplift is also necessary to explain features of the South Pacific Superswell [Stein and Abbott, 1990].

The hotspot region of French Polynesia is underlain by a low viscosity zone several hundred kilometers thick with a vicosity 50-100 times lower than is characteristic of the lower mantle in that region [McNutt and Judge, 1990]. A 2-dimensional Cartesian convection calculation shows that a narrow upwelling plume will spread out when it reaches a low viscosity zone producing large lateral temperature variations near the base of the zone. One model of P-wave tomography shows a hot temperature anomaly at depths of 300-600 km directly beneath the Superswell but with little structure at greater depth [McNutt and Judge, 1990].

The western section of SOPITA contains a high density of volcanoes, many with extremely radiogenic isotope ratios, which overlie a zone of low seismic velocity at the base of the lower mantle [Castillo, 1988]. Although the majority of hotspots within the superswell are found above low velocity regions, volcanoes that formed at hotspots beside the low velocity region, such as Tubuai, do not have Dupal chemical signatures [Castillo, 1988]. The correlation of Dupal chemistry with anomalously slow seismic velocities in the lower mantle suggests that the Dupal signature is originating within the lower mantle.

Regions of high seismic velocity are found at subduction zones; direct observations have been made of seismically fast extensions of subduction zones deep into the lower mantle suggesting that at least some subducted slabs may sink to the lower mantle or onto the core-mantle boundary [Creager and Jordan, 1986]. If a significant mass of lithospheric material sinks into the lower mantle an equal mass of material must return to the upper mantle. Low velocity regions probably represent return flow through upwelling mantle plumes. Persistent, focused volcanism at hotspots is the manifestation of that return flow [Castillo, 1988].

Geochemical characteristics of Pacific volcanism

Although spreading ridge lavas of the Pacific Ocean have a smaller range of isotopic variation than spreading ridge lavas within the Atlantic and Indian Oceans [White et al., 1987], chemical variations are found along and across ridge axes in both the north and south Pacific [Langmuir et al., 1986; Hegner and Tatsumoto, 1987]. A smaller range of compositions is found on the Juan de Fuca Ridge and Gorda Ridge than East Pacific Rise (Figure I.3), and although the EPR has a much greater length, the smaller range of compositions may reflect either a larger degree of melting and subsequent

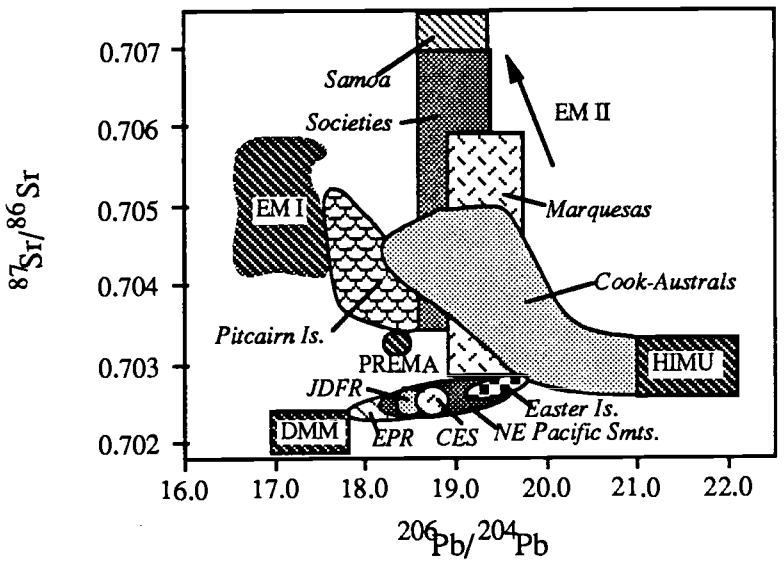

Figure I.3. $^{87}Sr/^{86}Sr$ versus $^{206}Pb/^{204}Pb$ for Pacific basalts. Basalt suites are from spreading ridges and some hotspot volcanic lineaments of the Pacific basin with mantle components after Zindler and Hart [1986]. Data sources are as follows: Juan de Fuca Ridge (JDFR) [Hegner and Tatsumoto, 1987], East Pacific Rise (EPR) [White et al., 1987]; Cobb-Eickelberg seamounts (CES) [Desonie and Duncan, 1990], Northeast Pacific seamounts [Cousens et al., 1985; Cousens, 1988; Hegner and Tatsumoto, 1989], Easter Island [White and Hofmann, 1982]; Society Islands [White and Hofmann, 1982; Cheng et al., 1987a; Devey et al., 1990]; Marquesas Islands [Vidal et al., 1984; Duncan et al., 1986; Dupuy et al., 1987; this study]; Cook and Austral Islands [Palacz and Saunders, 1986; Nakamura and Tatsumoto, 1988]; Pitcairn Island [Woodhead and McCulloch, 1989]; the Samoan Islands [Wright and White, 1986]; and the Louisville seamounts [Cheng et al., 1989b]; after Hart and Zindler [1989].

homogenization beneath eruption sites along those ridges or a smaller amount of heterogeneity in the upper mantle beneath the ridges. Less uniformity is found in Pb-isotopic compositions than in Sr and Nd isotopic compositions for all Pacific spreading ridges, although, again, the JDFR and GR are not as diverse in composition as the EPR [White et al., 1987]. Small seamount chains off of the EPR axis [Zindler et al., 1984; Fornari et al., 1988a, b] show a wider range of compositions than similar seamounts in the north Pacific [Hegner and Tatsumoto, 1989; Cousens et al., 1985; Cousens, 1988], again suggesting that the mantle beneath the central and south Pacific is more heterogeneous.

Small hotspots that lie near the spreading ridges may result from melting of a source similar to the spreading ridge source or may be diluted by the more voluminous ridge melts. In the northeastern Pacific, the Cobb-Eickelberg (CES) and Pratt-Welker seamounts are variably enriched in alkalies and incompatible elements relative to the nearby JDFR lavas. CES and Pratt-Welker basalts are virtually identical to the spreading ridge in their isotopic composition with a small enrichment in radiogenic Pb [Hegner and Tatsumoto, 1989; Desonie and Duncan, 1990] indicative of a larger component of HIMU within the source region, or a smaller degree of melting of the JDFR source, resulting in preferential melting of the HIMU component. Easter Island, which lies close to the EPR, also shows a larger amount of HIMU component than the EPR or than northeast Pacific seamounts. In the Pacific basin, basaltic products of the ridges, small near-ridge seamounts, and near-ridge hotspots are dominated by DMM component but show a distinct enrichment in Pb-isotopic composition, suggesting incorporation of HIMU component in the upper mantle source region that is being tapped by these different volcanic regimes (Figure I.3).

Some islands generated by hotspots, e.g. Tubuai in the Austral Islands and Mangaia in the Cook Islands, are formed of basalts that have extremely high Pb-isotopic ratios and that resulted in identification of the HIMU component. Other islands show some basaltic compositions, particularly the tholeiitic phase of volcanism found on some Marquesan shields [Duncan et al., 1986; Chapter III] that appear to be a mixture of DMM and HIMU component, with a small amount of enriched mantle incorporated, very similar in composition to Easter Island lavas. Hotspots lying outside of the Dupal region but not within a spreading ridge regime, e.g. Hawaii and Louisville, have relatively narrow ranges in isotopic composition and their lavas have a slightly larger enriched mantle component. These basalts are compositionally similar to the less enriched basalts of Dupal hotspots and may reflect the composition of ambient mantle in the Pacific (DMM + HIMU + EM).

This thesis is a study of two hotspot volcanic lineaments, the Cobb-Eickelberg, located near the Juan de Fuca Spreading Ridge (Chapter II) and the Marquesas, found within the Pacific plate (Chapter III). Each study reports age determinations from K-Ar and ^{40}Ar-^{39}Ar geochronology experiments and calculations of Pacific plate motion over the hotspot. Major and trace element compositions and Sr, Nd, and Pb isotopic analyses are also reported. We discuss the evolutionary paths that may relate samples within each province and changes that occur within the composition of a volcano or a volcanic lineament with time. Isotopic compositions are placed within the framework of mantle endmembers in Zindler and Hart [1986] terminology. For each hotspot, the data are discussed in terms of dynamic models of mantle plume and asthenosphere mixing. Chapter IV summarizes the results of the two studies and places them within the framework of volcanism within the Pacific basin, especially at mantle plumes.

THE COBB-EICKELBERG SEAMOUNT CHAIN: HOTSPOT VOLCANISM WITH MID-OCEAN RIDGE BASALT AFFINITY

ABSTRACT

Cobb hotspot, currently located beneath Axial seamount on the Juan de Fuca ridge, has the temporal but not the isotopic characteristics usually attributed to a mantle plume. The earlier volcanic products of the hotspot, from eight volcanoes in the Cobb-Eickelberg seamount (CES) chain, show a westward age progression away from the hotspot and a westward increase in the age difference between the seamounts and the crust on which they formed. These results are consistent with movement of the Pacific plate over a fixed Cobb hotspot and eventual encroachment by the westwardly migrating Juan de Fuca ridge. CES lavas are slightly enriched in alkalis and incompatible elements relative to those of the Juan de Fuca ridge but they have Sr, Nd, and Pb isotopic compositions virtually identical to those found along the ridge. Therefore, Cobb hotspot is a stationary, upper mantle melting anomaly whose volcanic products show strong mid-ocean ridge basalt affinity. These observations can be explained by low degrees of partial melting of entrained heterogeneous upper mantle MORB-source material within a thermally- driven lower mantle diapir or by an intrinsic MORB-like composition of the deeper mantle source region from which northeast Pacific plumes rise.

INTRODUCTION

Since hotspots were first described by Wilson [1963] and linked to convective mantle plumes by Morgan [1972], both temporal and chemical characteristics of these features

have been recognized. The linear array of volcanoes and the age-progressive distribution of hotspot tracks [Morgan, 1972] are two of the more distinguishing features of volcanism resulting from a fixed mantle plume. Some hotspots have been persistent over long periods, a feature clearly seen in the volumes of lava produced by the Hawaiian hotspot, while other Pacific plate hotspots have produced shorter or more intermittent seamount or island chains. Thus far, volcanic rocks formed at hotspots have been characterized by distinctive compositions, usually more radiogenic Sr, Nd and Pb and higher concentrations of incompatible elements, relative to basalts erupted at spreading ridges. The isotopic composition of lavas erupting over a given hotspot may not be constant with time, nor are all hotspots alike isotopically, but as a group these rocks have been termed ocean island basalts (OIB) as distinguished from basalts that form at mid-ocean ridges (MORB). The Cobb-Eickelberg seamount chain, and other hotspot-associated volcanic lineaments in the northeastern Pacific, are unusual in that they exhibit the temporal characteristics produced by other mantle plumes, but not the OIB isotopic signatures.

Based on different morphologic and tectonic characteristics, the Juan de Fuca ridge (JDFR) was divided into four spreading segments by Delaney et al. [1981]. Along-segment and between-segment variations in basalt chemistry give evidence of separate magmatic systems beneath the ridge [Liias, 1986]. The Endeavour segment, northernmost of the four, which lies north of the Cobb offset (Figure II.1) [Delaney et al., 1981] is chemically the most primitive (highest Mg-numbers) yet has the most incompatible element enriched lavas found along the ridge [Liias, 1986, Karsten, 1988]. The unusual chemistry of the Endeavour segment has been attributed to the contribution of the Heckle melting anomaly to the overriding Juan de Fuca spreading ridge melts [Karsten, 1988].

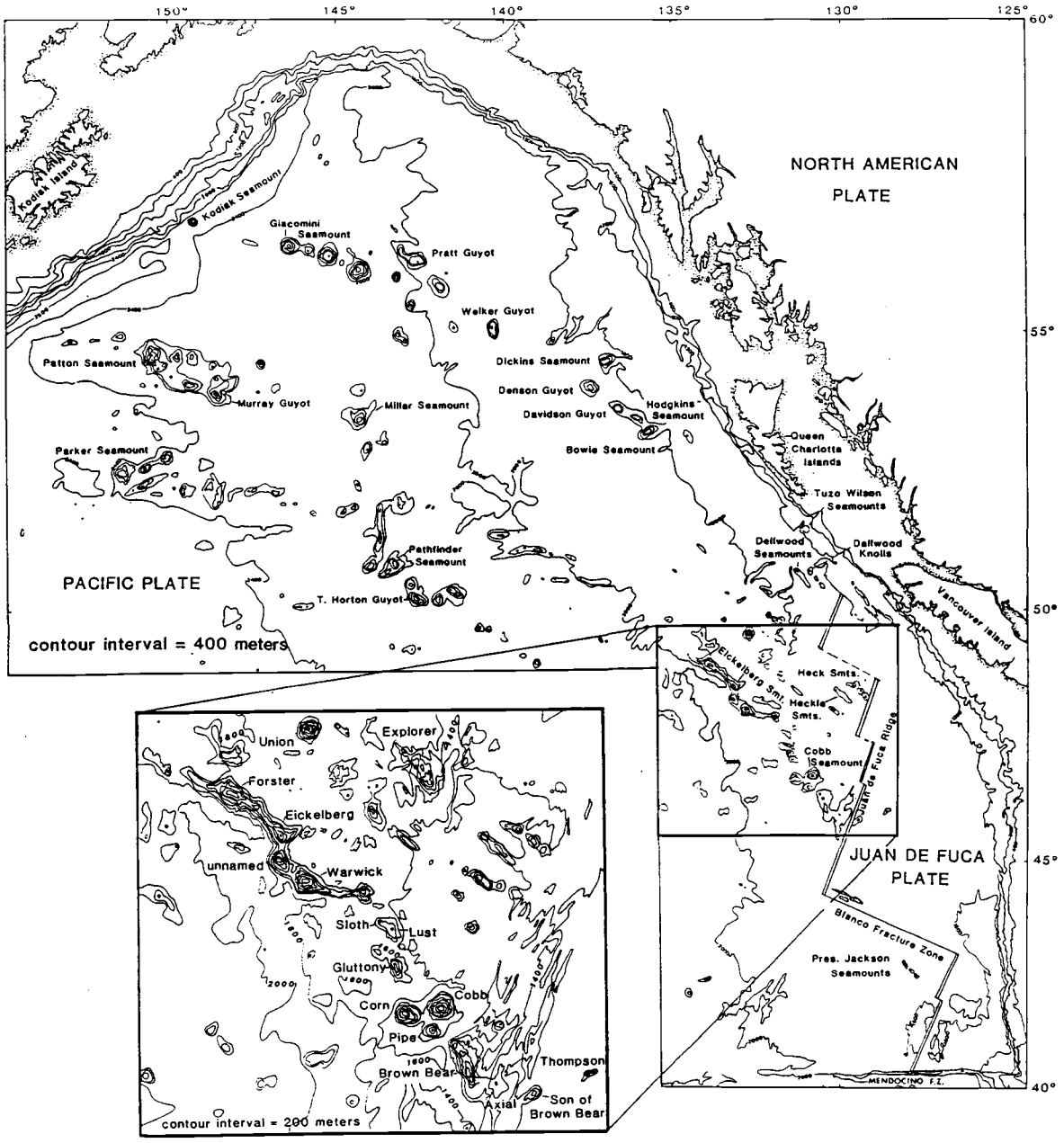

Figure II.1. Bathymetric map of northeastern Pacific and CES (inset). Bathymetric map showing seamounts, spreading ridges (double lines) and fracture zones (single lines) of the northeast Pacific, after Chase et al. [1970]. Inset shows seamounts of the Cobb-Eickelberg lineament and Explorer and Union volcanoes.

Axial seamount, which straddles the JDFR axis at ~46°N (segment 2) [Delaney et al., 1981] is the youngest expression of volcanism over an upper mantle melting anomaly termed the Cobb hotspot (Figure II.1). Older volcanic products of the hotspot, the Cobb-Eickelberg seamount (CES) chain, include a line of edifices on the Pacific plate, from Brown Bear northwest through Corn, Cobb and Pipe seamounts, a group of small volcanoes known as the Seven Deadly Sins seamounts, and finally the larger Warwick, Eickelberg, and Forster seamounts (Figure II.1). Two seamounts to the east of Axial seamount on the Juan de Fuca plate (Thompson and Son of Brown Bear) are inferred to be related to this linear volcanic province. Beyond Forster seamount, the westernmost edifice in the Eickelberg group, is a gap of 800 km before a line of seamounts which includes Miller, Murray, and Patton seamounts. These older volcanoes have been interpreted to be earlier products of volcanic activity at Cobb hotspot [Duncan and Clague, 1985; Smoot, 1985], but this suggestion has been questioned by Dalrymple et al. [1987] because seamount ages do not completely agree with rigid Pacific plate motion over a fixed hotspot.

The Pacific-mantle rotations proposed by Duncan and Clague [1985] and Pollitz [1988] place Miller seamount (26 Ma [Dalrymple et al., 1987]) directly over Cobb hotspot at the time of its formation. Basaltic rocks from this seamount have relatively low alkali contents and flat rare-earth element (REE) patterns [Dalrymple et al., 1987] similar to volcanic products of the CES lineament. Backtracking of Murray and Patton seamounts, however, places their positions at origin some 150-250 km west of Cobb hotspot. The higher alkali contents and light-REE enriched nature of the Murray and Patton seamount basalts would be consistent with their formation as a product of late-stage rejuvescent volcanism downstream from the Cobb hotspot, or with formation at another, now extinct, hotspot. Whether or not the three older seamounts formed at Cobb hotspot, there has been a lack of consistency of volcanism over the melting

anomaly; it either became active or it reactived after a long period of quiescence more than nine million years ago with the formation of Forster and Eickelberg seamounts. Since the hotspot began this latest pulse of activity, volcanic output has been continuous but has varied up to 20% [Karsten and Delaney, 1989] which is within the known variability of other hotspots [Bargar and Jackson, 1974; Lonsdale, 1988].

Within the northeast Pacific basin are several other linear volcanic chains, all of which are generally subparallel with more prominent Pacific chains to the southwest. These lineaments differ in length and volume and may have originated by different mechanisms. The longest and best known of these is the Pratt-Welker seamount chain (Figure II.1). Dalrymple et al. [1987] suggested a complex history involving at least two hotspots; some of the seamounts formed in a midplate setting while volcanism at or near a spreading ridge formed others [Turner et al., 1980]. The Pratt-Welker hotspot(s) may be located near the Tuzo Wilson seamounts [Chase, 1977; Cousens et al., 1985], Bowie seamount [Turner et al., 1980], or the Dellwood knolls [Silver et al., 1974]. All three of these young volcanic sites (Figure II.1) are proposed to reflect hotspot activity, although the Tuzo Wilson seamounts and Dellwood knolls may have originated by partial melting in a pull-apart basin [Allan et al., 1988]. A more southerly line of seamounts in the northwestern Gulf of Alaska, the Horton-Pathfinder-Parker group, cannot be attributed to a currently active hotspot.

Several shorter seamount chains lie close to and intersect the JDFR from the west. These appear to reflect a much shorter-lived and shallower-origin melting phenomenon. The Heck and Heckle seamount chains, for example, may be the result of passive upwelling and partial melting of heterogeneous upper mantle in advance of the northwestwardly migrating Juan de Fuca spreading ridge [Davis and Karsten, 1986] similar to the setting of the Lamont seamounts near the East Pacific Rise [Fornari et al., 1988a]. Other seamounts and small seamount chains, including Explorer and Union

seamounts which lie to the north of the CES (Figure II.1), are of unknown origin. All aforementioned seamount chains are found on the Pacific plate; only two edifices, Thompson and Son of Brown Bear, which are interpreted to be related to volcanism at Cobb hotspot [Desonie and Duncan, 1986; Karsten and Delaney, 1989] were formed on the Juan de Fuca plate.

In this paper we report new ^{40}Ar-^{39}Ar and K-Ar age determinations from eight volcanoes of the CES which document a clear age progression along the lineament, in concert with plate motion over a stationary hotspot. Major and trace element contents are slightly enriched over those for heterogeneous MORB erupted along the Juan de Fuca spreading ridge. In Sr, Nd and Pb isotopic compositions, the CES basalts are indistinguishable from nearby spreading ridge lavas. We discuss these data in terms of possible dynamic models of mantle plume and asthenosphere mixing, and conclude that the deep mantle under the northeast Pacific region is intrinsically more MORB-like than the central and south Pacific [Hart, 1984, 1988].

SAMPLE DESCRIPTIONS

Basalt samples from the Cobb-Eickelberg and Explorer-Union seamounts were obtained from Drs. John Delaney and Paul Johnson of the University of Washington, and were originally dredged during R/V Thomas Thompson cruises TT063, TT080 and TT175. The Cobb seamount sample was obtained by a diver from the pinnacle of the volcano. Dredge locations are given in Table II.1.

Samples used in this study for age determinations and compositional analyses were the freshest available, with little to no interstitial glass and only slight to moderate alteration. CES basalt samples are generally microcrystalline and aphyric. In some samples, phenocrysts of plagioclase, clinopyroxene and Fe-Ti oxides are found in an

Table II.1. Dredge Sample Locations and Whole Rock Descriptions for the Cobb-Eickelberg, and Explorer and Union Seamounts. A symbol for each seamount is included in parentheses behind seamount name and will be used throughout this study. Sample descriptions: v = vesicular, m = massive, mx = micro-crystalline, d = devitrified glass, pp = plagioclase phenocrysts, pm = plagioclase microlites, op = olivine phenocrysts, fo = Fe-Ti oxides.

Sample	Seamount Name	Latitude^{o}N	Longitude^{o}W	Nature of sample
TT080 DH 1-1	Eickelberg (E)	48.29	133.09	v, d
TT080 DH 2A	Eickelberg (E)	48.32	133.10	m, pp
TT080 DH 2-8	Eickelberg (E)	48.53	133.10	v, pp
TT080 DH 4-4	Warwick (W)	48.02	132.46	m, pm
TT080 DH 5-14	Warwick (W)	48.01	132.53	v, d
TT080 DH 8-8	Warwick (W)	48.03	132.45	m, pp
TT080 DH 9-1	Warwick (W)	48.02	132.47	pm
TT080 DH 10A	unnamed (X)	48.28	133.22	fo
TT080 DH 10-7	unnamed (X)	48.28	133.22	v, fo
TT175 DH 70-2	Sloth (S)	47.62	131.70	v, mx
TT175 DH 71-4	Lust (L)	47.50	131.51	v, mx
TT175 DH 74-17	Gluttony (G)	47.14	131.46	v, pp
CB-1	Cobb (C)	46.77	130.83	v, mx
TT080 DH 14A	Thompson (T)	46.03	128.63	v, mx
TT080 DH 14-5	Thompson (T)	46.03	128.63	m, mx
TT063 DH 34	Explorer (Ex)	48.96	131.03	op, pp
TT063 DH 35	Explorer (Ex)	48.98	130.98	v, op, pp
TT063 DH 36A	Union (U)	49.55	132.73	v, pp

intergranular or intersertal matrix. Plagioclase phenocrysts are generally fresh but may be slightly resorbed or zoned. Both samples from Eickelberg seamount used in this study contain plagioclase glomerocrysts. Several basalt samples are highly vesicular, indicating that the magmas degassed as they cooled and were probably erupted at a relatively shallow depth or had high ascent rates [Dixon et al., 1988]. Secondary mineralization is slight; the matrix of some samples is partially altered to reddish-brown clays. One Warwick seamount sample (TT080 DH04-4) has zeolites lining some vesicles.

COBB-EICKELBERG SEAMOUNT COMPOSITIONS

Analytical procedures

Major and some trace element analyses for dredged basalts were determined from pressed powder pellets by X-ray fluoresence spectroscopy [Hooper, 1981]. Rare earth element (REE) and Sc concentrations were determined from instrumental neutron activation analysis (INAA) [Laul, 1979]. Isotope dilution techniques were employed to measure Sr, Rb, Cs, K, Sm and Nd concentrations [White et al., 1990]. Where any of those elements is available by another analytical technique, the isotope dilution values are preferred.

Sr, Nd, and Pb isotopic ratios were measured on a VG Sector thermal ionization mass spectrometer at Cornell University, following the procedure of White et al. [in press]. All samples were leached in 6N HCl to eliminate effects of seawater alteration. In order to compare the CES results with those from previously published studies of other northeast Pacific basalts, only samples that were similarly leached before isotopic analysis were considered.

Major and trace elements

The older Pacific plate CES lavas (Cobb through Eickelberg seamounts) show a narrow range of variation with respect to many chemical parameters, often smaller than previously analysed samples from the JDFR (Table II.2) [Liias, 1986; Karsten, 1988]. However, a larger variation in chemical parameters exists in seamounts of the CES chain that lie close to the spreading ridge (Figure II.2) [Morgan, 1985]. Variations in Brown Bear seamount are reported in Rhodes et al. [1990].

The basalts from Thompson seamount, considered part of the CES chain [Delaney et al., 1981] although moving eastward with the Juan de Fuca plate, are more primitive and depleted in incompatible elements than other CES lavas (Figure II.3) and, in some chemical parameters, JDFR lavas. Chemical analyses of the Seven Deadly Sins cluster are reported by Rhodes et al. [1990]. For almost all chemical criteria, the two samples from Explorer and Union seamounts (TT063 DH 34 and 36A, respectively) have a far greater compositional range than do the Pacific plate CES, e.g. the most extreme Mg-numbers and $(La/Sm)_N$ analysed are from those two volcanoes (Table II.2) and they encompass a greater range than the older CES on a plot of incompatible elements (Figure II.3).

Although many northeast Pacific seamount basalts are strongly enriched in alkali and incompatible elements and ratios relative to JDFR lavas [Cousens et al., 1985; Dalrymple et al., 1987; Cousens, 1988], the Cobb-Eickelberg, Explorer and Union seamount samples straddle the line dividing alkalic from tholeiitic basalts on a plot of alkalies vs. silica (Figure II.4) and are transitional in their incompatible elements and ratios as well (Table II.2). In some chemical parameters (i.e. Zr/Nb, Zr/Y, P_2O_5, and K_2O) CES lavas resemble the Endeavour segment basalts, which are enriched relative to

TABLE II.2. Geochemical Analyses for the Cobb-Eickelberg, Explorer, and Union Seamounts

	DH1-1	DH2A	DH2-8	DH4-4	DH5-14	DH8-8	DH9-1	DH10A	DH10-7	CB-1	DH14A	DH14-5	DH34	DH36A
SiO_2	50.21	51.35	51.33	50.76	51.63	50.26	51.56	48.44	47.95	51.18	50.44	50.68	48.16	51.03
TiO_2	1.89	2.32	1.83	1.76	2.06	1.87	1.94	2.41	2.27	1.85	1.03	1.02	1.32	2.85
Al_2O_3	16.50	15.40	16.81	16.44	15.44	14.97	15.89	15.29	15.23	14.95	16.58	16.65	16.62	17.46
FeO	9.45	9.12	8.12	8.65	8.69	8.95	8.15	9.37	9.81	10.58	7.11	7.10	9.05	8.10
Fe_2O_3	1.05	1.01	0.90	0.96	0.97	1.49	1.36	1.56	1.09	1.18	1.19	1.18	1.01	0.90
MnO	0.16	0.19	0.26	0.14	0.17	0.14	0.17	1.11	1.41	0.19	0.13	0.12	0.18	0.15
MgO	4.77	4.98	4.50	5.69	5.99	7.12	5.43	4.23	4.31	6.86	7.65	7.93	10.12	2.94
CaO	12.25	11.95	12.51	12.30	12.07	11.24	12.07	12.32	12.75	11.32	13.25	12.59	11.17	11.89
Na_2O	3.31	3.50	3.56	3.02	3.32	3.11	3.11	3.37	3.41	3.09	2.52	2.54	2.73	3.63
K_2O	0.31	0.57	0.51	0.43	0.35	0.44	0.67	0.43	0.31	0.24	0.13	0.15	0.24	0.71
P_2O_5	0.24	0.35	0.47	0.23	0.25	0.23	0.25	1.21	1.38	0.20	0.09	0.08	0.14	0.48
Mg#	47	49	50	54	55	59	54	45	44	54	66	66	67	39
Ba	39	69	66	29	60	47	60	190	177	40		10	18	110
Cr	173	150	183	295	84	133	135	41	68	164	323	331	433	139
Cs	0.164	0.335	0.279	1.39		0.237				0.019		0.321	0.022	0.195
Cu	86	82	41	81	83	84	93	39	46	83	124	107	90	41
Ga	19	21	19	18	19	15	22	22	21	21	18	16	12	25
Nb	9.3	10.2	9.3	10.1	10.7	10.4	10.1	11.6	12.9	9.5		2.5	5.3	28
Ni	26	33	33	60	38	48	32	79	142	50	108	113	293	11
Rb	4.5	10.6	9.63	12.3	4.82	4.67	13	8	2.78	1.84	5	3.1	5.6	10.3
Sr	281	248	281	256	264	226	265	328	328	236	210	122	204	373
V	296	325	275	273	297	275	303	366	346	252	246	226	209	280
Y	35	40	33	30	34	31	32	54	51	31	24	24	25	40
Zn	102	104	82	83	96	79	95	112	124	85	81	69	71	120
Zr	141	165	132	132	146	138	137	156	164	139	66	76	100	221
Hf	3.3	3.9	2.9	3.0	3.3	3.2			3.9	2.9		1.8	2.3	4.6
Sc	47.1	48.9	41.9	44.2	49.0	45.2	44	50	50.6	41.8	41	38.6	37.9	38.8
La	9.4	9.2	7.7	8.1	7.9	8.6			12.7	7.8		2.1	4.4	19.7
Ce	24.5	24.2	16.2	23.1	21.1	21.1			30.4	24.2		5.1	13.0	57.5
Nd	15.58	17.78	19.00	13.73	15.83	14.92			19.4	22.0				40.3
Sm	4.39	5.50	4.17	4.06	4.68	4.18			5.48	4.41		2.24	2.92	7.13
Eu	1.66	1.87	1.50	1.44	1.71	1.49			1.99	1.61		0.85	1.12	2.25
Tb	0.99	1.11	0.75	0.75	1.01	1.00			1.28	0.96		0.68	0.71	1.29
Yb	3.12	4.21	3.20	3.22	3.47	2.81			4.17	2.76		2.44	2.98	3.66
Lu	0.45	0.62	0.48	0.41	0.51	0.44			0.65	0.46		0.31	0.41	0.52
$(La/Sm)_N$	1.37	1.07	1.18	1.27	1.09	1.27			1.49	1.14		0.59	0.97	1.77
$^{87}Sr/^{86}Sr$	0.702467	0.702507	0.702518	0.702596	0.720485	0.702515			0.702505	0.702454		0.702501	0.702461	0.702537
$^{143}Nd/^{144}Nd$	0.513109	0.513122	0.513128	0.513109	0.513120	0.513103			0.513098	0.513135		0.513201	0.513119	0.513077
$^{206}Pb/^{204}Pb$	18.663	18.624	18.609	18.620	18.844	18.646			18.675	18.823			18.807	19.464
$^{207}Pb/^{204}Pb$	15.447	15.491	15.521	15.498	15.521	15.438			15.494	15.494			15.520	15.553
$^{208}Pb/^{204}Pb$	37.895	37.985	38.028	37.985	38.188	37.832			38.037	38.233			38.291	38.619

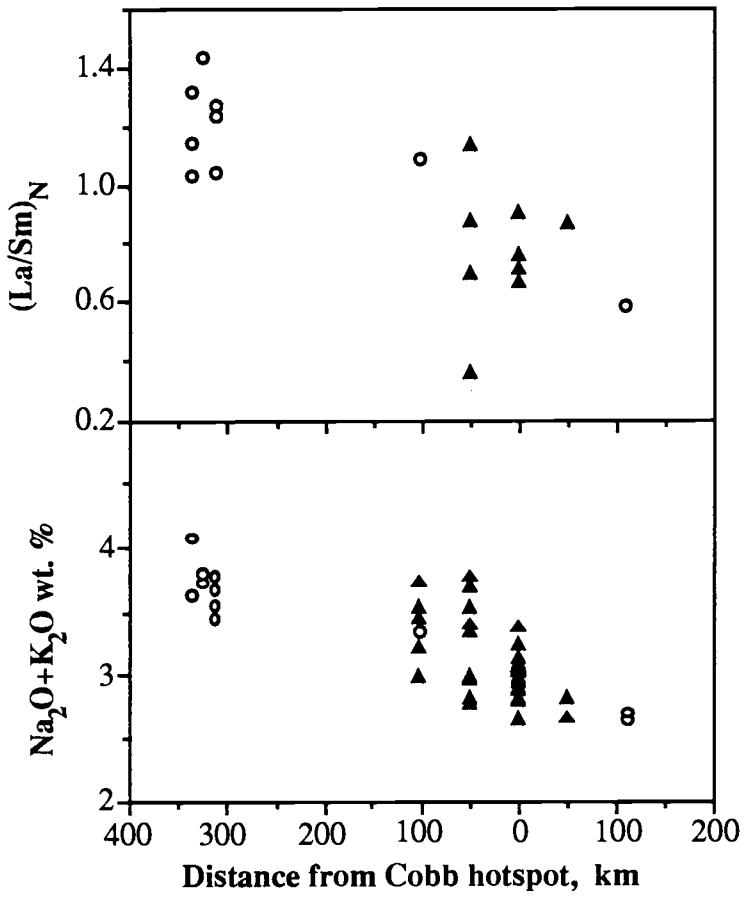

Figure II.2. $(La/Sm)_N$ and $Na_2O+ K_2O$ wt. % versus distance from Cobb hotspot. Variation in alkali and light-REE enrichment with distance from Axial seamount. Basalts dredged from seamounts farthest west of Cobb hotspot show greater enrichment and less variability than seamount basalts dredged near the ridge. Filled triangles represent analyses of Cobb, Brown Bear, Axial and Son of Brown Bear seamounts by Morgan [1985].

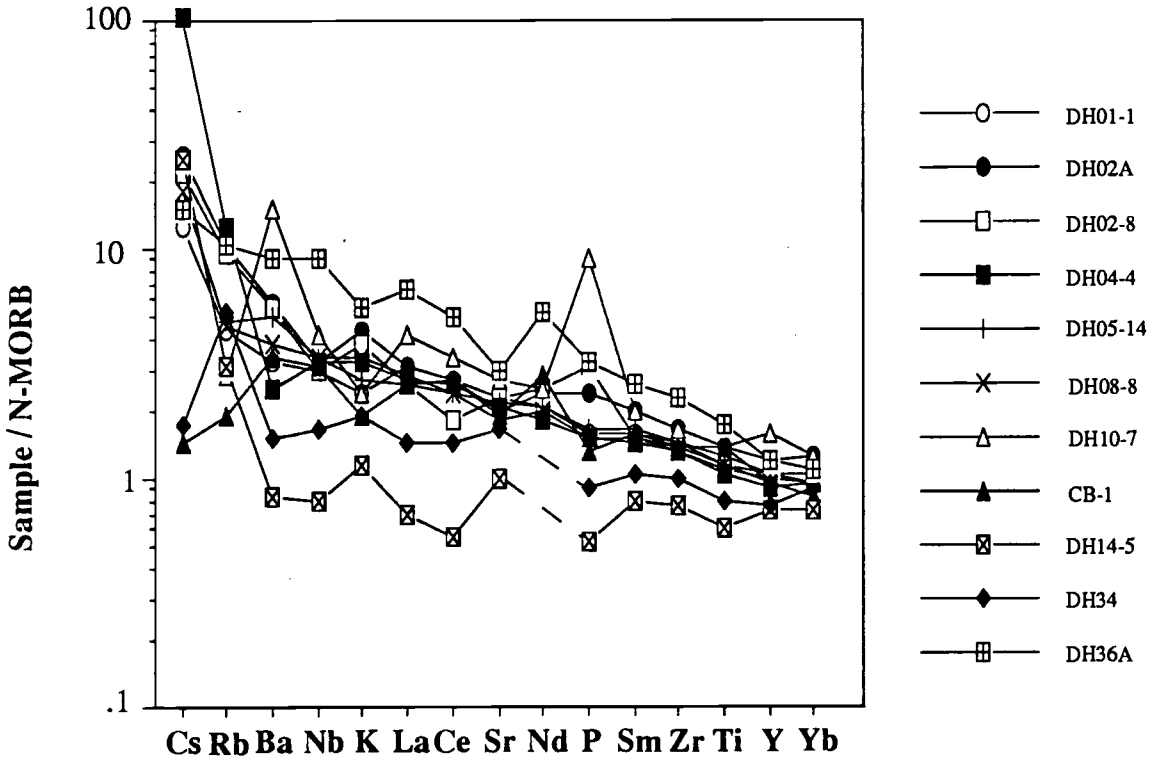

Figure II.3. Spider diagram for CES lavas. Geochemical patterns normalized to N-MORB [after Sun and Nesbitt, 1977]; incompatibility of an element in N-MORB decreases to the right.

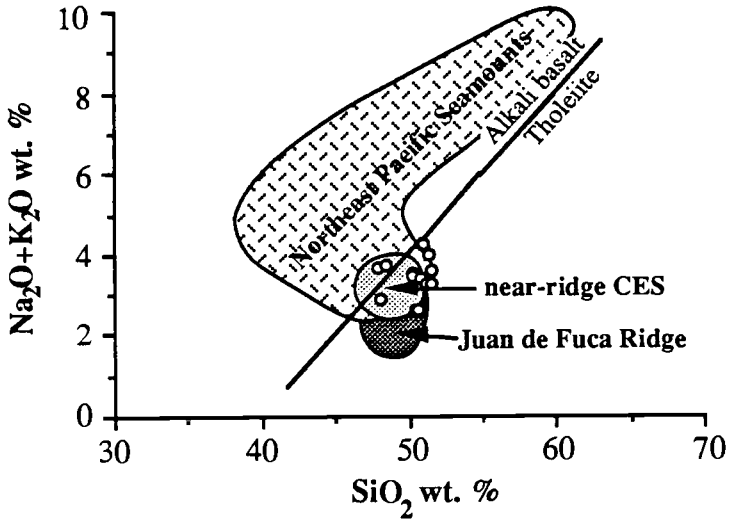

Figure II.4. Na_2O+K_2O wt. % versus SiO_2 wt. % for northeastern Pacific basalts. Northeast Pacific seamount field includes data from seamounts of the Pratt-Welker [Dalrymple et al., 1987], Tuzo Wilson, Bowie, and Dellwood knoll seamount chains Cousens et al., 1985; Cousens, 1988]. Near-ridge CES field includes data from Brown Bear, Son of Brown Bear and Axial seamounts [Morgan, 1985]. The JDFR field is from Liias [1986] and Karsten [1988] and includes the Endeavour segment. Alkali basalt-tholeiite boundary from Macdonald and Katsura [1964].

Table II.3. Average Compositions of Selected Chemical Elements and Ratios for Different Tectonic Settings in the Juan de Fuca Region

Chemical Parameter	JDFR Segments 1-3[a]	Endeavour Segment[b]	Near-Ridge Seamounts[c]	Axial Seamount[a]	Near-Ridge CES[d]	Pacific Plate CES[e]
K_2O (wt.%)	0.18	0.42	0.12	0.15	0.17	0.43
P_2O_5 (wt.%)	0.17	0.23	0.07	0.13	0.13	0.28
Sr ppm	113	211	158	136	159	271
Zr ppm	104	134	54	92	93	145
Nb ppm	5.3	13.9	2.0	4.3	4.2	10.4
Zr/Nb	22.1	9.7	28.1	23.3	28.1	14.0
Zr/Y	3.10	4.58	2.17	3.26	3.66	3.84
$(La/Sm)_N$	0.86	[1]0.70	---	0.76	0.74	1.24

[a] From *Liias* [1986].
[b] From *Karsten* [1988].
[c] Includes Heck, Heckle and Springfield seamount chains, from *Karsten* [1988].
[d] Includes Cobb, Brown Bear, and Son of Brown Bear seamounts, data from *Morgan* [1985], averaged by *Liias* [1986].
[e] Includes Eickelberg, unnamed (except for P_2O_5 wt. %), Warwick, and Cobb seamounts, from this study.

segments 1 through 3 of the JDFR (Table II.3) [Liias, 1986; Karsten, 1988]. However, on the average CES basalts are enriched in Sr, Zr, and P_2O_5 but are depleted in Nb and have higher Zr/Nb and $(La/Sm)_N$ relative to Endeavour segment lavas (Table II.3). CES lavas derive from a source (or sources) enriched over the JDFR source that resembles but is distinguishable from the Endeavour segment source.

On a chondrite-normalized REE plot (Figure II.5), the CES exhibit greater variability than the JDFR basalts (stippled field), although the older Pacific plate CES have rather uniform REE concentrations. Cobb through Eickelberg seamount basalts show slight enrichment in light-REEs relative to the JDFR field (including the Endeavour segment which lies virtually within the field for segments 1 through 3) and a steeper light- to heavy-REE pattern [and thus greater $(La/Sm)_N$)] than the spreading ridge samples. Crossing REE patterns within the Pacific plate CES (Figure II.5, inset) may indicate that the basalts originated from variable partial melting of a mildly heterogeneous source or dynamic partial melting of a homogeneous source [Langmuir et al., 1977].

The moderate MgO content and Mg-number [=100Mg/(Mg+Fe^2)] of many CES and Explorer and Union samples indicate that the basalts have undergone low pressure fractionation away from primary melt compositions. Olivine phenocrysts are present only in the sample from Explorer seamount. However, low Ni contents and a constant CaO/Al_2O_3 with decreasing Mg-number indicate significant olivine removal from the mantle-derived melts (Figure II.6). The absence of a Eu anomaly in the REE patterns of CES samples (Figure II.5) and roughly constant Sr/Zr ratios (Table II.2) provide evidence that although plagioclase was on the liquidus, a large amount of it was not removed from the melt during crystallization. From the lack of correlation between Sc and CaO/Al_2O_3 with Mg-number (Table II.2, Figure II.6) it appears that clinopyroxene was not an important fractionating phase. REE patterns (Figure II.5) and heavy-REE ratios show no evidence for garnet in the CES source. Probably, as with basalts of the

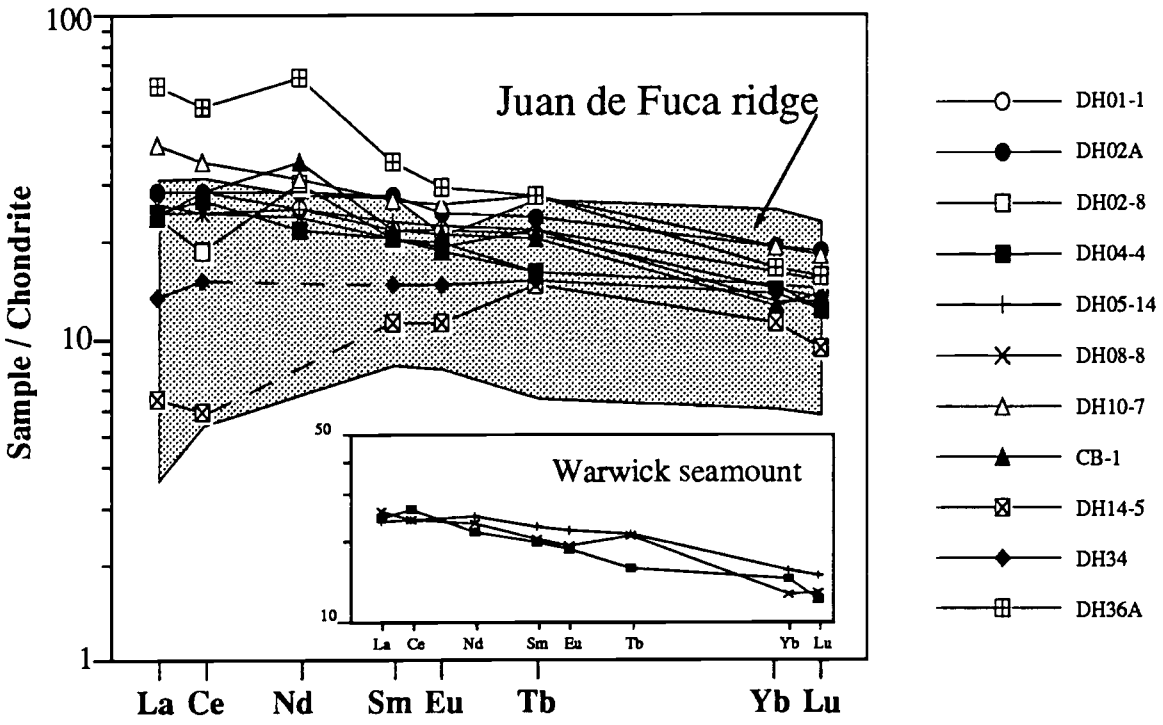

Figure II.5. REE patterns for CES lavas. Chondrite-normalized [after Nakamura, 1974] REE patterns for seamounts of the CES, Explorer and Union seamounts. JDFR (including Endeavour segment) field shown in stipple pattern [Wakeham, 1978; Liias, 1986]. Analyses from samples dredged near the Blanco fracture zone (Dredges 6 and 7) from Wakeham [1978] were not included. Inset shows REE patterns for three basalts from Warwick seamount.

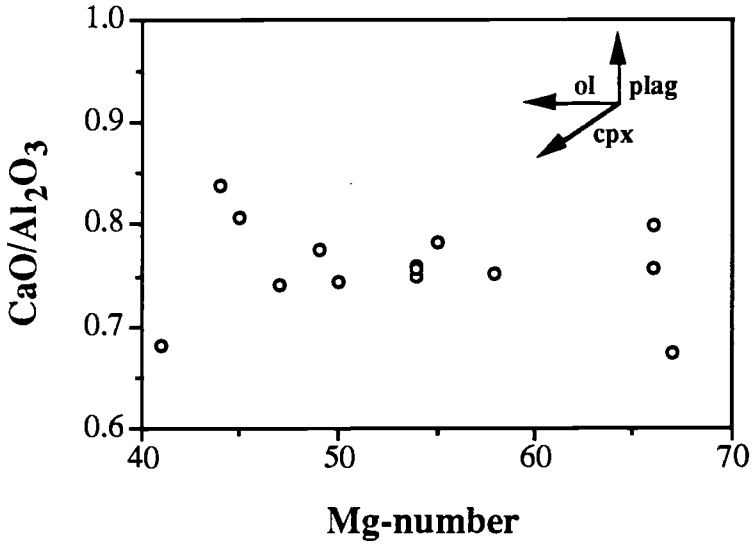

Figure II.6. CaO/Al_2O_3 versus Mg-number for CES basalts. Fractionation trends for olivine (ol), clinopyroxene (cpx) and plagioclase (plag) and variation of of CaO/Al_2O_3 with Mg-number for Cobb-Eickelberg, Explorer and Union seamount basalts.

JDFR [Liias, 1986], the depth of melt segregation for CES lavas was within the spinel stability field.

Determining the petrogenesis of this basaltic suite is limited by the small number of analyses from several volcanic edifices erupted in a changing tectonic setting over 9 Ma. However, the compositional similarity of the older Pacific plate CES allow a common history for these seamounts, which could range from multiple stages of melting of a single homogeneous source (dynamic partial melting) to similar melt conditions acting on a heterogeneous source. In their studies of the JDFR and near-ridge seamounts (including Brown Bear and Son of Brown Bear), Morgan [1985], Liias [1986] and Karsten [1988] concluded that the mantle beneath the Juan de Fuca region must be heterogeneous on a small scale (hundreds of meters to a few kilometers). The variability of lavas within Brown Bear seamount [Morgan, 1985] is one line of evidence for heterogeneity of the upper mantle beneath the Cobb-Eickelberg region. Overlapping REE patterns (Figure II.5) in CES basalts with similar chemical characteristics and a range in TiO_2 and other chemical parameters at constant MgO for basalts of the Juan de Fuca region (Figure II.7) allow us to conclude that the entire CES lineament was produced by preferential melting of compositionally similar, incompatible-element rich pods within a heterogeneous mantle source.

Ratio-ratio plots involving four different elements that are incompatible in fractionating phases (i.e. Zr/Y vs Ti/Nb) indicate mixing of two sources or magmas if sample compositions are linked by a curve [Langmuir et al., 1978]. In a companion plot, one in which the ratios shown have the same incompatible element in the denominator (i.e. Zr/Nb vs Ti/Nb), sample compositions will fall on a line if mixing has occurred. In both plots the sample compositions should lie in the same relative positions unless fractionation has affected the less incompatible elements [Langmuir et al., 1978]. On most ratio-ratio plots (i.e. Figure II.8a and b), CES lavas and near-ridge CES

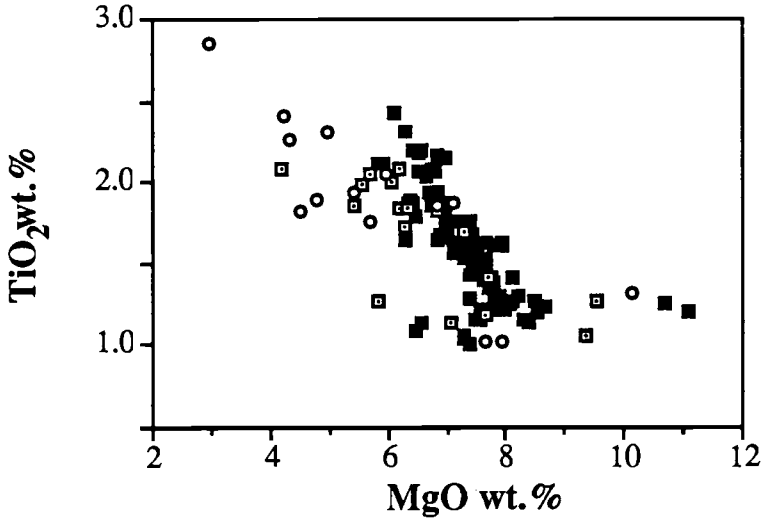

Figure II.7. TiO_2 wt. % versus MgO wt. % variation diagram for northeast Pacific basalts. Symbols as follows: JDFR (filled squares), [Liias, 1986], Axial and the near-ridge CES (open squares) [Morgan, 1985], and the older CES (circles, this study).

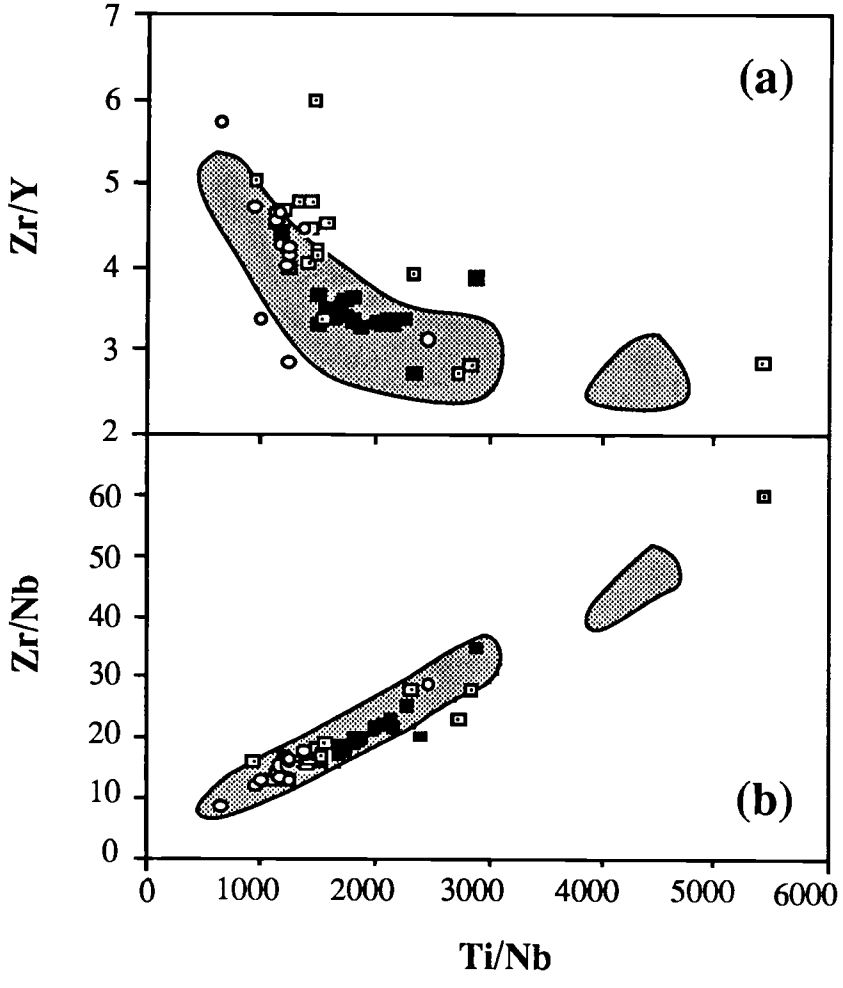

Figure II.8. Incompatible element ratio-ratio mixing plots. Diagram (a) Zr/Y versus Ti/Nb, diagram (b) Zr/Nb versus Ti/Nb. Axial seamount samples are shown in filled squares [Morgan, 1985], near-ridge CES (including Brown Bear, Cobb, Axial and Son of Brown Bear seamounts) are shown in open squares [Morgan, 1985], and older CES analyses are shown in open circles (this study). JDFR and Endeavour segment fields are in dotted pattern [Liias, 1986; Karsten, 1988]; after Langmuir et al. [1978].

[Morgan, 1985] plot close to a mixing curve or line. These data suggest mixing of a low alkalies and $(La/Sm)_N$, high Zr/Nb end-member expressed most strongly near the spreading ridge, with a higher alkalies and $(La/Sm)_N$, lower Zr/Nb end-member seen in the older CES basalts (Figures II.8a and b). However, scatter within these plots precludes simple mixing of two discrete end-members. Rather, the patterns seen are more compatible with partial melting of incompatible-element enriched segregations within the heterogeneous northeastern Pacific upper mantle and variable mixing with a relatively depleted JDFR source. To a first order, mixing between enriched and depleted sources can also be seen along strike of the CES lineament, with more enriched values of incompatible elements ($K_2O + Na_2O$) and ratios $(La/Sm)_N$ at the older end of the chain and more variable (Brown Bear seamount) or less enriched values (Cobb or Axial seamounts) at the younger end (Figures II.2a and b).

Sr, Nd, and Pb isotopes

Although CES lavas are slightly enriched in incompatible element concentrations relative to normal-MORB (N-MORB) from the JDFR (Table II.3), Sr, Nd and Pb isotopic ratios for the CES and Explorer and Union seamounts plot well within the range expected for N-MORB. Samples from the seamounts fall virtually within the JDFR field in their Sr and Nd isotopic ratios (Figure II.9a) [Eaby et al., 1984; Morgan, 1985; Liias, 1986] and there is little isotopic variation along the seamount lineament (Figure II.9b). Only in Pb-isotopic ratios is there a difference in composition between the seamount basalts analysed and the Juan de Fuca ridge (Figure II.10a and b). All CES samples fall in or near the JDFR field [Church and Tatsumoto, 1975; Hegner and Tatsumoto, 1987] but range to somewhat elevated $^{206}Pb/^{204}Pb$, but well within the larger field for northeast Pacific seamounts.

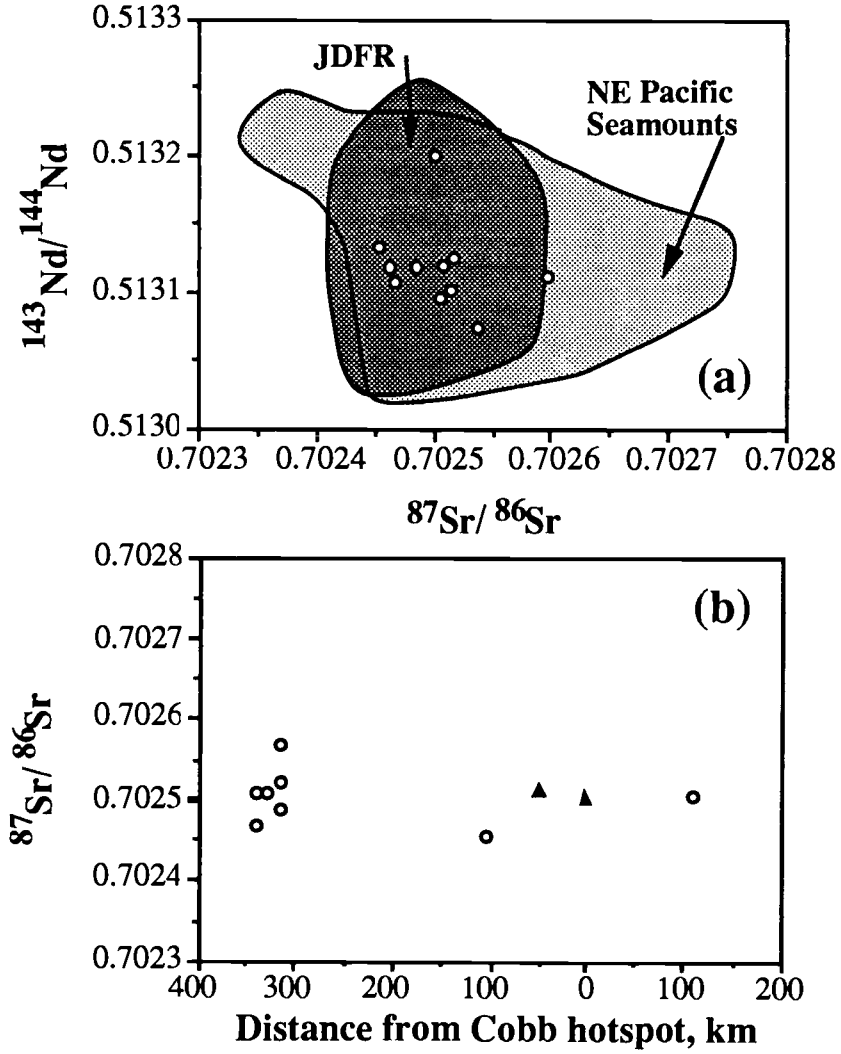

Figure II.9. Sr- and Nd-isotope compositions for northeast Pacific basalts. Diagram (a) $^{143}Nd/^{144}$ Nd vs. $^{87}Sr/^{86}Sr$, diagram (b) $^{87}Sr/^{86}Sr$ vs. distance from Cobb hotspot. CES and Explorer and Union samples with JDFR [Hegner and Tatsumoto, 1987] and other NE Pacific seamount [Hegner and Tatsumoto, 1989; Cousens et al., 1985; Cousens, 1988] fields superimposed. Range in isotopic ratios shown is equal to N-MORB field. for samples from the CES lineament. Filled triangles represent analyses of Brown Bear and Axial seamounts by Eaby et al., [1984].

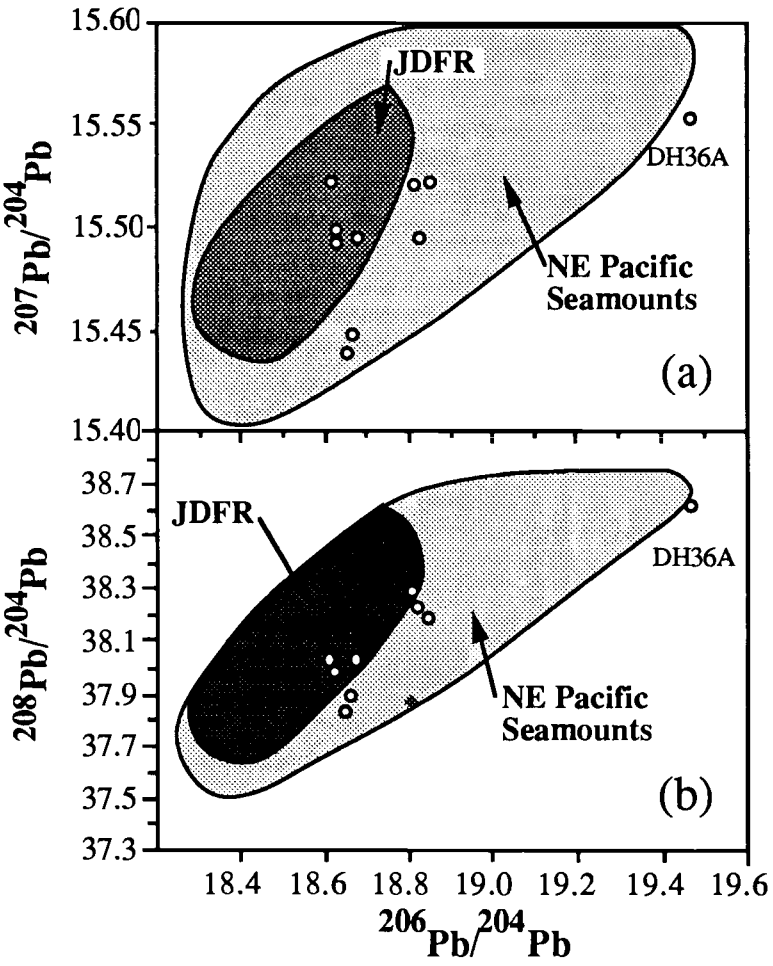

Figure II.10. Pb-isotope compositions for northeast Pacific basalts. Diagram (a) $^{207}Pb/^{204}Pb$ versus $^{206}Pb/^{204}Pb$,diagram (b) $^{208}Pb/^{204}Pb$ versus $^{206}Pb/^{204}Pb$. CES, Explorer and Union samples compared with Juan de Fuca ridge [Church and Tatsumoto, 1975; Hegner and Tatsumoto, 1987] and NE Pacific seamounts [Church and Tatsumoto, 1975; Hegner and Tatsumoto, 1989; Cousens, 1988] fields. The sample from Union seamount (DH36A) is distinct. Range in isotopic ratios shown is slightly larger than values seen in N-MORB basalts.

The single sample from Union seamount is clearly distinct from the CES basalts in Pb isotopic composition.

GEOCHRONOLOGY

Eleven of the freshest basalt samples from the Cobb-Eickelberg, Explorer and Union seamounts were chosen for age determinations by ^{40}Ar-^{39}Ar total fusion and conventional K-Ar radiometric dating methods [McDougall and Harrison, 1988; Dalrymple and Lanphere, 1969]. Because of the young ages and low potassium concentrations in these lavas and sample size limitations for irradition, not enough radiogenic ^{40}Ar was present for analysis by ^{40}Ar-^{39}Ar incremental heating experiments. Basalt samples were crushed and sieved to obtain the 0.5 and 1.0 mm size fraction, then washed ultrasonically in distilled water. For ^{40}Ar-^{39}Ar total fusion experiments, samples were irradiated for 6 to 10 hours in the core of the Oregon State University TRIGA reactor, where they received a neutron flux of 0.6 to 1.0 x 10^{17} nvt. Isotopes of argon were measured on an AEI MS-10S mass spectrometer, after sample fusion via radio-frequency induction heating and gas purification; potassium contents were determined by atomic absorption spectrophotometry. Analytical data and age calculations from the ^{40}Ar-^{39}Ar and K-Ar experiments are given in Table II.4. The relatively large age uncertainties result from measuring small amounts of radiogenic ^{40}Ar within a total ^{40}Ar signal of largely atmospheric origin. A replicate ^{40}Ar-^{39}Ar total fusion analysis was performed on one sample from Eickelberg seamount (Table II.4). Ages coincide within their two sigma errors. Reactor irradiation is known to increase the atmospheric argon component [McDougall and Harrison, 1988] so conventional K-Ar ages were determined for Explorer seamount where samples were

TABLE II.4. ^{40}Ar-^{39}Ar and K-Ar Total Fusion Ages and Analytical Data for Whole Rock Basalt Samples From the Cobb-Eickelberg and Explorer and Union Seamounts

Sample	J-Factor	$^{40}Ar/^{39}Ar$	$^{36}Ar/^{39}Ar$	$^{37}Ar^{c}/^{39}Ar$	%K	$^{*40}Ar$ mol/g ($x10^{-9}$)	$\%^{40}Ar$	Age (± 1 sigma) Ma
TT080 DH01-1	0.001957	21.269	0.06435	22.052			11.91	9.03 (0.41)
TT080 DH02A	0.002446	15.865	0.05083	15.574			12.69	8.98 (0.75)
replicate	0.002446	40.990	0.13615	12.812			4.16	7.52 (0.46)
TT080 DH02-8	0.002446	21.768	0.07212	14.542			7.35	7.05 (0.15)
TT080 DH08-8	0.001957	28.394	0.09047	16.109			6.85	6.91 (0.30)
TT080 DH 10-7	0.001292	23.862	0.77980	22.765			12.61	7.73 (0.33)
TT175 DH 70-2	0.003050	35.811	0.12171	14.064			2.64	5.20 (0.32)
TT175 DH 71-4	0.003050	29.516	0.10218	18.908			2.72	4.40 (1.07)
TT175 DH 74-17	0.003050	55.674	0.19423	25.713			0.51	1.55 (1.40)
CB-1	0.003050	11.161	0.04158	22.013				3.27 (0.30)
TT080 DH 14-5	0.002446	163.580	0.56704	60.010			0.44	3.19 (1.30)
TT063 DH 34	0.003050	30.274	0.11003	29.057			0.07	0.12 (0.57)
					0.666	4.375		0.17 (0.03)
TT063 DH 35	0.003050	35.303	0.13252	50.211			0.16	0.31 (0.37)
					0.489	6.510		0.35 (0.04)
TT063 DH 36A	0.003050	8.875	0.29922	8.696			1.14	5.78 (0.65)

Ages calculated using the following decay and abundance constants: $\lambda_{\varepsilon}=0.581x10^{-10}\ yr^{-1}$; $\lambda_{\beta}=4.963x10^{-10}\ yr^{-1}$; $^{40}K/K=1.167x10^{-4}$ mol/mol. Neutron flux monitored with hornblende standard MMhb-1.

[c]Corrected for decay since irradiation.

expected to be the youngest analysed (i.e. smallest radiogenic ^{40}Ar) and Explorer samples were absolutely fresh (no alteration). Crustal ages were based on magnetic anomaly interpretations by Wilson et al. [1984] and tectonic reconstructions by Karsten and Delaney [1989].

Figure II.11 shows the variation in age of eight seamounts with distance along the seamount chain from Cobb hotspot, assuming its location is defined by the center of Axial volcano (zero age). Distances were measured along the lineament, in the direction of Pacific plate motion over the mantle [Duncan and Clague, 1985; Pollitz, 1988]. Also shown on this figure are the ages determined for Union and Explorer seamounts plotted against distance from Endeavour and Middle Valley spreading segments, respectively (Figure II.1). Volcanic activity may continue for as long as three million years at a given seamount [e.g. Pratt-Welker seamounts, Turner et al., 1980]; a two million year span was recorded in the three samples analysed from Eickelberg seamount. Therefore, we have used the oldest sample from each seamount where more than one sample was analysed as an estimate of the time when the volcano was located directly over the hotspot. Replicate analyses for Eickelberg sample DH02A were averaged. Oldest seamount ages were used in a least-squares linear regression to determine an average rate of plate motion over the hotspot of 43 ± 3 km/my A least-squares regression of all Pacific plate CES including all three Eickelberg points gives a rate of plate motion over the hotspot of 47 ± 3 km/my. Ages from Union and Explorer seamounts were not included in the regression, being from separate provinces, but these data are generally consistent with the Pacific plate motion inferred from the CES age-distance relationship.

Two age patterns can be seen in Figure II.11:

(1) Ages increase to the northwest along the CES chain from Axial seamount at zero age on the spreading ridge, to 3.3 Ma at Cobb seamount, some 105 km from the ridge, and on to 9.0 Ma at Eickelberg seamount, about 340 km from the ridge. Union seamount is

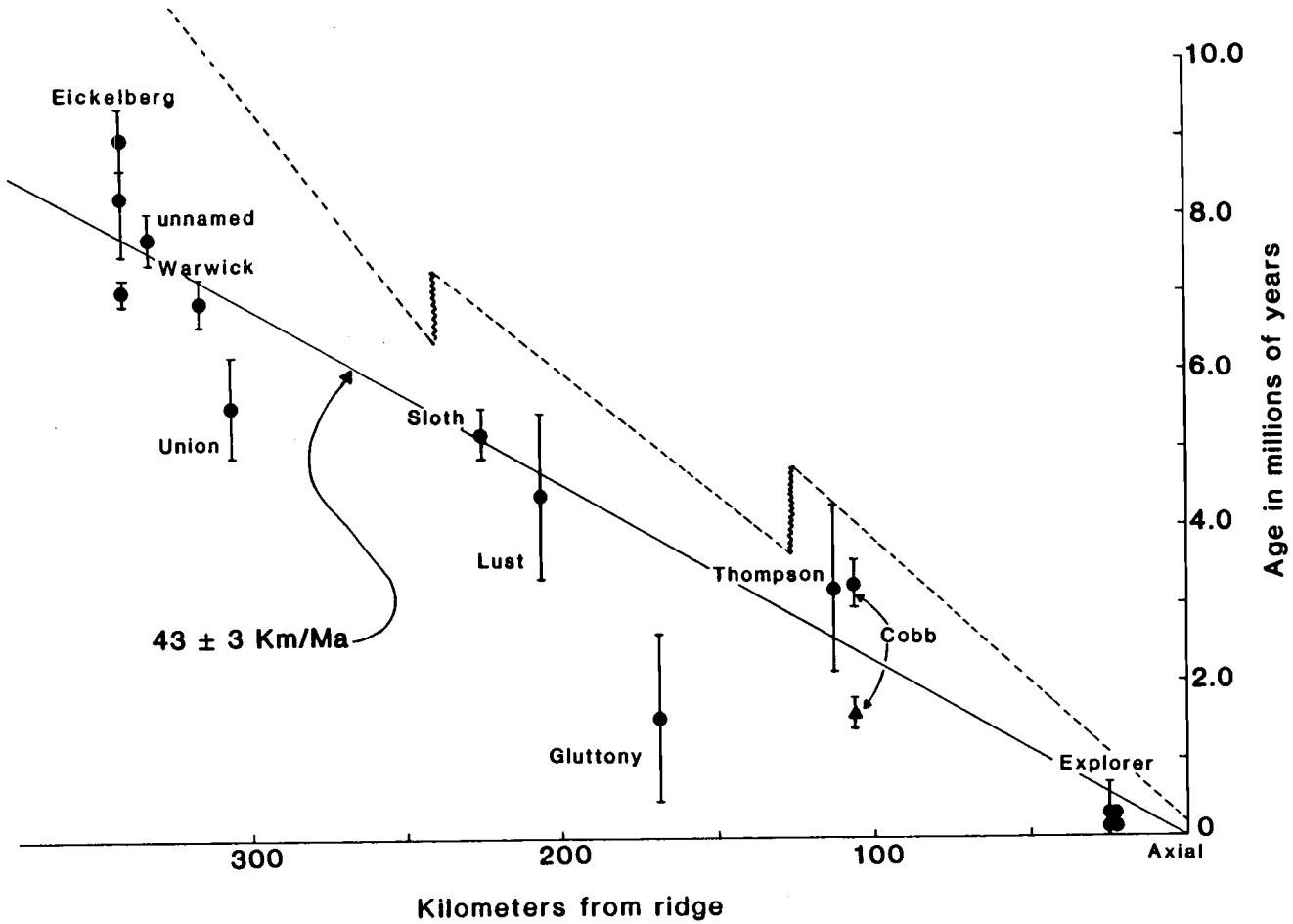

Figure II.11. Seamount age versus distance from spreading ridge. $^{40}Ar/^{39}Ar$ and K-Ar age determinations for CES and Explorer and Union seamounts. K-Ar age of Cobb seamount by Dymond et al. [1968] shown as triangle. Measured distance for CES is from Cobb hotspot, defined as the center of Axial volcano (46°N, 130°W), along the direction of Pacific plate motion [Pollitz, 1988]. Crustal ages [after Wilson et al., 1984] are shown by the dashed line; a break indicates location of a pseudofault. Average rate of motion of the Pacific plate over the hotspot was calculated to be 43 + 3 km/Ma. Replicate analyses of sample DH02A from Eickelberg seamount were averaged.

one member of a short Pacific plate volcanic chain further to the north. The zero age position of the associated melting anomaly is unknown; we have assumed it to be the Endeavour ridge segment (Table II.4).

(2) There is a northwesterly increase in the difference in the age of the seamounts and the crust on which they formed. Axial seamount is currently forming on the ridge on zero-age crust but Eickelberg seamount formed on crust that was 2-3 Ma. This change in the crustal age at the time of seamount volcanism is due to the westward migration of the JDFR, toward Cobb hotspot, since at least 10 Ma [Riddihough, 1984; Karsten and Delaney, 1989].

The line of seamounts from Axial through Eickelberg, although short, is subparallel with other more prominent Pacific chains that are associated with stationary long-lived mantle hotspots. The volcanic migration rate of 43$\pm$ 3 km/Ma is consistent with a plate-mantle velocity of 44 km/Ma predicted from the latest Pacific plate rotation pole at 62^{o}N, 94^{o}W and rotation rate of 0.95^{o}/Ma [Pollitz, 1988], which applies for the period 0-9 Ma. New age data from the CES, as well as the Pratt-Welker seamounts [Dalrymple et al., 1987], Samoa [McDougall, 1985] and the Louisville seamount chain [Watts et al., 1988] support the idea of rigid Pacific plate motion over a fixed constellation of hotspots (Figure II.12).

DISCUSSION

Summary of temporal and chemical characteristics of the CES

The CES chain has the temporal and morphologic characteristics of volcanism generated over a hotspot fed by a mantle plume. The seamount chain is age progressive and the linear geometry and age distribution of volcanoes are compatible with the motion

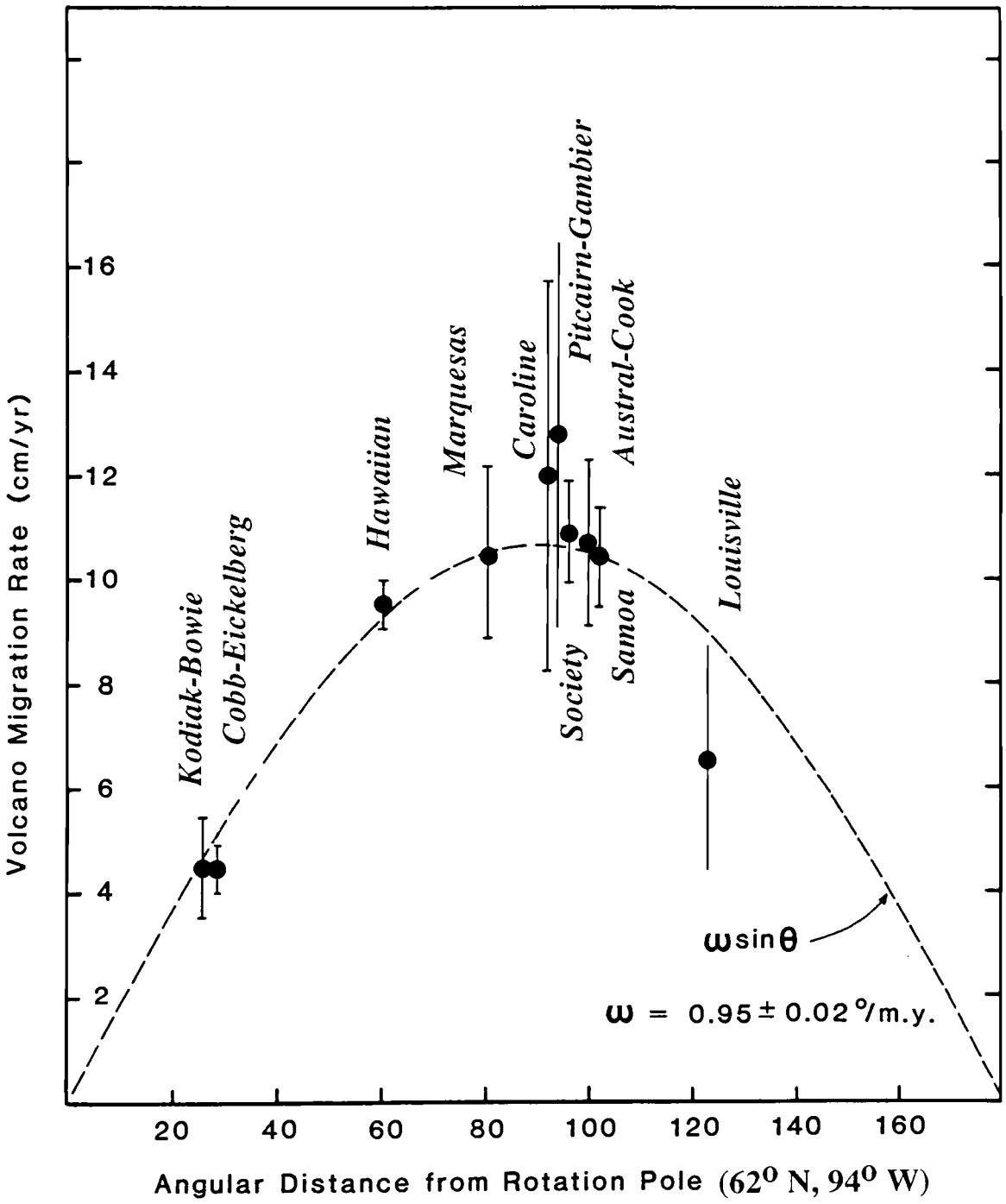

Figure II.12. Volcanic migration rate versus angular distance from rotation pole. Rotation pole located at 62° N, 94° W [Pollitz, 1988]. The dotted curve is a least-squares best-fit with an angular rotation rate of 0.95 ± 0.02°/Ma.

of the Pacific plate over other well-established hotspots. Age relationships along the CES chain, determined by ^{40}Ar-^{39}Ar and K-Ar analyses, in conjunction with the tectonic reconstruction of the Juan de Fuca region of Karsten and Delaney [1989] require a fixed source for the CES lineament and a westwardly migrating spreading ridge. Our data demonstrate that the melting anomaly currently beneath Axial seamount is a stationary, persistent focus of unusually high magma supply, even though volcanic activity along the lineament may have been intermittent, with the Eickelberg to Axial seamount section being the latest "pulse" of plume flow.

In most respects, CES lavas are transitional between basalts characteristic of hotspots and those of segments 1 through 3 of the JDFR; they are similar to those of the Endeavour segment. Compositional variability among CES basalts probably reflects a range of partial melting of the mantle supplied to the melting anomaly, which is heterogeneous with respect to incompatible elements [Morgan, 1985; Liias, 1986; Karsten, 1988]. The eastward trend toward depleted compositions indicates that progressively greater proportions of the source for JDFR basalts participated in melting for CES basalts. In terms of the Sr, Nd and Pb isotopic compositions, which usually distinguish hotspot from spreading ridge lavas, the CES basalts cannot be separated from MORB compositions. The lack of distinguishing Sr, Nd, Pb and He isotopic ratios is a feature of other northeast Pacific seamount and spreading ridge lavas [Church and Tatsumoto, 1975; Lupton, 1982; Eaby et al., 1984; Morgan, 1985; Liias, 1986]. No significant isotopic variation has yet been found in basalts from the Pratt-Welker [Church and Tatsumoto, 1975; Hegner and Tatsumoto, 1989], Heckle [Hegner and Tatsumoto, 1989], Tuzo Wilson [Cousens et al., 1985], Bowie [Cousens et al., 1985; Cousens, 1988], Dellwood knolls [Cousens et al., 1984], or President Jackson [W. M. White, pers. comm., 1988] seamount groups.

Models

Several models may explain the age distribution and chemical compositions of the CES basalts.

(1) *Passively upwelling heterogeneous mantle and a migrating spreading ridge:* The CES may be the result of the same processes that form near-ridge seamounts along the East Pacific Rise [Batiza and Vanko, 1983, 1984; Zindler et al., 1984; Fornari et al., 1988a,b], Juan de Fuca and Gorda Ridges [Davis and Karsten, 1986; Karsten and Delaney, 1989]. Most of these small near-ridge seamount clusters are thought to be the result of volcanism above a short-lived melting anomaly embedded in the upper mantle lateral flow, rather than a deep mantle plume. Following the Batiza and Vanko [1983, 1984] and Zindler et al. [1984] model for small seamounts near the East Pacific Rise, a somewhat smaller degree of partial melting of the same heterogeneous upper mantle source that is producing the JDFR lavas would result in melts somewhat enriched in incompatible elements and alkalis but with essentially MORB-like isotopic composition. This mechanism could easily explain the modest enrichment in alkalies of the CES lavas and might, with an even smaller degree of partial melting, explain the alkali basalts and hawaiites of other northeastern Pacific seamounts.

The scale of volcanic activity at such near-ridge seamounts is, however, much smaller than in the CES province. A typical near-ridge seamount is 100 km^3, compared with 1000 km^3 for a Cobb-Eickelberg cone. The duration of volcanism for an entire near-ridge seamount chain can be brief - the Heckle chain near the Juan de Fuca ridge began activity at ~2 Ma and ceased at 0.5 Ma [Karsten and Delaney, 1989]. Volcanism along the CES chain has persisted for at least 9 Ma.

Although it is possible that a large passive upper mantle melting anomaly could account for the increased volume and duration of volcanism at Cobb hotspot, we believe that a melting anomaly that has been fixed with respect to the hotspot reference frame for at least 9 Ma must be rooted below the asthenosphere. A melting anomaly, of the type responsible for volcanism at small near-ridge seamount chains, would be swept along with upper mantle flow over the time scale required. Therefore, we believe that Cobb hotspot has been maintained by a mantle plume during the CES formation. Also, near-ridge seamount basalts in the Juan de Fuca region, i.e. Heck, Heckle, and Springfield [Karsten, 1988], are more depleted in alkali and incompatible elements at a given MgO content than the spreading ridge basalts, in contrast with the CES lavas.

(2) *Compositionally buoyant mantle plume and a migrating spreading ridge:* Compositional buoyancy occurs when plume flow is driven by intrinsic density differences between the diapir and its surroundings [Griffiths, 1986a]. Chemical diffusion proceeds extremely slowly so that compositional diapirs maintain their chemical identity relative to the upper mantle material through which they rise [Griffiths, 1986a].

A compositional plume that has moderately enriched trace element contents but a nonradiogenic isotopic character could originate in several ways. For example, the MORB-like isotopic composition of all seamounts of the northeastern Pacific may reflect a broad regional difference in mantle composition from the equatorial oceanic regions where Dupal hotspots are found [Hart, 1984]. Hart [1988], who noticed a poleward trend toward less radiogenic isotopic compositions in hotspot-associated basalts, termed the regional isotopic homogeneity of the northeastern Pacific the anti-Dupal anomaly. He proposed that the lower mantle which feeds plumes may be compositionally variable on a very long lengthscale (10^4 km) and some regions may be isotopically MORB-like if large amounts of melts have been previously extracted from them.

A metasomatic event that enriched the mantle in the region in Rb, Sm and U, along with other incompatible elements [Menzies and Murthy, 1980], but so recently that their elevated concentrations have not yet significantly shifted the Sr and Nd isotope ratios from the MORB field was suggested by Cousens et al. [1985] to explain the alkalic but isotopically MORB-like compositions of the Tuzo Wilson seamounts. This explanation could also apply to the transitional lavas of the CES chain.

The proximity of Cobb hotspot to the Juan de Fuca ridge may provide another explanation for the unusual chemistry of the CES basalts. A weak supply of relatively enriched plume material to a hotspot in a spreading ridge setting may be diluted by mixing with the MORB partial melt zone. That is, the zone of partial melting below the ridge may extend at least 130 km away from the spreading axis. This model of hotspot and spreading ridge interaction is easily testable. Older Gulf of Alaska seamounts (e.g. Miller, Patton and Murray) proposed to have formed at hotspots far removed from a spreading ridge at the time of seamount formation should exhibit a more typical OIB signature if they formed from a plume with OIB composition. If basalts from such seamounts are found to have MORB compositions they would almost certainly have resulted from a plume with MORB chemical characteristics since melts from those hotspots could not easily have mixed with spreading ridge melts. The alkalic lavas from Murray and Patton seamounts, which erupted through 11-12 Ma oceanic crust [Dalrymple et al., 1987], would have been 550 km west of the spreading ridge system and isotopic data could be expected to detect an OIB isotopic plume signature, if one existed.

Interaction of a plume of enriched mantle composition with oceanic lithosphere cannot explain CES chemistry. For the Hawaiian Islands, a model of mixing between the enriched mantle (EM) plume and a small degree of melting of oceanic lithosphere through which the plume rises, can explain the distinct incompatible element and

isotopic compositions of tholeiitic and alkalic lavas [Chen and Frey, 1983]. A similar mixing model can also be applied to the CES lavas and other seamount lavas of the northeast Pacific [Cousens et al., 1985]. A plot of La/Ce vs $^{87}Sr/^{86}Sr$ [Chen and Frey, 1983, figure 3] shows that CES lavas could result from 0.25% to more than 3.0% partial melt of lithospheric (MORB) material mixed with EM, in proportions of about 1:4, a larger MORB component than is seen in Hawaii. Samples such as the basalt from Cobb seamount could be generated only if the La/Ce of the upper mantle beneath the northeast Pacific is lower than the one postulated in the Chen and Frey [1983] model for Hawaii. However, the required variation in degree of melting of the lithosphere, followed by mixing of nearly constant proportions of MORB and EM components would result in $^{87}Sr/^{86}Sr$ enrichment with increasing degree of melting of the lithosphere, a trend not seen in the CES lineament. The observed compositions seem to point strongly to the absence of a long-term enriched mantle component in lavas of the CES and other northeast Pacific lineaments.

(3) *Thermally buoyant plume and a migrating spreading ridge:* Formation of a plume that has MORB isotopic characteristics might result from thermal entrainment of MORB upper mantle by a plume of lower mantle composition. Thermally buoyant plumes are driven entirely by viscosity and density differences created by a temperature gradient across a thermal boundary layer [Griffiths, 1986a]. Diffusion of heat from such thermal diapirs warms the surrounding mantle and lowers its density sufficiently for the plume to entrain its initially cooler surroundings but conserve its total heat content, buoyancy and driving force. The thermal plume will be a mixture of the diapiric material and surrounding material entrained toward its center [Griffiths, 1986a]. Recently, Geist et al. [1988] have argued that the unusual isotopic structure of the Galapagos archipelago, in which Sr-isotopic ratios decrease toward the center of the hotspot, may result from the thermal entrainment process proposed by Griffiths [1986a,b].

Thermal entrainment can also occur in a continuous plume which is deflected by mantle shear flow beneath a spreading ridge [Richards, 1988]. In this case, as well as for discrete diapirs, the most MORB-like magmas are to be expected from the center of the plume. Therefore, the isotopic composition of erupted magmas may be an important distinction between chemical and thermal plumes, regardless of possible small-scale heterogeneity and variable source. A large volume of entrained material implies a sharply reduced temperature contrast between plume and normal mantle.

In reality plumes may occur from a combination of thermal and compositional instabilities, but one effect may dominate. The hotspot that produced the Louisville seamount chain (LSC) may have been supplied by a largely compositional plume. Like many hotspot tracks, the LSC has an associated topographic swell, in this case several hundreds of meters high, and a volcanic eruption rate of 3-4000 km^3/Ma from 70 Ma until 20 Ma, when it waned sharply [Lonsdale, 1988]. The LSC shows a very narrow range of Sr, Nd, and Pb isotopic values over the 65 m.y. range of available samples. These basalts show radiogenic Sr, Nd, and Pb isotopic compositions, typical of OIB lavas [Cheng et al., 1987b]. Based on the consistently enriched compositions of Louisville samples, Cheng et al. [1987b] suggested that the LSC was formed by a compositional plume that originated from a long-lived, stationary and homogeneous mantle source. This plume was not noticeably contaminated by overlying asthenosphere or lithosphere as were plumes that form other hotspot chains [Cheng et al., 1987b and references therein].

In contrast, the more intermittent and consistently MORB-like melts from Cobb hotspot perhaps manifest a thermal plume. Such a plume may rise through and entrain the MORB-like upper mantle, supplying the melting anomaly at the base of the lithosphere. To produce the observed isotopic compositions, we would expect the proportion of MORB-component to be large. If a large amount of the final plume

volume is entrained material, the plume might be broad but would be thermally dilute (cooled); thus, resulting volcanism might be volumetrically small compared with that of other hotspots. Furthermore, thermal entrainment increases strongly with decreasing thermal plume Rayleigh number [Griffiths, 1986b]. Plumes that start off weaker (smaller diameter and lower temperature contrast) suffer stronger entrainment. This is consistent with a relatively "weak" (thermal) plume source for the CES.

Summary model

The major and trace element chemical characteristics of the CES are best explained by mixing of enriched and depleted lavas resulting from partial melting of a heterogeneous upper mantle in both a hotspot and spreading ridge melting regime. Like JDFR melts, CES liquids probably segregate in the spinel lherzolite stability field. CES lavas are also similar to all northeastern Pacific seamount and spreading ridge basalts analysed thus far in that they show no enrichment in radiogenic isotopes over normal-MORB. Thus, there is no evidence to suggest that Cobb hotspot is a compositionally buoyant mantle plume. Although, the chemical characteristics of the lavas can be explained by a large passive upper mantle melting anomaly, we believe that, to have remained stationary, the source of the CES lineament must be rooted beneath upper mantle lateral flow. The most likely explanation for the unusual geochemical characteristics of Cobb hotspot is a deeply rooted, thermally buoyant diapir which has entrained nonradiogenic upper mantle MORB-source material. The large, thermally dilute plume supplies the hotspot with volumes of warm mantle in excess of that upwelling along the spreading ridge, resulting in the buildup of the volcanic cones of the CES chain. Progressively greater mixing of plume and spreading ridge mantle sources has occurred as the JDFR approached the hotspot.

Age relationships along the CES lineament since 9 Ma permit greater resolution of the Karsten and Delaney [1989] model for hotspot-spreading ridge interaction. In this model a westward migration of the JDFR toward a fixed Cobb hotspot was determined from analysis of the propogating rift and spreading history of the ridge [Wilson et al., 1984; Riddihough, 1984]. At 8 Ma the JDFR lay about 130 km east of Cobb hotspot (Figure II.13). Eickelberg seamount was then forming above the hotspot on seafloor aged 2-3 m.y.. Proximity of the Cobb hotspot to the JDFR may have resulted in dilution of plume material by mixing with the MORB partial melt. The next seamount to the east (unnamed) had begun forming while Eickelberg seamount was still active, ~7.8 Ma. By 6 Ma Eickelberg seamount had moved 88 km west of the hotspot, the Juan de Fuca ridge had moved 35 km closer to the hotspot and Warwick seamount was forming on ~2 Ma crust. At ~4 Ma Sloth seamount had formed on 1.6 m.y. crust and had moved more than 50 km to the west, Lust seamount had formed on 1.8 m.y. crust while the ridge was only 65 km from the hotspot. Although a large uncertainty is associated with the age of Thompson seamount it is consistent with an origin at the ridge at ~3.2 Ma, followed by transport *east* at a rate of ~34 km/Ma with the Juan de Fuca plate [Desonie and Duncan, 1986; Karsten and Delaney, 1989]. Cobb seamount formed at approximately the same time as Thompson seamount on crust of age 0.4 m.y.. Interaction of spreading ridge and hotspot partial melt zones resulted in less enriched (Cobb seamount) or more variable (Brown Bear seamount) chemical characteristics in the seamounts near the Juan de Fuca spreading ridge. Axial seamount is currently forming over the ridge-centered hotspot.

Figure II.13. Hotspot-ridge interactions from 8 Ma to present. Locations of Cobb hotspot and Juan de Fuca ridge, in 2 m.y. time increments [after Karsten and Delaney, 1989] with improved resolution by ^{40}Ar-^{39}Ar total fusion age determinations on basalts of the CES chain. Large arrows indicate motion of the Pacific and Juan de Fuca plates. Age of crust at the time of eruption of each seamount is given. Symbols for seamount names as in Table 1.

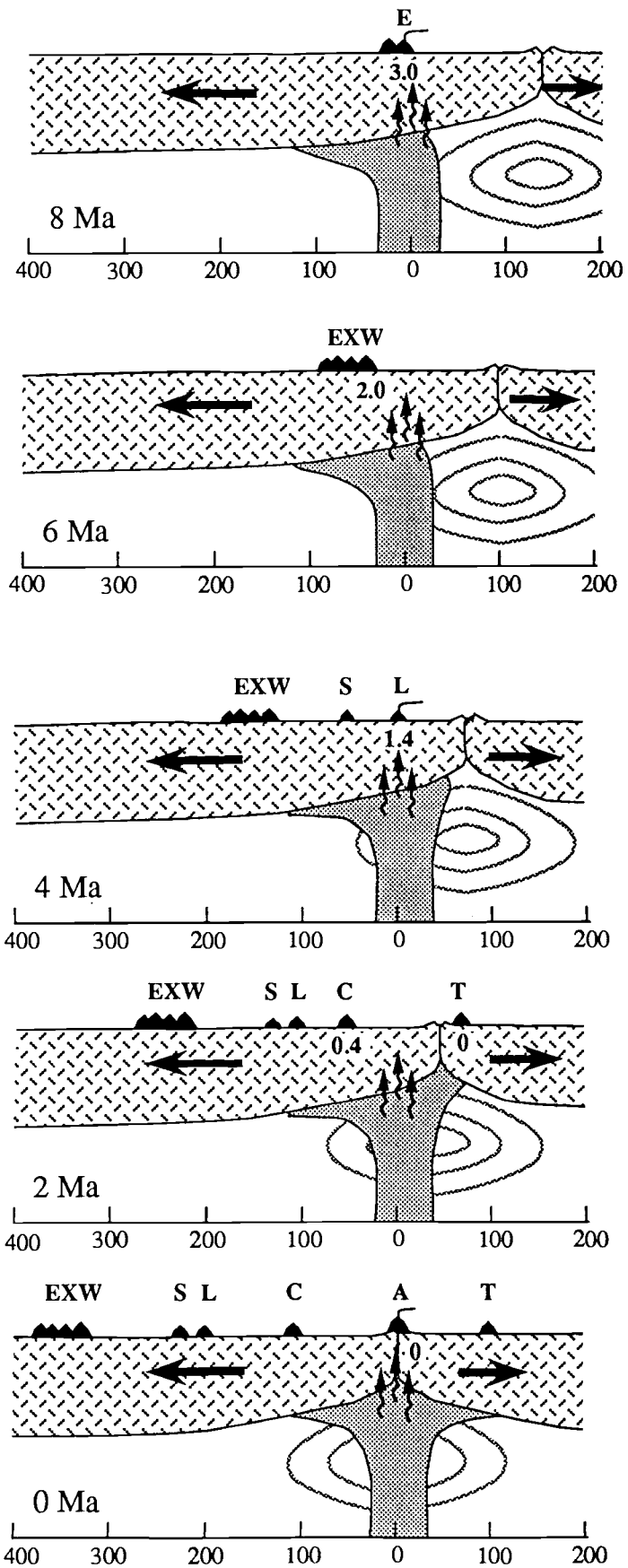
E
3.0
8 Ma
400 300 200 100 0 100 200
EXW
2.0
6 Ma
400 300 200 100 0 100 200
EXW S L
1.4
4 Ma
400 300 200 100 0 100 200
EXW S L C T
0.4
0
2 Ma
400 300 200 100 0 100 200
EXW S L C A T
0
0 Ma
400 300 200 100 0 100 200

Figure II.13.

TEMPORAL AND GEOCHEMICAL VARIABILITY OF VOLCANISM OVER THE MARQUESAS HOTSPOT

ABSTRACT

The Marquesas archipelago, which lies within the chemically heterogeneous and geophysically anomalous French Polynesian region of the south central Pacific, is a linear volcanic chain that formed as the result of melting above the Marquesas hotspot. Samples dredged from volcanoes along the lineament on the Crossgrain 02 Expedition decrease in age from northwest to southeast; the youngest known volcanism in the Marquesas is at a group of seamounts southeast of the island of Fatu Hiva. Tholeiitic and transitional basalts compose the typical shield of a Marquesan volcano; alkalic lavas form a later phase. Fractional crystallization models performed on the most primitive dredged lavas can relate evolved lavas to tholeiitic, transitional, and alkalic parental compositions.

Subaerial and submarine basalts are the result of mixing of at least two mantle sources distinguished by trace element and Sr, Nd, and Pb isotope compositions. Tholeiitic and transitional lavas compositions can be explained in terms of variable degrees of melting of a depleted mantle source (DMM) which contains pods of incorporated enriched material (HIMU). Alkalic lava compositions can be explained in terms of smaller degrees of melting of a more enriched mantle source (EM II). In our preferred model, a thermally buoyant diapir of EM II composition may have entrained upper mantle MORB-source material, composed of DMM + HIMU, as it rose. Tholeiitic melts were formed by melting the entrained material at the center of the hotspot, explaining the larger degree of melting and larger volume of tholeiitic and

transitional basalts in the main shield-building phase of volcano development. Alkali basalts resulted from melting of mantle of EM II composition at the edges of the hotspot.

INTRODUCTION

French Polynesia, in the south-central Pacific (Figure III.1), is a region uniquely suited for studies of mantle heterogeneity [Duncan and Compston, 1976; Vidal et al., 1984]. The high density of volcanoes found within this 2,200,000 km^2 area allow an excellent sampling of the mantle and lithosphere beneath. French Polynesian volcanoes are far from plate boundaries, well away from seafloor spreading at the East Pacific Rise and subduction processes at the Tonga Trench. The islands of French Polynesia are on the western side of a geophysically anomalous region, the South Pacific Isotopic and Thermal Anomaly (SOPITA), thought to be a zone of broad scale mantle upwelling. Within the Society, Marquesas, Cook-Austral and Pitcairn-Gambier volcanic lineaments are some of the most extreme Sr, Nd, and Pb isotopic compositions measured in the ocean basins.

Age relationships

Each of the linear volcanic chains of French Polynesia is subparallel with other young intraplate Pacific island chains and each shows an age progression in volcanism, with the youngest activity at the southeastern end of the chain [Duncan and McDougall, 1974, 1976; McDougall and Duncan, 1980; Duncan and Clague, 1985]. Age progressive volcanism along an absolute plate motion vector is a distinguishing feature of volcanism resulting from a mantle-fixed hotspot supplied by a stationary, convective plume [Morgan, 1972].

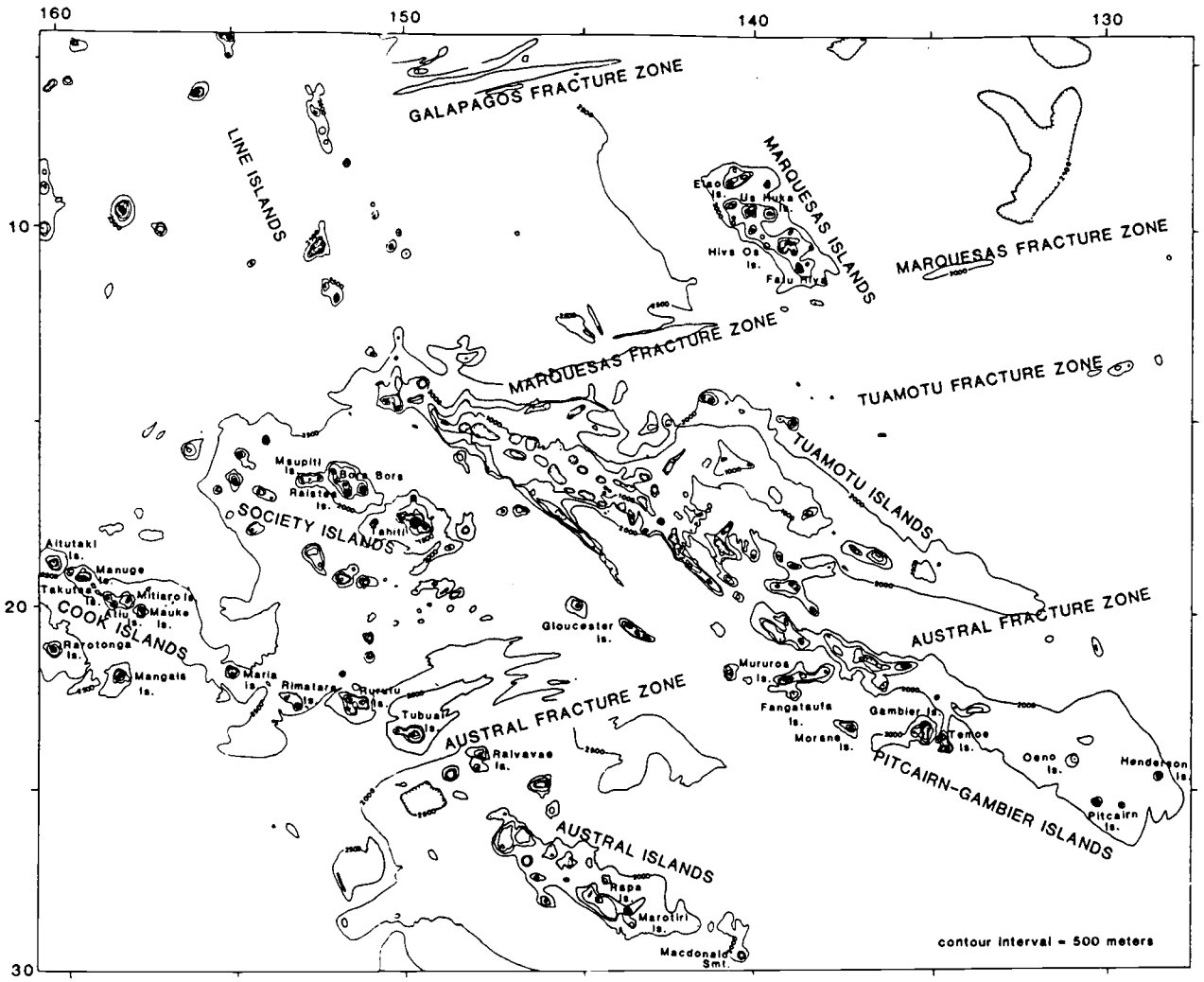

Figure III.1. Bathymetric map of linear volcanic chains and fracture zones of the south-central Pacific. After GEBCO Map 297, Centre National pour l'Exploitation des Oceans, Paris, 1973. Contour interval = 500 m.

The recognized duration of volcanism for the hotspots of French Polynesia is short relative to many other Pacific hotspots. Whereas volcanism at the Hawaiian and Louisville hotspots has continued for more than 65 m.y. [Jackson et al., 1972; Dalrymple et al., 1980; Lonsdale, 1988], the oldest measured ages for a volcano in the French Polynesian region is 19.3 Ma for Mangaia, an island in the Cook chain [Dalrymple et al., 1975; Turner and Jarrard, 1982]. The oldest ages measured from island lavas within the other lineaments is less than 7 Ma; submerged volcanoes to the west are presumably older.

It has been recently suggested that activity at the French Polynesian hotspots may be long-lived but intermittent. Two volcanoes in the Magellan seamounts (northwest Pacific) with ages 100 and 120 Ma exhibit the isotopic and depth anomalies expected for volcanoes located in French Polynesia. Backtracking of these seamounts places them over Rurutu and Rarotonga Islands, proposed as the locations of two hotspots within the Cook-Austral lineament [Smith et al., 1989]. Volcanism at ridges along the Galapagos Fracture Zone and the Nova-Canton trough has been proposed to have originated at 13 and 30 Ma respectively, as a result of volcanism over the Marquesas hotspot [McNutt et al., 1989]. A long broad swell, termed the Line-Cross trend, lies on the western extension of the Marquesas Islands and has allowed speculation that at least some of the central Line Islands formed above the Marquesas hotspot [Crough and Jarrard, 1981]. Three of the volcanoes, with ages between 38 and 60 Ma, show an age progression which could be related to volcanism along the Marquesas-Line trend [Schlanger et al., 1984].

Active volcanoes are found at the southeastern ends of three of the French Polynesian hotspot chains. Macdonald seamount, of the Austral chain, is currently active [Norris and Johnson, 1969], as are several seamounts near Mehetia in the Society Islands [Talandier and Okal, 1984; Cheminee et al., 1989], and seamounts southeast of

Pitcairn Island [P. Stoffers and C. Devey, pers. comm., 1990]. No active volcanism has been found in the Marquesas region [McNutt et al., 1989].

Mantle source compositions for hotspot-derived magmas

Geochemical studies of Sr, Nd, and Pb isotopic relationships on spreading ridge and ocean island basalts have led to the identification of 4 to 6 mantle components which can be visualized as endmember source compositions in oceanic volcanism [Zindler and Hart, 1986]. Volcanism resulting from partial melting of a source composed of depleted MORB-mantle (DMM), with low $^{87}Sr/^{86}Sr$, $^{206}Pb/^{204}Pb$ and high $^{143}Nd/^{144}Nd$, is observed at spreading ridge segments that are geographically separate from all hotspot activity. DMM is thought to be the residue left behind in the upper mantle after extraction of continental crust; it is the geochemical complement of continental crust.

HIMU component, named for its inferred, long-term, high μ (=U/Pb), exhibits high $^{206}Pb/^{204}Pb$ and $^{208}Pb/^{204}Pb$ but low $^{87}Sr/^{86}Sr$ values, is ubiquitously present in the convective mantle [Zindler and Hart, 1986]. Development of these isotopic compositions requires time integrated low Rb/Sr to produce the nonradiogenic $^{87}Sr/^{86}Sr$ with associated high U/Th and U/Pb for growth of $^{206}Pb/^{204}Pb$ and $^{208}Pb/^{204}Pb$ [Palacz and Saunders, 1986]. At some ocean islands, including Mangaia in the Cook Islands and Tubuai in the Austral Islands (Figure III.1), HIMU is the dominant melt component. At Mangaia and Tubuai, basalts are enriched in incompatible trace elements although trace element ratios (e.g. Rb/Ta and K/Ta) suggest that the magmas derived from a source more depleted than MORB. Smaller enrichments of radiogenic $^{206}Pb/^{204}Pb$ and $^{208}Pb/^{204}Pb$, without equivalent increases in radiogenic Sr, are found along some ridge segments, e.g. Indian Ocean MORB, or within some volcanic phases at ocean islands, e.g. the early tholeiitic basalt phase at Ua Pou in the Marquesas

[Duncan et al., 1986], suggesting that HIMU is present as a dispersed component in DMM-dominated mantle [Hart and Zindler, 1989]. These unusual isotopic compositions may have resulted from melting of previously subducted oceanic crust that was altered by seawater or mantle metasomatism, which enriched it in U, depleted it in Pb, and fractionated large-ion lithophile elements from the high field strength elements. During subduction the crust may have been preferentially stripped of volatile elements such as K and Rb. Ba, light-REE, and Pb may also have been lost, resulting in low K/Ta,Nb and La/Ta,Nb [Palacz and Saunders, 1986; Hart and Zindler, 1989].

Enriched mantle components, with relatively low (EM I) or relatively high (EM II) radiogenic Sr and variable radiogenic Pb, are tapped primarily in parts of the southern hemisphere. Chemical characteristics of EM I are those expected of recycled lower continental crust or metasomatized mantle, both associated with subduction processes [Hart and Zindler, 1989]. Based on its elevated $^{207}Pb/^{204}Pb$ values, EM II is thought to represent ancient continental material that was reincorporated into the mantle more than 3 billion years ago [Hart and Zindler, 1989]. High Rb/Sr, Th/U and Pb/U through time are necessary for development of the current isotopic ratios. This composition is also enriched in Pb, Rb, K, Th, and La relative to Nb and Ta by comparison with HIMU. The large ion lithophile enriched ancient sedimentary source that has resulted in mantle of EM II composition has remained isolated from the convecting depleted mantle for long periods of time.

A cluster of isotopic compositions, at approximately $^{87}Sr/^{86}Sr \sim 0.7033$ and $^{143}Nd/^{144}Nd \sim 0.5130$, are frequently found in basalts of ocean islands, continental regions and island arcs. Although mixing of mantle components such as EM I, EM II, HIMU, and DMM could produce melt of this isotopic composition, the wide-spread occurrence of this composition is evidence that it represents the prevalent composition of the mantle, PREMA. Like DMM, PREMA could also be a geochemical complement of

continental crust, the residue of separation of crustal material from the mantle over time; alternatively, PREMA could represent the initial product of differentiation of the silicate fraction of material from the metallic core very early in Earth history. PREMA is less depleted in radiogenic isotopic ratios than is DMM [Zindler and Hart, 1986].

French Polynesian basalts are extremely variable in their isotopic compositions. The quartz-normative tholeiites from Ua Pou in the Marquesas islands are the most depleted basalts in $^{87}Sr/^{86}Sr$ but are somewhat enriched in Pb-isotope ratios relative to MORB. The depleted mantle component that serves as the source of MORB volcanism (DMM) at spreading ridges may contribute to the Ua Pou tholeiites and other island and seamount basalts with non-radiogenic isotopic ratios within French Polynesia. The enrichment of these tholeiites in Pb-isotope ratios relative to MORB may be due to the incorporation of pods of HIMU component within the DMM matrix [Duncan et al., 1986; Hart and Zindler, 1989]. Basalts from the island of Mangaia have among the highest Pb-isotope ratios yet measured at an oceanic island; however, their Sr and Nd isotope ratios are relatively non-radiogenic [Palacz and Saunders, 1986; Nakamura and Tatsumoto, 1988]. Lavas from this island, along with Tubuai in the Austral Islands and St. Helena in the Indian Ocean, define the isotopic compositions of the HIMU endmember (Figure III.2) [Zindler and Hart, 1986].

Many of the islands of French Polynesia, helped to define the Dupal anomaly, a zone of high $^{87}Sr/^{86}Sr$ and moderately high $^{207}Pb/^{204}Pb$ and $^{208}Pb/^{204}Pb$ found between 0 and 45° S [Hart, 1984]. The anomaly results from melting of mantle with characteristics of one of the enriched mantle components (EM I and EM II) [Hart and Zindler, 1989]. Lavas comprising the shield of Pitcairn Island, for example, are partial melts of mantle with an EM I signature (Figure III.2) [Woodhead and McCulloch, 1989]. The other enriched mantle component, EM II, has been tapped by lavas from the Marquesas and Society Islands in French Polynesia and Kerguelen and others in the

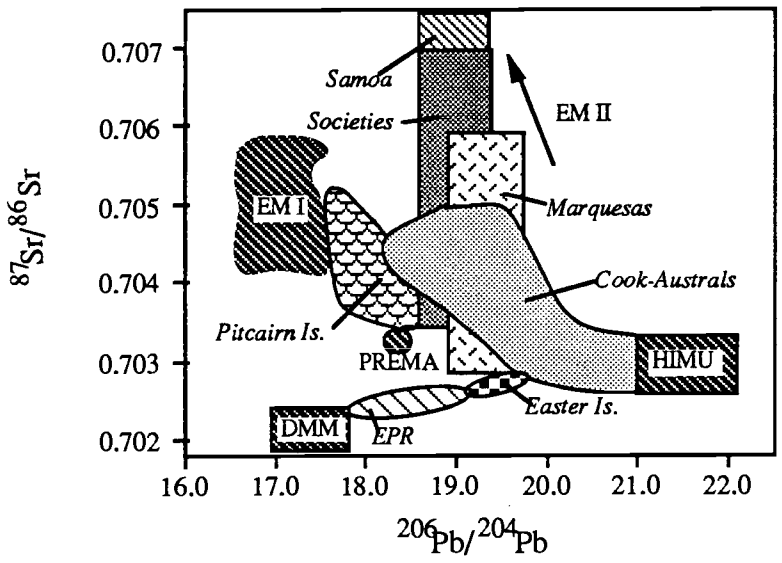

Figure III.2. $^{87}Sr/^{86}Sr$ versus $^{206}Pb/^{204}Pb$ for South Pacific basalts. Isotopic ratios for basalt suites from the East Pacific Rise (EPR), Easter Island, and the islands of French Polynesia with mantle components after Zindler and Hart [1986]. Data sources are as follows: EPR [White et al., 1987]; Easter Island[White and Hofmann, 1982]; Societiy Islands [White and Hofmann, 1982; Cheng et al., 1987a; Devey et al., 1990]; Marquesas Islands [Vidal et al., 1984; Duncan et al., 1986; Dupuy et al., 1987; this study]; Cook and Austral Islands [Palacz and Saunders, 1986; Nakamura and Tatsumoto, 1988]; Pitcairn Island [Woodhead and McCulloch, 1989]; and the Samoan Islands [Wright and White, 1986]; after Hart and Zindler [1989].

Atlantic and Indian Oceans [Zindler and Hart, 1986]. Nowhere other than in French Polynesia is such diversity seen within a single physiographic province in the ocean basins.

South Pacific Superswell and Dupal anomaly

A broad area of the south-central Pacific, including French Polynesia, is characterized by anomalous geophysical properties. Seafloor depths are 250-750 m shallower than lithosphere of the same age in the North Pacific and North Atlantic [McNutt and Fischer, 1987]. Lithosphere in this region follows the predicted thermal subsidence curve for a 75 km thick plate, whereas to the north of this anomalous zone the lithosphere behaves as a 125 km thick plate [McNutt and Menard, 1978; Calmant and Cazenave, 1987]. This region also has anomalously low upper mantle seismic velocities [Nishimura and Forsyth, 1985]. A high density of volcanoes, some composed of basalts with highly radiogenic isotope ratios are also features of this region. Broad-scale upwelling of warm material from the deep mantle, as imaged by seismic tomography [Dziewonski and Woodhouse, 1987], has probably thinned the lithosphere and allowed its penetration by hotspots. This region of anomalous geophysical and geochemical features has been named the South Pacific Superswell by McNutt and Fischer [1987].

The hotspots of French Polynesia helped to define part of a globe-encircling region of anomalous mantle composition centered around 30° S, termed the Dupal anomaly [Hart, 1984]. Melting of this large-scale (>1000 km) heterogeneous mantle results in some basalts with elevated $^{87}Sr/^{86}Sr$, $^{207}Pb/^{206}Pb$ and $^{208}Pb/^{204}Pb$. Recent investigations of the extent of this geochemical province have revealed that lavas of the East Pacific Rise do not show Dupal signatures [White et al., 1987], but enriched

radiogenic Pb isotope signatures are found at Indian Ocean spreading ridges. Duncan et al. [1986] noticed that tholeiitic basalts found at Ua Pou in the Marquesas Islands did not share the Dupal Sr isotope signature with their alkalic counterparts although they are enriched in $^{206}Pb/^{204}Pb$ relative to MORB. They suggested that perhaps the geochemical anomaly would not be such a striking feature if tholeiitic basalts were found in other French Polynesian volcanic chains [Duncan et al., 1986].

Geochemical variability within Pacific hotspot volcanic chains

Recent detailed studies of hotspot volcanic chains have revealed geochemical variations on a number of scales. The Dupal anomaly belt separates hotspots of French Polynesia, which have high radiogenic isotopic ratios from other nearby hotspots with more moderate radiogenic isotopic ratios, such as Louisville, only 2000 km to the south [Cheng et al., 1987b]. In the group of young volcanoes of the Societies chain, southeast of Tahiti , an isotopic gradient in $^{87}Sr/^{86}Sr$ is found from north to south with values of 0.7060 at Rockard seamount to the north, decreasing to values of 0.7031 at Moua Pihaa to the south. At least in the younger members of the Society lineament, isotopic composition is related to position above the hotspot [Devey et al., 1990]. On the island of Ua Pou in the Marquesas archipelago, tholeiitic basalts predate alkalic basalts by $\geq$ 1.5 Ma, yet tholeiitic and alkalic basalts show nearly the variation in Sr-isotopic ratios that is found in hotspot lavas globally. Duncan et al. [1986] suggested that the composition of the eruptive products at Ua Pou was related to position of the volcano above a compositionally segregated hotspot.

In this paper we report new ^{40}Ar-^{39}Ar and K-Ar age determinations from eight dredge hauls and from the island of Fatu Hiva in the Marquesas lineament which fit with the age progression previously established by island studies. Major and trace element

contents are consistent with fractional crystallization of two parental compositions, one tholeiitic/transitional and another alkalic. Isotopic ratios identify the parental mantle compositions as having DMM + HIMU and EM II signatures in Zindler and Hart [1986] terminology. We discuss these data in terms of possible dynamic models of mantle plume and asthenosphere mixing.

MARQUESAS ISLANDS AND SWELL

The Marquesas lineament includes 12 islands and at least 8 seamounts, that extend for nearly 500 km between the Marquesas and Galapagos Fracture Zones (Figure III.3). Volcanic cones rise up to 5000 m from 50-65 m.y. old oceanic lithosphere [Kruse, 1988] that formed at the Galapagos Rise, predecessor to the East Pacific Rise spreading boundary.

Age relationships

Previous results of K-Ar age determinations from the Marquesas [Duncan and McDougall, 1974; Duncan et al., 1986] have shown a southeastward migration of volcanism along the Marquesas chain from 5.8 Ma at Eiao [Barsczus, pers. comm., 1988] through 1.3 Ma at Fatu Hiva [McDougall and Duncan, 1980]. The resultant volcanic migration rate of 104 $\pm$ 18 km/my [McDougall and Duncan, 1980] closely matches those calculated for other French Polynesian volcanic chains: 107 $\pm$ 6 km/my for the Australs Islands, 109 $\pm$ 10 km/my for the Society Islands and 128 $\pm$ 92 km/my for the Pitcairn-Gambier Islands [McDougall and Duncan, 1980]. Differences in these rates may reflect minor differences in the angular distance of the lineaments from the rotation pole.

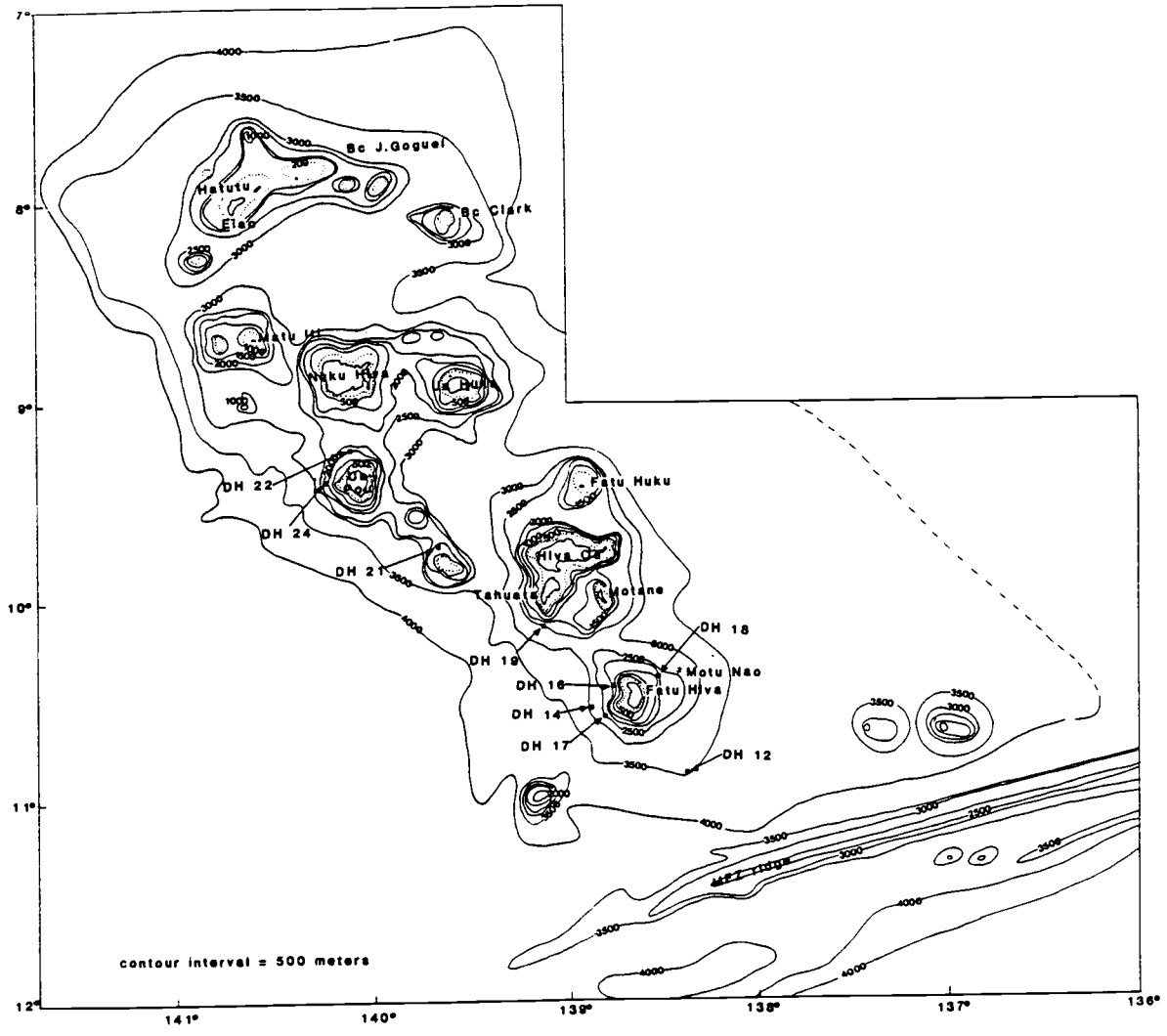

Figure III.3. Bathymetric map of the Marquesas lineament. Arrows indicate locations of dredge hauls; after GEBCO Map 297, Centre National pour l'Exploitation des Oceans, Paris, 1973. Contour interval = 500 m, dotted line = 200 m.

Although the current location of the Marquesas hotspot is unknown, McNutt et al. [1989] have proposed that the most recent expression of its volcanism is found in the Marquesas Fracture Zone (MFZ). The Marquesas Fracture Zone ridge (MFZ ridge) is a presumed volcanic feature 20 km wide, 1.5 km high and at least 350 km long, with northern and southern scarps that dip between 11° and 14°. The sediment free summit is dotted with small cones. Although thermal disturbance of the lithosphere by the Marquesas hotspot has caused a distinct swell to the north of the MFZ, no thermal effects on seafloor south of the MFZ have been found [McNutt et al., 1989]. These observations serve as evidence that the MFZ ridge is the most recent expression of the Marquesas hotspot [McNutt et al., 1989]. No samples have been collected from the MFZ ridge to test this prediction.

At several French Polynesian volcanoes the duration of volcanism seen at a single edifice has been found to be unusually long compared with the duration measured at other hotspot locations, although the sequence of volcanic events parallels those seen at the Hawaiian hotspot. For example, a 10 m.y. hiatus separates eruption of the early shield-building phase and a minor alkalic phase on the island of Rurutu, in the Austral chain [Duncan and McDougall, 1976; Turner and Jarrard, 1982]. Recently, Duncan et al. [1986] discovered that the 3.8 m.y. history of volcanism at Ua Pou followed a sequence similar to that at Hawaii as well. Shield lavas exposed in stream valleys, road cuts and wave cut cliffs around the perimeter of Ua Pou represent a tholeiitic basalt phase of volcanism which took place from 5.6 to 4.5 Ma. Volcanism began again after a 1.6 m.y. hiatus, with eruption of alkali basalts from 2.9 to 2.7 Ma and finally more evolved lavas, such as trachytes and phonolites, from 2.5 to 1.8 Ma [Duncan et al., 1986].

Geophysical characteristics

Although the Marquesas lineament trends northwest-southeast, as do all hotspot generated volcanic features of the Pacific Basin, the orientation of the volcanic chain deviates 20-30° from the trends of the other large hotspot lineaments on the Pacific plate [Crough and Jarrard, 1981]. This deviation, coupled with the intermittent nature of the volcanism in the Marquesas region, has caused some researchers to suggest that the Marquesas hotspot has moved at a rate of up to 20 mm/yr relative to other Pacific hotspots [Crough and Jarrard, 1981] or that Marquesas volcanism is actually controlled by a "hot line" rather than a hotspot [Turner and Jarrard, 1982]. A change in the direction of plate motion at 5 Ma [Pollitz, 1988] could also account for the orientation of the Marquesas volcanism. Alternatively, McNutt et al. [1989] proposed that the Marquesas hotspot is a fixed mantle plume that is simply too weak to penetrate the old, thick oceanic lithosphere found north of the MFZ except where there is a conduit to the surface. They suggested that a lithospheric weakness, such as a fracture zone, exists between the Galapagos fracture zone and MFZ and that volcanism from the mantle plume is found only along that lineation [McNutt et al., 1989]. The shortness of the Marquesas chain relative to other Pacific hotspot lineaments, then, could be the result of a 275 km wide plume being intersected by the lithospheric weakness for only a 500 km distance [McNutt et al., 1989].

The age of the lithosphere decreases abruptly across the MFZ from ~63 Ma to the south to ~49 Ma to the north possibly due to a ridge jump at ~49 Ma [Kruse, 1988]. Geoid height and gravity data indicate that oceanic lithosphere beneath the Marquesas swell has been thinned relative to normal lithosphere of the same age [Fischer et al., 1986] by the Marquesas hotspot. The northern boundary of the South Pacific Superswell, as defined by McNutt and Fischer [1987], is the Marquesas Fracture Zone,

thus excluding the Marquesas from the superswell region. Although a large swell resulting from thermal input of the Marquesas hotspot has been superimposed on the oceanic lithosphere, they suggest that lack of a depth anomaly and normal elastic plate thickness surrounding the Marquesas swell are more typical of the effects of a hotspot on normal oceanic lithosphere and that there is no evidence for anomalous lithospheric characteristics in the Marquesas region. Smith et al. [1989], however, interpret reduced elastic plate thickness and isotopic anomalies to include the Marquesas in their South Pacific Isotopic and Thermal Anomaly (SOPITA). Clearly, the Marquesas are similar to nearby superswell volcanoes in their isotopic compositions and are a part of the south-central Pacific geochemically anomalous region. The term SOPITA will be used here to include the Marquesas.

Geochemical compositions

Basalts sampled from the Marquesas Islands range in composition from tholeiitic to alkalic, including compositions as evolved as trachytic and phonolitic [Bishop and Woolley, 1973; Liotard et al., 1986; Duncan et al., 1986]. Although quartz normative tholeiitic basalts (~1% quartz) are found on the island of Ua Pou [Liotard et al., 1986], most tholeiitic basalts from the Marquesas have olivine-normative compositions [Liotard et al., 1986]. The tholeiitic basalts can be distinguished from alkalic basalts by lower rare-earth element (REE) concentrations especially in the light-REEs and by lower total incompatible element concentrations and ratios [Liotard et al., 1986]. Isotopic composition does not uniformly correlate with major and trace element composition. In general, however, alkali basalts are enriched in $^{87}Sr/^{86}Sr$ and moderately enriched in radiogenic Pb, indicating that they were derived from sources enriched in radiogenic isotopes and tholeiitic/transitional basalts are depleted in $^{87}Sr/^{86}Sr$ and variable in

radiogenic Pb, indicating derivation from depleted mantle sources with variable Pb isotope ratios [Dupuy et al., 1987].

SAMPLES AND ANALYTICAL METHODS

Basalt samples used in this study were dredged in March and April of 1987 by the R/V Thomas Washington (expedition Crossgrain [CRGN 02]). The objectives of the program were two-fold: to study the thermo-mechanical properties of the lithosphere underlying the Marquesas lineament and to determine the chemical composition of the submarine portions of the volcanoes. A portion of the results of Seabeam swath mapping, a single channel seismic acquisition system, and gravity and magnetic surveys were reported in McNutt et al. [1989].

In this paper we report analyses of rocks recovered on nine dredge hauls of seamounts, banks, and the submarine portions of islands from CRGN 02. Dredge locations from which basaltic rocks were recovered are shown in Figure III.3 and descriptions of the dredge targets are given in Table III.1. Previous studies of Marquesan volcanism have relied solely on samples from the emergent portions of the volcanoes which represent less than 2% of the mass of any edifice.

The dredge hauls contained the same rock types found on the islands: olivine tholeiite, transitional basalt, and alkali basalt (including mugearite and basanite). Most of the dredge hauls collected rocks very similar to each other in composition. For example, nearly identical ages and compositons from all analyzed samples from DH 12 provide evidence that only one flow sequence was sampled. A few dredge hauls contained a greater number of rock types. The most diverse haul, DH 19, from the side of the island of Tahuata, returned olivine tholeiites (19-1, 19-2), transitional basalts (19-

Table III.1. Location and Description of CRGN 02 Dredge Hauls in Which Basaltic Rocks Were Recovered.

Station	Lat. (S)	Long. (W)	Depth (m)	Feature
DH 12	10°49.1'	138°25.9'	2985-3136	small smt group 50 km SE of Fatu Hiva
DH 14	10°32.3'	138°50.8'	2442-2077	upper fault scarp SW of Fatu Hiva
DH 16	10°26.0'	138°45.8'	2307-1936	base N-S fault scarp N flank of Fatu Hiva
DH 17	10°31.5'	138°48.7'	2437-2348	upper fault scarp SW of Fatu Hiva
DH 18	10°23.8'	138°32.2'	1992-1758	SW rift zone of Motu Nao
DH 19	10°05.9'	139°08.8'	1936-1717	flank of N-S ridge 6 km S of Tahuata
DH 21	9°39.6'	139°43.7'	2524-2296	W flank Dumont D'Urville Nord rift zone
DH 22	9°13.6'	140°07.6'	2036-1692	small cone at change in slope N Ua Pou
DH 24	9°25.2'	140°14.6'	2780-2006	rift zone on steep slope W of Ua Pou

3, 19-11), and basanites (19-8). The diversity of compositions from this sample site is similar to that of the island of Ua Pou.

Samples used for age determinations and compositional analyses were the freshest available, with only slight to moderate alteration and little or no interstitial glass. All CRGN 02 samples, except the mugearites, are highly vesicular, indicating that the magmas degassed as they cooled and were erupted at shallow depth or that they had high ascent rates and retained gas upon cooling [Dixon et al., 1988]. Tholeiitic basalts include olivine (some embayed) and abundant clinopyroxene phenocrysts. Fe-Ti oxides, clinopyroxene, and small amounts of interstitial glass are found in the groundmass. Transitional basalts are similar to olivine tholeiites but include small laths of groundmass plagioclase. Abundant embayed olivine crystals are found as phenocrysts and in the groundmass of alkali olivine basalts. Augitic clinopyroxene is abundant as well. The basanites are fine-grained with abundant olivine, clinopyroxene, and plagioclase phenocrysts and microphenocrysts; some also include nepheline. Mugearites contain fine-grained plagioclase laths and minor clinopyroxene, Fe-Ti oxides, and nepheline in a trachytic matrix.

Age determinations by ^{40}Ar-^{39}Ar incremental heating and total fusion experiments [e.g., McDougall and Harrison, 1988] and conventional K-Ar radiometric dating methods [Dalrymple and Lanphere, 1969] were performed on 23 fresh basalt samples from the CRGN 02 dredge collection and six samples from the island of Fatu Hiva. Sample preparation and analysis of samples by K-Ar and ^{40}Ar-^{39}Ar total fusion methods followed the techniques outlined in Desonie and Duncan [1990]. Experimental methods for ^{40}Ar-^{39}Ar incremental heating are described in Duncan and Hargraves [1990]. Analytical data and age calculations from the K-Ar and ^{40}Ar-^{39}Ar total fusion and incremental heating experiments are given in Tables III.2 and III.3. Air measurements to determine the mass discrimination factor, critical to correction for

Table III.2. K-Ar and ^{40}Ar-^{39}Ar Total Fusion Ages For Basalts From CRGN 02 and the Island of Fatu Hiva, Marquesas Swell.

Sample No.	% K	^{40}Ar radiogenic ($x10^{-8}$ mol/g)	$\%^{40}Ar$	Age $\pm$ 1 σ (Ma)
CRGN 02				
DH 12-1	2.11	3.176	4.4	0.39 $\pm$ 0.04
DH 12-10	[n.d.]		4.3	0.35 $\pm$ 0.04
	[2.02]		4.5	0.45 $\pm$ 0.10
DH 12-11	[2.07]		5.2	0.48 $\pm$ 0.10
DH 17-1	1.49	4.877	18.7	0.84 $\pm$ 0.03
DH 17-2	[1.14]		9.4	1.31 $\pm$ 0.12
DH 18-26	[0.71]		4.1	0.74 $\pm$ 0.12
DH 18-40	[n.d.]			1.27 $\pm$ 0.03
DH 19-1	0.73	4.448	6.9	1.57 $\pm$ 0.05
	[n.d.]			1.58 $\pm$ 0.08
DH 19-8	2.31	15.777	26.1	1.76 $\pm$ 0.10
DH 21-8	[1.12]		11.4	3.13 $\pm$ 0.14
DH 21-14	[n.d.]			2.81 $\pm$ 0.04
DH 22-1	1.54	14.966	32.8	2.49 $\pm$ 0.04
DH 24-4	2.57	29.567	27.4	2.97 $\pm$ 0.04
DH 24-7	2.62	30.151	31.9	2.96 $\pm$ 0.03
DH 24-8	[n.d.]		7.8	2.45 $\pm$ 0.14
Fatu Hiva				
FT 01-02	0.95	4.350	6.6	1.18 $\pm$ 0.06
FT 01-23	1.41	9.996	5.2	1.84 $\pm$ 0.14
FT 01-39	1.47	8.157	5.5	1.43 $\pm$ 0.05
FT 01-42	1.47	7.157	17.5	1.24 $\pm$ 0.02
FT 01-61	1.02	7.606	7.1	1.91 $\pm$ 0.09
FT 01-65	1.07	7.310	5.7	1.76 + 0.12

Ages calculated using the following decay and abundance constants: $\lambda_\varepsilon = 0.581x10^{-10}$ yr^{-1}; $\lambda_\beta = 4.963x10^{-10}$ yr^{-1}; $^{40}K/K = 1.167x10^{-4}$ mol/mol.

% K determined by atomic absorption spectrophotometry, or calculated from measured ^{39}Ar (in brackets; n.d. = not determined).spectra and inverse isochron correlation diagrams for incremental heating experiments are shown in the appendix.

Table III.3. ^{40}Ar-^{39}Ar Plateau and Isochron Ages From CRGN 02 Basalts.

Sample Number	Plateau Age ± 1 σ (Ma) wgt by $1/\sigma^2$	wgt by $\%^{39}Ar$	^{39}Ar (% of total)	Integrated Age (Ma)	Corrchron Age + 1σ (Ma)	N	SUMS (N-2)	$^{40}Ar/^{36}Ar$ intercept
DH 12-17	0.76 ± 0.10	0.76 ± 0.24	100.0	0.76	0.60 ± 0.05	6	0.3	295.6 ± 2.4
DH 16-1	1.31 ± 0.04	1.28 ± 0.13	94.7	1.22	1.22 ± 0.03	4	0.0	296.5 ± 0.7
DH 17-1	1.70 + 0.07	1.60 ± 0.20	87.0	1.73	1.54 ± 0.37	5	0.8	283.4 ± 9.9
DH 17-5	1.69 ± 0.11	1.60 ± 0.38	100.0	1.60	1.25 ± 1.52	6	3.1	298.1 ± 11.0
DH 18-13	1.27 ± 0.10	1.29 ± 0.20	67.0	1.92	2.28 ± 0.36	4	1.0	286.2 ± 2.5
DH 19-2	1.74 ± 0.08	1.58 ± 0.23	96.2	1.58	1.85 ± 0.12	3	0.7	291.6 ± 0.5
DH 19-3	1.97 ± 0.12	1.86 ± 0.19	99.4	1.82	-	2	-	-
DH 19-8	1.87 ± 0.00	1.83 ± 0.06	99.4	1.82	1.75 ± 0.18	5	2.4	293.4 ± 2.8
DH 19-11	none developed		_	1.60	-	-	-	-
DH 21-14	2.63 + 0.19	2.60 ± 0.28	73.8	2.61	-	2	-	-
DH 22-1	2.69 ± 0.07	2.69 ± 0.24	92.3	2.87	-	2	-	-
DH 22-2	3.50 ± 0.08	3.43 ± 0.16	75.2	3.85	3.57 + 0.12	3	0.2	280.9 ± 4.4
DH 24-4	3.24 ± 0.09	3.36 ± 0.20	81.8	3.12	3.17 + 0.14	5	1.0	290.1 ± 4.4
DH 24-7	3.28 ± 0.07	3.27 ± 0.17	94.6	3.23	3.03 + 0.20	5	0.4	296.1 ± 11.9

corrected for ^{37}Ar decay since irradiation, half-life = 35.1 days

Ages calculated using the following decay and abundance constants: $\lambda_\varepsilon = 0.581 \times 10^{-10}\ yr^{-1}$; $\lambda_\beta = 4.963 \times 10^{-10}\ yr^{-1}$;

$^{40}K/K = 1.167 \times 10^{-4}$ mol/mol.

Neutron flux monitored with hornblende standard MMhb-1.

atmospheric argon, were performed after each two sample runs for total fusion analyses and between each stepwise heating experiment.

Because of the potential for potassium addition and argon loss in seawater, K-Ar analyses provide only a minimum age. ^{40}Ar-^{39}Ar incremental heating experiments can provide a reliable crystallization age if a plateau is formed and appropriate statistical criteria are met. For a plateau to be defined, two contiguous steps with age calculations within one sigma error and representing at least 50% of the ^{39}Ar released were required. If more than two steps were used in the calculation an inverse isochron age was also calculated. The atmospheric $^{40}Ar/^{36}Ar$ intercept in each of these calculations shows no evidence for excess argon. Plateau and inverse isochron diagrams are shown in the appendix. Because of the expected young ages and only moderate potassium contents in some of these lavas, ^{40}Ar-^{39}Ar total fusion experiments were done on some dredged samples.

Major and trace element analyses of the dredged basalts were carried out by X-ray fluorescence spectroscopy (XRF) using fused glass disks by the technique of Hooper [1981]. Rare earth element (REE) and Hf concentrations were determined by instrumental neutron activation analysis (INAA) using Laul [1979]. Five basalt fragments (14-1, 16-1, 16-2, 16-3, and 19-11), too small for analysis by XRF, were powdered, fused under controlled atmosphere (QFM) and analysed for major elements by a Cameca SX-50 electron microprobe at Oregon State University. For analyses of radiogenic isotope ratios, 0.5 to 1.0 mm chips of all samples were leached in warm 6 N HCl for two hours to eliminate effects of seawater alteration. Sr, Nd, and Pb concentrates were then obtained from dissolved powders by ion exchange and isotopic ratios were measured on a VG Sector thermal ionization mass spectrometer at Cornell University, following the procedure of White et al. [1990].

RESULTS AND DISCUSSION

Age determinations

Figure III.4 shows the variation in age of 11 islands and 8 dredge sites with distance along the lineament, measured from DH 12. Samples from CRGN 02 expand the age range previously seen at some volcanoes. Because the current location of the Marquesas hotspot relative to the Pacific plate is unknown, we use the location of DH 12 as the youngest point in the Marquesas lineament for plate motion calculations. DH 12 is the most southeasterly location from which Marquesan basalts have been recovered; the age of basalts from these seamounts is younger than those from Fatu Hiva. Distances from DH 12 were measured in the direction of the Pacific plate absolute motion vector (~N 70° W).

Because volcanism at a single volcano can last for at least 3.8 m.y. in the Marquesas [Duncan et al., 1986], we have calculated the rate of plate motion over the Marquesas hotspot in three ways. For all calculations, the most reliable age determinations available (^{40}Ar-^{39}Ar total fusion or incremental heating for submerged basalts, K-Ar for island samples) were used in a least-squares linear regression. In one regression analysis, the oldest age from each island and dredge location was used. In another analysis, only basalts known to be of tholeiitic or transitional composition were used. Regression rates for both of these methods, which we take to estimate the time when the volcano was located over the center of the hotspot, were virtually the same at 70 $\pm$ 4 km/my and 72 $\pm$ 6 km/my, respectively. The better estimate was for all tholeiitic and transitional basalts which had a correlation coefficient of 0.94. These estimates are low relative to those calculated for average ages of all samples for which age determinations have been performed. A third regression of all 70 age determinations [Duncan and

Figure III.4. Basalt age versus distance from DH 12 for seamounts and islands of the Marquesas lineament. Distances from DH 12 were measured in the direction of absolute motion of the Pacific plate, ~N 70° W. Data for basalts from CRGN 02 and the island of Fatu Hiva from this study are represented by squares, circles represent data from Duncan and McDougall [1974] and Duncan et al. [1986], the diamond represents ages for the islands of Hatutu, Eiao, and Bc J.Goguel from Hans Barsczus [pers. comm., 1988]. Filled symbols represent rocks analyzed by the ^{40}Ar-^{39}Ar incremental heating technique for which a plateau age was calculated. Open symbols represent data generated by ^{40}Ar-^{39}Ar or K-Ar total fusion experiments. Error bars are given for CRGN 02 analyses. Two least-squares regression lines are pictured: one with a slope of 70 ± 4 km/my calculated from oldest ages and one with a slope of 108 ± 2 km/my calculated from all available Marquesas age determinations. A third regression line for all tholeiitic and transitional basalt samples for which ages have been determined, with slope 72 ± 2 km/my, is not pictured.

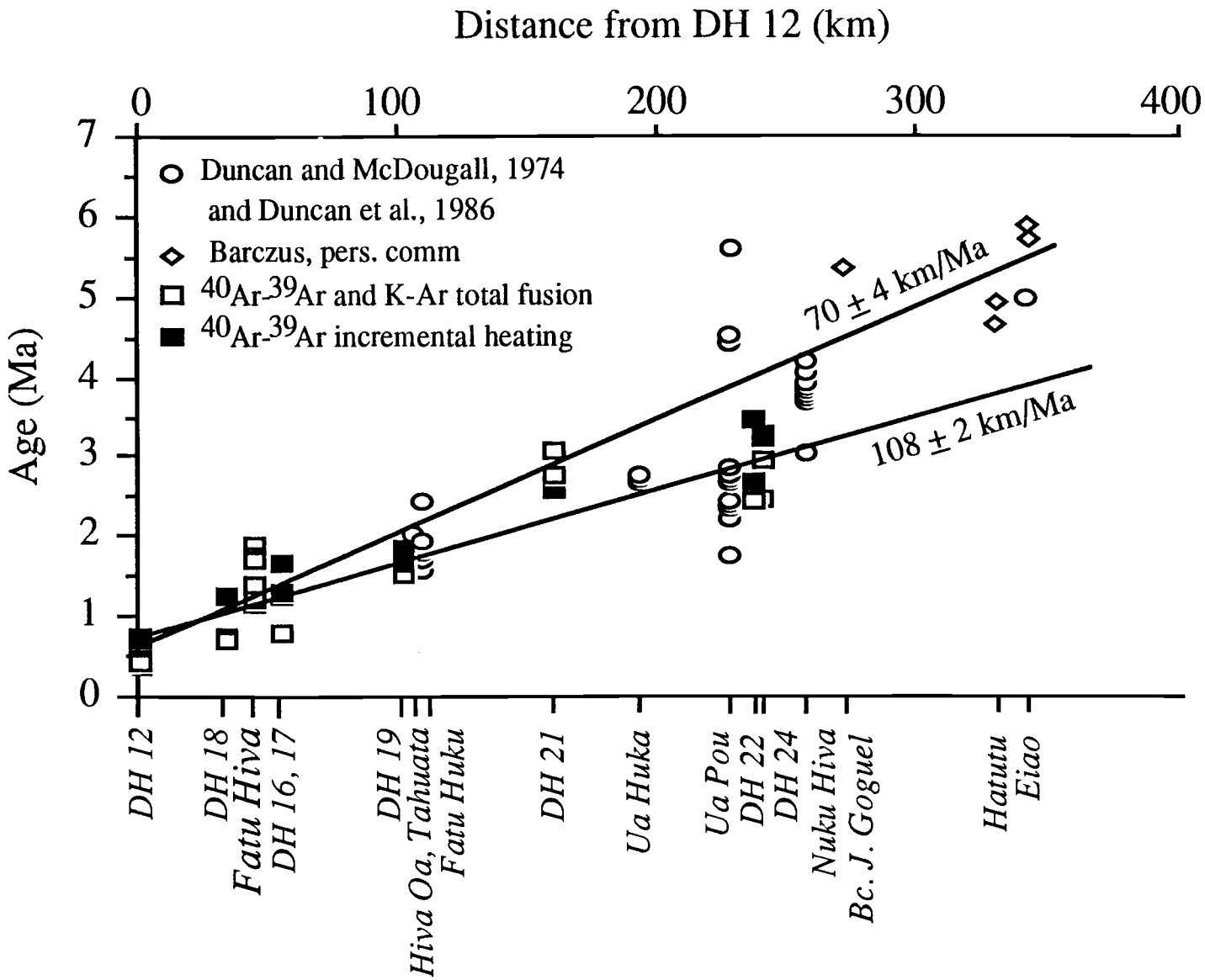
Distance from DH 12 (km)
0
100
200
300
400
Age (Ma)
0
1
2
3
4
5
6
7
Duncan and McDougall, 1974
and Duncan et al., 1986
Barczus, pers. comm
40Ar-39Ar and K-Ar total fusion
40Ar-39Ar incremental heating
70 ± 4 km/Ma
108 ± 2 km/Ma
DH 12
DH 18
Fatu Hiva
DH 16, 17
DH 19
Hiva Oa, Tahuata
Fatu Huku
DH 21
Ua Huka
Ua Pou
DH 22
DH 24
Nuku Hiva
Bc. J. Goguel
Hatutu
Eiao

McDougall, 1974; Duncan et al., 1986; Hans Barsczus, pers. comm., 1988; this study] leads to a rate of 113 ± 8 km/my. This rate is virtually the same as the rate of 104 ± 18 km/my calculated by McDougall and Duncan [1980] and is comparable to plate motion rates calculated for other French Polynesian chains [McDougall and Duncan, 1980]. Both regression lines were extrapolated to zero age to determine the current location of the Marquesas hotspot. For the regression rate calculated for the tholeiitic/transitional basalts the current hotspot location is 43 km southeast of DH 12. For the rate calculated for all Marquesan basalts the current hotspot location is 85 km southeast of DH 12. The MFZ ridge is thought by McNutt et al. [1989] to be the current location of the Marquesas hotspot and it is within the range of locations possible for the hotspot.

DH 19 is the only dredge haul that contains representatives of tholeiitic, transitional, and alkalic magmatic types. Lack of stratigraphic information from dredge sampling does not allow relative position of the three compositional phases of volcanism to be known. Ages of each of the three phases of volcanism can be compared with the sequence found on Ua Pou where tholeiitic shield lavas predate alkalic cap rocks [Duncan et al., 1986]. The youngest sample from DH 19 is tholeiitic (19-1: 1.58 ± 0.08 Ma, 19-2: 1.70 ± 0.08 Ma), but the age is similar to ages from transitional (19-3: 1.97 ± 0.12 Ma) and alkalic (19-8: 1.87 ± 0.03 Ma) basalts. Although at Ua Pou a distinct age versus compositional relationship is seen, samples from DH 19 show that the two compositional types sometimes overlap each other in time.

During the CRGN 02 expedition samples were collected from the emergent portion of the island of Fatu Hiva. Age determinations, performed by K-Ar methods, expand the age range previously seen at that edifice and are included in Table III.2. Compositional analyses have yet to be performed on this sample suite [Kevin Johnson, pers. comm., 1990].

Chemical compositions

Although tholeiitic, transitional, and alkalic basalts are represented in the CRGN 02 sample suite (Tables III.4 and III.5), highly alkalic rocks (>30% normative nepheline), which are abundant among subaerial samples, were not recovered. Among the dredge hauls five rock types can be distinguished on the basis of petrography, modal mineralogy, bulk rock major and trace element chemistry, and normative mineralogy. Although specific criteria were defined only for CRGN lavas, the rock groupings are generally coincident with those of other ocean islands, i.e. Hawaii. Subalkaline basalts fall into two groups: olivine tholeiites (>10% normative hypersthene, ~3% total alkalies) and transitional basalts (<10% normative hypersthene, 3.5-4.5% total alkalies). All other samples contain normative nepheline: alkali basalts (<2% normative nepheline, moderate alkalies and SiO_2), mugearites (<5% normative nepheline, >51% SiO_2, ~8% alkalies) and basanites (>10% normative nepheline, <45% SiO_2). Although none of these criteria alone are sufficient to identify all basalts by rock type, normative nepheline and feldspar proportions provide the most concise groupings for dredge samples (Figure III.5).

The distribution of basalt compositions along the lineament gives an indication of the structure of a Marquesan volcano. Only tholeiitic basalts are found on the northwesternmost island of Eiao, where the capping alkali basalt, if it existed, has presumably been eroded away [Liotard et al., 1986]. Tholeiitic basalts have also been collected from the exposed shield areas that underlie the alkalic capping lavas of the central islands of Ua Pou [Liotard et al., 1986] and Nuku Hiva [Duncan, 1975]. In dredge hauls on the younger volcanoes of Tahuata (DH 19) and Fatu Hiva (DH 16), tholeiites have been recovered where only alkalic basalts have been found subaerially (Figure III.3). Transitional basalts are often found with tholeiitic basalt lavas within the

Table III.4. Major Element Analyses and CIPW-Normative Compositions for CRGN 02 Basalts.

	12-1	12-6	12-10	12-11	12-12	12-17	14-1	16-1	16-2	16-3	17-1	17-2	17-5	18-13
SiO_2	51.73	51.53	51.64	51.67	51.60	51.23	48.49	49.10	48.90	48.17	46.37	43.57	46.36	51.21
TiO_2	2.26	2.20	2.27	2.27	2.27	2.26	3.84	1.97	3.78	4.14	3.87	3.66	3.85	2.21
Al_2O_3	17.44	17.48	17.56	17.51	17.68	17.41	14.67	13.26	14.44	14.69	12.31	11.28	12.25	17.28
FeO	8.29	8.16	8.30	8.24	8.25	8.20	10.23	9.63	8.95	9.97	10.31	9.88	8.13	8.13
Fe_2O_3	1.38	1.36	1.38	1.37	1.38	1.37	1.53	1.44	1.34	1.50	1.72	1.65	1.36	1.36
MnO	0.20	0.20	0.20	0.20	0.20	0.20	0.15	0.14	0.12	0.16	0.16	0.16	0.16	0.22
MgO	2.84	2.93	2.52	2.77	2.89	2.89	6.54	11.16	7.57	5.73	9.63	9.59	9.99	2.91
CaO	7.19	7.01	7.20	7.19	7.17	7.17	8.79	10.01	9.90	10.17	9.53	8.98	9.50	7.00
Na_2O	4.98	4.74	5.23	4.98	4.92	4.97	3.18	2.42	2.72	2.82	2.53	2.33	2.57	4.92
K_2O	2.54	2.82	2.55	2.58	2.56	2.85	1.55	0.57	1.16	1.26	1.80	1.66	1.78	2.79
P_2O_5	1.28	1.25	1.32	1.29	1.29	1.29	0.69	0.21	0.41	0.50	0.53	0.50	0.53	1.27
Total	99.99	99.55	100.03	99.93	100.07	99.71	99.50	99.76	99.16	98.96	98.59	93.09	99.03	99.15
Mg#	38	39	39	37	38	39	50	65	48	57	62	63	60	39
CIPW-normative compositions														
or	15.01	16.67	15.07	15.25	15.13	16.87	9.16	3.37	6.86	7.45	10.64	9.82	10.52	16.49
ab	37.01	35.75	36.68	36.89	36.84	33.77	26.91	20.48	23.02	23.86	19.14	17.27	18.37	34.84
an	17.73	17.98	16.91	17.81	18.60	16.81	21.18	23.64	23.77	23.70	16.92	15.42	16.63	16.83
ne	2.78	2.36	4.10	2.85	2.60	4.53	0	0	0	0	1.23	1.32	1.83	3.68
lc	0	0	0	0	0	0	0	0	0	0	0	0	0	0
di	8.05	7.24	8.59	7.93	7.17	8.72	14.66	19.95	18.35	19.24	21.75	20.92	21.87	8.06
hy	0	0	0	0	0	0	6.00	11.79	11.84	9.02	0	0	0	0
ol	10.45	10.60	9.45	10.07	10.58	10.20	10.64	14.38	5.39	4.64	18.01	18.21	19.12	10.46
mt	1.83	1.97	2.00	1.99	2.00	1.81	2.22	2.09	1.94	2.17	2.49	2.18	2.13	1.79
il	4.29	4.18	4.31	4.31	4.31	4.30	7.29	3.74	7.18	7.86	7.35	6.95	7.31	4.20
ap	3.03	2.96	3.12	3.05	3.05	3.06	1.63	0.50	0.97	1.18	1.25	1.18	1.25	3.01
rock type	muge-arite	muge-arite	muge-arite	muge-arite	muge-arite	muge-arite	trans. basalt	olivine tholeiite	trans. basalt	trans. basalt	alklali basalt	basanite	alkali basalt	muge-arite

Table III.4. continued.

	18-26	18-40	19-1	19-2	19-3	19-8	19-11	21-8	21-14	22-1	22-2	22-3	24-4	24-7	24-8
SiO_2	47.92	47.40	48.25	48.34	47.48	45.07	48.33	48.68	47.59	43.43	42.88	43.43	44.58	44.35	44.29
TiO_2	3.76	3.37	2.93	2.91	3.19	3.73	3.82	3.57	4.09	3.46	3.31	3.33	3.37	3.42	3.38
Al_2O_3	12.23	13.06	12.02	11.81	11.30	13.74	14.74	15.50	15.30	12.92	12.57	12.81	15.12	15.04	15.47
FeO	10.15	9.96	10.47	10.08	9.91	10.92	10.01	10.38	11.39	11.26	11.48	11.55	10.41	10.56	10.21
Fe_2O_3	1.52	1.49	1.57	1.51	1.49	1.64	1.50	1.56	1.71	1.69	1.72	1.73	1.56	1.58	1.53
MnO	0.17	0.30	0.20	0.16	0.16	0.18	0.18	0.19	0.19	0.23	0.20	0.26	0.22	0.22	0.20
CaO	10.42	9.24	10.56	10.53	10.40	10.91	10.03	8.42	9.26	12.30	11.70	11.91	10.02	9.93	9.77
MgO	10.00	9.48	10.06	9.93	11.30	7.55	5.28	4.05	4.58	9.92	10.26	9.95	6:10	5.87	5.56
Na_2O	2.56	2.99	2.09	2.08	2.32	3.20	2.69	4.07	3.58	2.53	2.69	2.82	4.07	4.52	4.20
K_2O	1.22	1.77	0.88	0.95	1.19	2.78	1.95	1.75	1.37	1.86	1.93	1.96	3.09	3.16	3.25
P_2O_5	0.52	0.56	0.34	0.34	0.40	0.65	0.55	0.78	0.77	0.45	0.43	0.43	0.75	0.76	0.78
Total	100.32	99.47	99.21	98.49	98.99	100.20	98.92	98.79	99.66	99.88	99.00	100.00	99.14	99.26	98.50
Mg#	64	63	63	64	67	56	46	41	42	61	62	61	51	50	50
CIPW-normative compositions															
or	7.21	10.46	5.20	5.61	7.03	16.43	11.52	10.34	8.10	10.99	9.71	10.04	18.26	18.67	19.21
ab	21.66	20.76	17.69	17.60	19.63	4.14	22.76	31.35	29.28	0.04	0	0	3.08	1.32	2.68
an	18.28	16.99	20.82	20.08	16.91	14.92	22.39	18.86	21.63	18.40	16.52	16.51	13.86	11.42	13.76
ne	0	2.46	0	0	0	12.43	0	1.68	0.55	11.58	12.33	12.93	16.99	20.01	17.80
lc	0	0	0	00	0	0	0	0	0	0	1.33	1.21	0	0	0
di	24.25	20.41	23.81	24.26	25.86	28.58	19.57	14.84	16.03	32.24	31.46	32.37	25.46	27.09	24.41
hy	2.41	0	13.34	14.28	2.80	0	5.12	0	0	0	0	0	0	0	0
ol	16.10	18.68	9.88	8.30	17.97	12.92	7.01	11.04	12.22	16.73	18.04	17.30	11.25	10.36	10.34
mt	2.21	2.16	2.28	2.19	2.16	2.37	2.17	2.26	2.48	2.45	2.50	2.51	2.26	2.29	2.22
il	7.14	6.40	5.56	5.53	6.06	7.08	7.26	6.78	7.77	6.57	6.29	6.32	6.40	6.50	6.42
ap	1.23	1.33	0.80	0.80	0.95	1.54	1.30	1.85	1.82	1.07	1.02	1.02	1.78	1.80	1.85
rock type	trans. basalt	alkali basalt	olivine tholeiite	olivine tholeiite	trans. basalt	basanite	trans. basalt	alkali basalt	alkali basalt	basan-ite	basan-ite	basan-ite	basan-ite	basan-ite	basan-ite

Table III.5. Trace Element Analyses For Samples Dredged on CRGN 02. Data in the first set of columns are from XRF; data from the set of columns are from INAA.

	12-1	12-6	12-10	12-11	12-12	12-17	16-2	17-1	17-2	17-5	18-13	18-26	18-40
Ba	569	577	584	592	565	555		246	249	249	567	254	327
Cr	1	2	0	0	1	0	34	376	390	391	0	537	380
Cu	14	17	36	20	14	6		66	65	71	0	79	46
Ga	20	24	27	22	23	24		23	21	23	22	24	22
Nb	112	113	114	110	114	114		64	62	63	116	60	60
Ni	3	5	4	3	2	2		236	269	257	6	234	228
Pb	8	10	7	8	7	8		7	8	7	10	6	10
Rb	57	49	58	55	56	56		29	29	30	60	29	34
Sc	12	7	13	10	10	8		22	25	24	13	30	25
Sr	1231	1222	1247	1235	1225	1227		673	655	670	1225	605	783
Th	9	12	10	10	8	9		6	6	5	11	6	4
V	106	94	115	119	108	106		259	243	275	94	292	217
Y	44	44	43	43	45	44		30	31	34	44	31	30
Zn	132	137	155	132	133	128		120	123	122	133	112	128
Zr	439	460	452	439	448	459		289	282	289	464	276	316
Hf	12.2	12.4	11.5	12.3	12.5	12.2	7.7	6.6	8.1	7.5	12.1	7.1	8.4
La	93.9	91.8	92.6	95.2	93.5	91.0	36.7	34.6	44.0	43.5	94.8	44.9	48.8
Ce	198.6	199.9	187.4	190.8	196.1	192.7	85.3	69.8	92.9	92.0	188.8	85.2	103.0
Nd	98.2	103.0	98.9	97.2	96.6	93.5	47.7	37.9	47.1	50.4	89.8	43.9	64.2
Sm	16.5	15.2	16.3	16.4	16.1	15.5	8.1	8.3	9.3	9.4	16.0	9.2	10.6
Eu	5.07	4.96	4.90	5.07	5.17	5.02	2.94	2.72	3.14	3.35	4.90	3.02	3.37
Tb	1.55	1.94	1.61	1.58	1.43	1.68	0.88	0.95	1.18	1.27	1.41	1.01	1.12
Yb	3.39	3.10	3.57	2.71	2.86	2.84	1.94	1.96	1.68	2.05	3.32	1.91	2.45
Lu	0.43	0.40	0.45	0.42	0.44	0.46	0.18	0.25	0.23	0.25	0.39	0.26	0.42
$(La/Sm)_N$	3.51	3.72	3.51	3.58	3.58	3.63	2.93	2.85	3.66	3.93	3.85	3.66	3.01

Table III.5. continued.

	19-1	19-2	19-3	19-8	21-8	21-14	22-1	22-2	22-3	24-4	24-7	24-8
Ba	133	144	262	616	311	263	557	525	562	709	743	755
Cr	522	522	711	147	3	4	406	392	355	117	124	99
Cu	75	73	82	49	41	14	11	16	31	28	28	28
Ga	18	17	20	22	30	26	20	18	21	23	21	23
Nb	32	35	43	88	69	60	72	71	70	100	100	103
Ni	234	224	296	110	8	0	145	148	153	54	51	40
Pb	6	4	6	8	6	8	7	7	8	7	12	10
Rb	19	19	29	77	27	21	55	59	61	85	88	91
Sc	32	28	31	27	16	22	35	31	29	23	19	21
Th	3	2	6	10	2	5	8	8	9	10	12	11
V	259	256	267	307	238	280	353	339	338	267	268	266
Y	29	29	27	35	50	45	30	28	26	32	32	35
Zn	104	96	108	120	169	154	103	102	107	114	116	118
Zr	198	199	221	331	447	394	201	199	199	302	301	315
Hf	6.7	5.0	6.0	9.5	12.4	11.3	5.7	5.5	5.9	7.5	7.7	8.0
La	32.7	25.4	33.6	81.2	49.4	43.2	67.6	59.4	61.8	77.2	86.0	78.2
Ce	69.3	49.7	67.	151.0	109.8	98.1	111.1	103.7	102.5	145.5	154.7	153.8
Nd	41.6	29.3	43.33	76.5	81.6	77.4	54.4	49.2	47.8	72.9	67.1	62.6
Sm	8.1	6.5	7.2	10.9	16.0	14.2	8.1	8.2	8.3	10.0	10.4	10.1
Eu	2.52	2.16	2.46	3.54	5.33	4.80	2.64	2.48	2.33	2.96	3.22	3.12
Tb	1.01	0.97	0.98	1.51	1.94	1.64	1.03	0.92	1.06	1.05	1.00	1.20
Yb	2.09	2.04	1.55	2.57	3.09	2.95	2.55	2.20	2.55	2.40	2.31	2.92
Lu	0.28	0.29	0.18	0.26	0.42	0.38	0.29	0.29	0.28	0.29	0.30	0.39
$(La/Sm)_N$	2.48	2.42	2.86	4.58	1.91	1.88	5.12	4.47	4.58	4.76	5.09	4.76

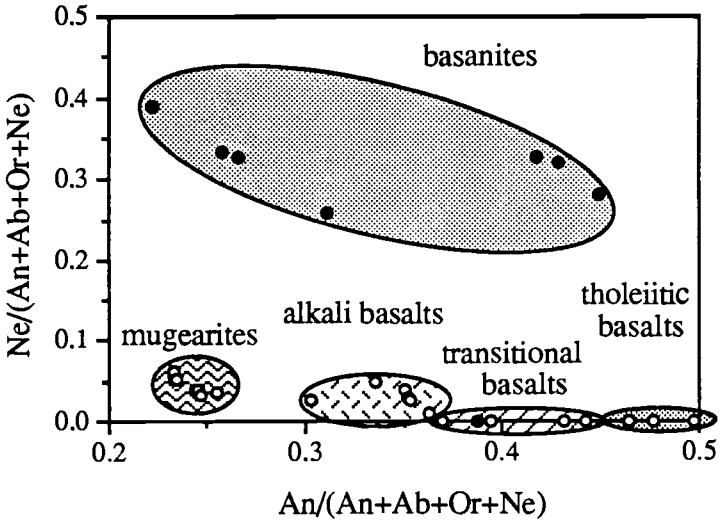

Figure III.5. Ne/(An+Ab+Or+Ne) versus An/(An+Ab+Or+Ne) for CRGN lavas. Five rock types identified from samples dredged on CRGN 02 based on normative feldspar and nepheline compositions; after Wright [1986]. Filled circles represent samples with $^{87}Sr/^{86}Sr > 0.7045$.

volcanic shield. These compositional distributions provide evidence that the bulk of the submerged shield of a Marquesan volcano is composed of hypersthene-normative tholeiitic and transitional basalts with later-stage, alkalic volcanism rising above sea level.

Substantial fractionation of these lavas is indicated by the wide range of MgO content (11.16-2.52 wt.%) and Mg-numbers (67-37) [$=100Mg^{+2}/(Mg^{+2}+Fe^{+2})$] in CRGN 02 samples (Table III.4). None of the lavas, even the most primitive (highest Mg-number) among the dredged samples, appear to have fractionated olivine alone. This is supported by the drop in CaO/Al_2O_3 as a function of Mg-number (Figure III.6) represented in the compositional trends for each group, suggesting clinopyroxene fractionation. Although fractional crystallization has occurred in all lava groups, the primitive compositions in each group cannot be derived from one another by that process because of the diversity of CaO/Al_2O_3 at a given Mg-number. Variation in degree of partial melting in the more primitive lavas, however, can produce the observed trend of decreasing CaO/Al_2O_3 with increasing Mg-number. Paired fractional crystallization and mixing can produce some of the observed characteristics [Defant and Nielsen, 1990], but it cannot produce a range of nepheline-normative compositions at a fixed, high Mg-number (Table III.4).

Source heterogeneity in trace element and isotopic compositions has been suggested for the Marquesas lineament by authors of all recent studies [Liotard et al., 1986; Duncan et al., 1986; Dupuy et al., 1987]. Whether this heterogeneity is found within a single source region (i.e. small pods of one material within a matrix of another) resulting in the development of a range of lava compositions by different degrees of partial melting, or whether two physically separate sources have been tapped, or a combination of both scenarios, cannot be established.

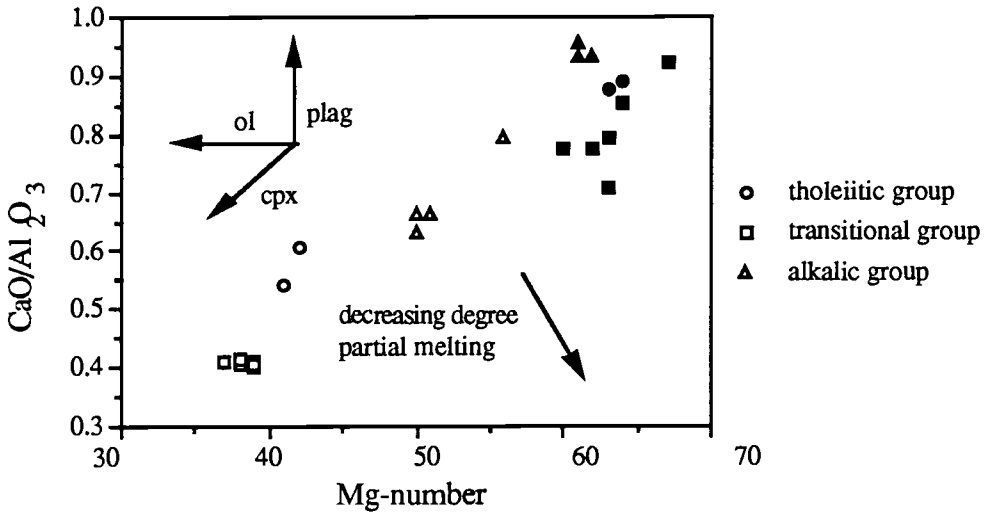

Figure III.6. CaO/Al_2O_3 versus Mg-number for CRGN lavas. Directions of the change of liquid compositions with olivine (ol), clinopyroxene (cpx), and plagioclase (plag) removal are shown. Where the most primitive compositions within a trend are tholeiitic, those lavas and their possible differentiates are called the tholeiitic trend; transitional and alkalic trends are defined similarly. Filled symbols have Mg-number >60. The most primitive lavas from each compositional type have undergone ol and some cpx removal. Primitive alkalic group lavas may represent a lower degree of partial melting than the primitive tholeiitic group lavas.

Rather primitive CRGN 02 lavas with Mg-numbers >60 can be divided into three groups in which incompatible trace element concentrations and ratios and Sr and Nd isotopic ratios are clustered. The most primitive lavas of one group are tholeiitic basalts; they are relatively depleted in incompatible elements and radiogenic isotope ratios (19-1, 19-2). The most primitive lavas of one alkalic group (22-1, 22-2, 22-3) are relatively enriched in incompatible elements and isotopic ratios while another alkalic group (17-1, 17-2, 17-5, 18-40) exhibits relatively unradiogenic isotopic ratios. These are the more primitive compositions of the alkalic trend and transitional trend, respectively.

In a plot of Y versus Nb (Figure III.7) the compositional groups identified above (tholeiitic, transitional, and alkalic) define linear trends. Primitive lavas in each group have lower concentrations of both elements. The primitive members of tholeiitic and transitional groups are similar in Y and Nb contents (Figure III.7); their differences might be explained by different degrees of melting of a single source. The most primitive alkalic lavas are enriched in Nb over the most primitive of the tholeiitic/transitional groups but are similar in Y, and indicate an origin at a different source and (or) the influence of residual clinopyroxene or garnet in the source region.

Differentiation modelling

One method for evaluating the relative importance of the different active processes responsible for the variety of compositions observed in a natural suite of lavas is phase equilibria based differentiation modelling. The product of this type of modelling is a simulated liquid line of descent produced by a known set of processes. The calculated trends can then be compared to those of the natural suite. In the CRGN basalt suite, differentiation paths were calculated for the most primitive lava from each of the three major chemical groups (tholeiitic, transitional, and alkali basalts) in order to test whether the more differentiated lavas can be related to the more primitive lavas by assimilation or fractionation processes, using the model of Nielsen [1988]. This model uses a set of

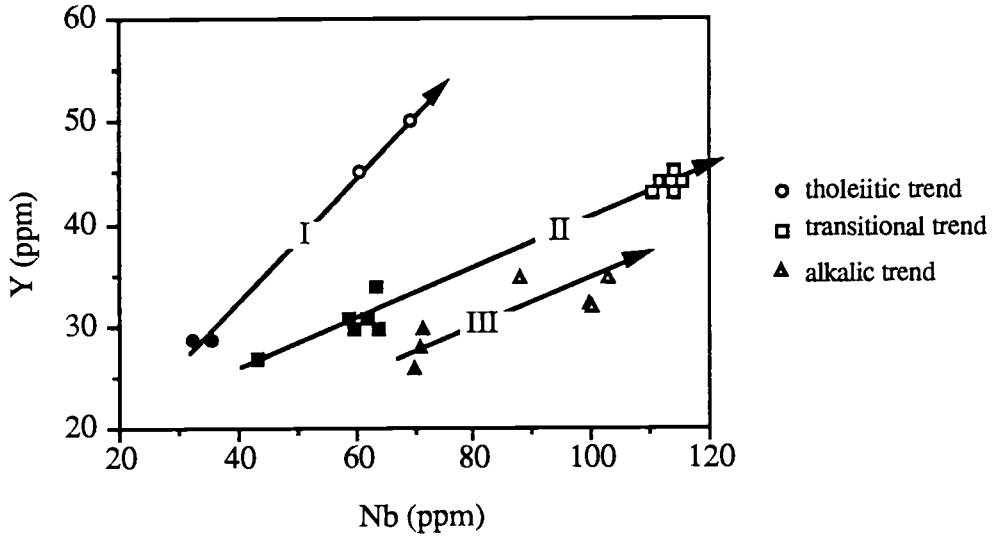

Figure III.7. Y (ppm) versus Nb (ppm) for CRGN basalts. Arrows showing fractionation relationships within the three compositional groups as described in Figure 6. Filled symbols represent lavas with Mg-number. > 60.

empirical and theoretical constraints to calculate the major and trace element path a magma will take as it undergoes fractional crystallization, magma mixing, assimilation, and eruption. Since this model is calibrated using low pressure experimental data, the calculated liquid lines of descent may be used only as a minimum pressure baseline against which we can measure the observed trends.

Three types of model were chosen: (model 1) homogeneous fractionation of olivine, clinopyroxene, orthopyroxene, plagioclase, spinel, and apatite, (model 2) fractionation of the same phases by in situ crystallization, that is, with crystallization only along the walls of the cooling magma chamber [Langmuir, 1989], and (model 3) assimilation of olivine (Fo_{90}), thought to simulate perculation of the liquid through an olivine mush, and continued fractionation of the above phases. In each case the most primitive composition within the lava series was chosen as parental; sample DH 19-1 was chosen as parent for the tholeiitic series and transitional series, and sample DH 22-1 for the alkalic series. Simulations of fractionation or fractionation/assimilation were calculated beginning with these more primitive compositions, and these results were compared with observed trends involving the more evolved compositions. All samples analyzed show geochemical characteristics indicative of clinopyroxene fractionation (e. g. a simultaneous drop in Ca and Sc with decreasing Mg). Therefore, parental compositions could not be obtained by back-calculation with olivine addition.

The modelling results support the view that in all three compositional series the lavas with low Mg-number can be related to the high Mg-number lavas by crystal fractionation, but not at low pressure. In addition, because magma mixing paired with fractionation produces major element trends similar to fractionation alone [Defant and Nielsen, 1990], it is possible that the natural system was open to recharge. However, the present natural lava compositional data base is too small to adequately evaluate this possibility. The effect of pressure on the differentiation trend can be seen in Figure

III.8a. The homogeneous fractionation trend for the transitional and tholeiitic lavas calculated at low pressure is characterized by a relatively shallow slope of Ca/Al versus Sc (Figure III.8a) and a significant Fe enrichment (versus Al , Figure III.8b) compared with the natural trends. This Fe enrichment and Al depletion in the calculated liquid paths is due to the role of plagioclase fractionation. At higher pressure where plagioclase saturation is suppressed, the plagioclase-in inflection in the trend (Figure 8III.b) will be offset to higher Al. The in situ fractionation trend is more similar to the natural data in terms of Ca/Al versus Sc and Fe enrichment, however, other characteristics such as MgO versus SiO_2 paths are significantly different (Figure III.8c).

Scatter of the data, especially in the more primitive compositions of transitional basalts, may reflect the differences in source compositions of the individual members of the sample suite. As would be expected for a suite collected by random sampling of several edifices with ages spanning an almost 4 m.y. period, calculated fractionation trends only match the observed lavas in a general way. Nonetheless, although the tholeiitic and transitional suites show differences in source compositions with regard to trace elements and isotopic ratios, they plot on the same fractionation trends. From this we can infer that they originated from parents with similar major element compositions. The compositional scatter of the data suggests that the tholeiitic/ transitional basalts can be explained by different degrees of partial melting of a heterogeneous source or by a range of degrees of partial melting and variable mixing of two sources. Alkalic lavas are related to each other by fractionation of a source of different composition from the tholeiitic and transitional lavas. High pressure fractionation is indicated by the deviation of the series from expected fractionation trends for total alkalies versus silica (Figure III.9a) suggesting increased Ca-Tschermak component in the pyroxene. High pressure clinopyroxene fractionation is indicated by the downward trend in Ca/Al versus Sc (Figure III.9b). We conclude that the fractionated lavas are the result primarily of

Figure III.8. Modelled differentiation trends of tholeiitic/transitional series lavas. Diagram (a) Ca/Al versus Sc, diagram (b) FeO* versus Al_2O_3, diagram (c) SiO_2 versus MgO. Fractionation trends for three models described in text with CRGN basalt sample 19-1 as parent. Percent fractionation for model 1 shown as tic marks.

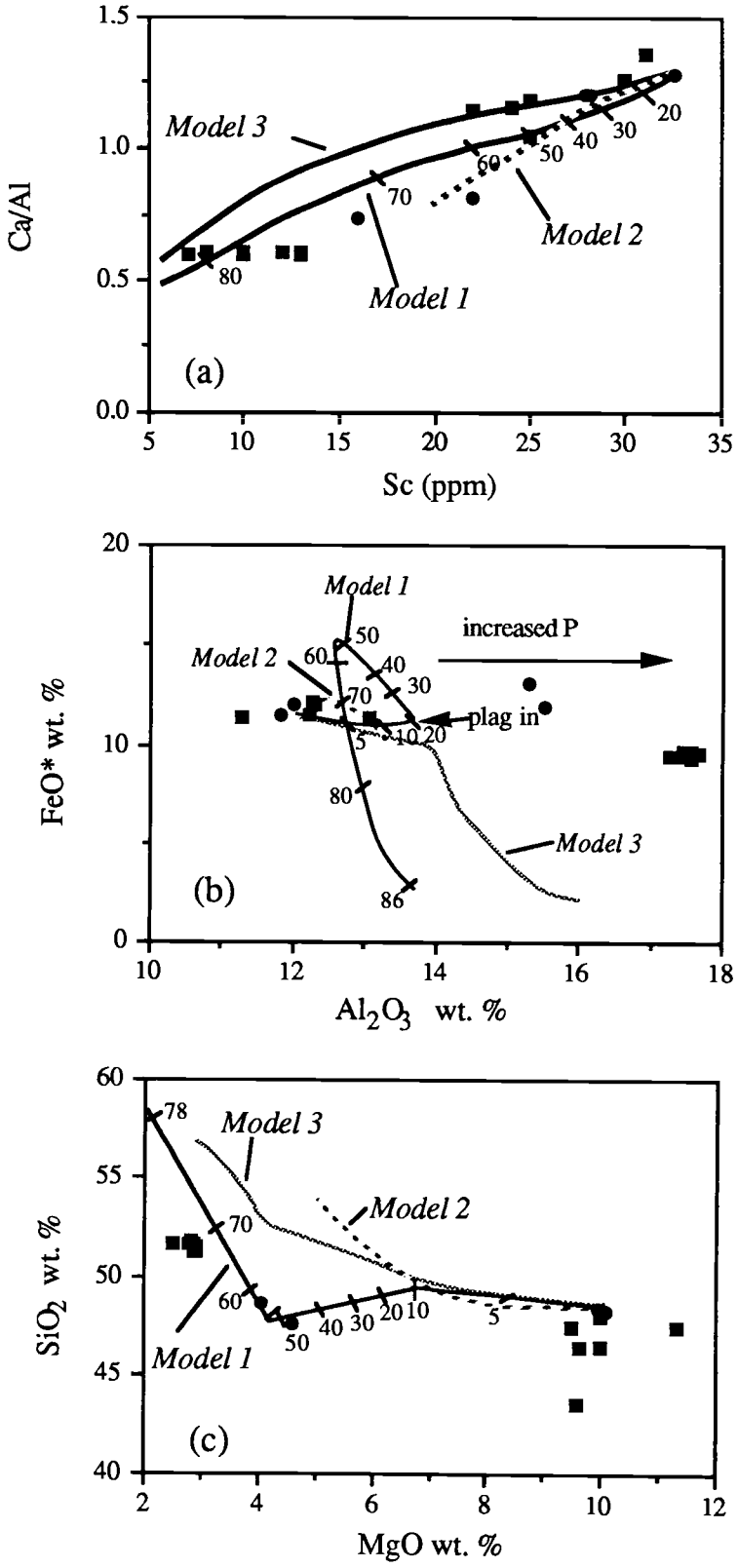
Ca/Al
Sc (ppm)
Model 3
Model 2
Model 1
(a)
FeO* wt. %
Al_2O_3 wt. %
increased P
plag in
(b)
SiO_2 wt. %
MgO wt. %
(c)

Figure III.8

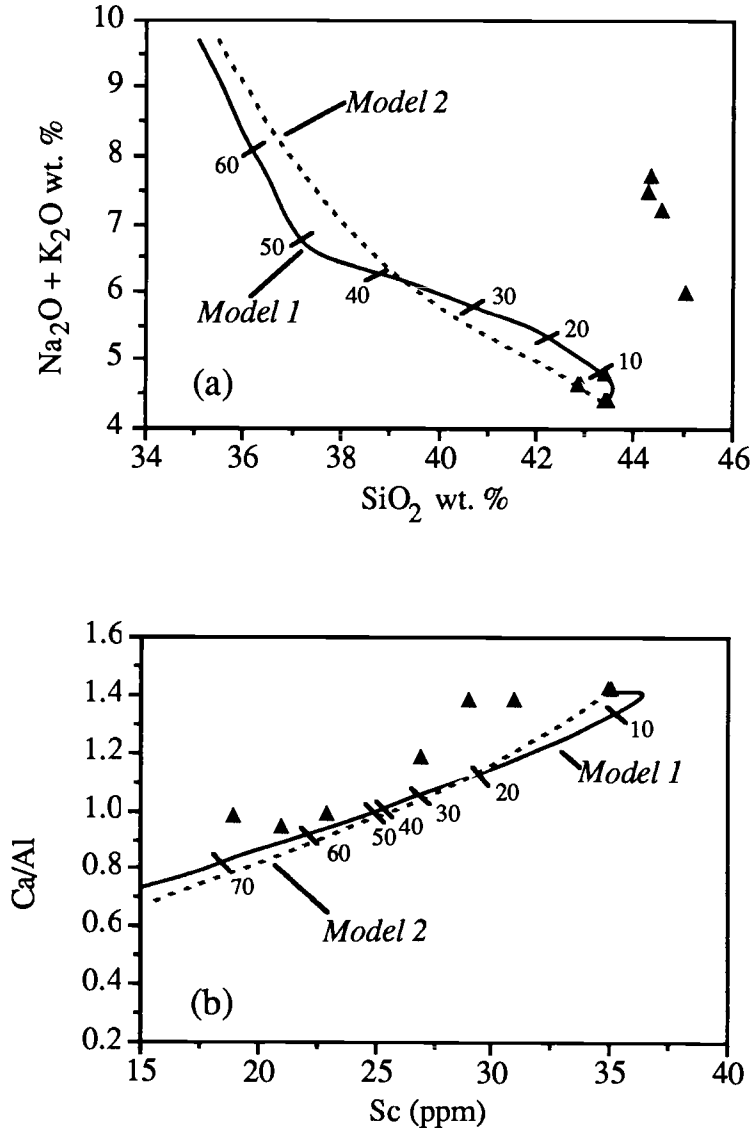

Figure III.9. Modelled fractionation trend of alkalic series lavas. Diagram (a) Na_2O + K_2O wt. % versus SiO_2 wt. %, diagram (b) Ca/Al versus Sc. Percent fractionation for model 1 shown as tic marks. Models as described in text.

olivine, clinopyroxene and relatively less orthopyroxene, plagioclase fractionation from several compositionally distinct parental magmas. The alkalic lavas formed at greater depth than the tholeiitic and transitional lavas.

Trace elements

All CRGN basalts analyzed are enriched in trace elements, especially in incompatible trace elements, relative to spreading ridge lavas. As expected, alkalic lavas are more enriched in incompatible elements than tholeiitic and transitional lavas (Table III.5), consistent with their formation by smaller degrees of partial melting, or by melting of a more enriched source. However, incompatible element ratios, which are an indicator of source composition, vary widely. For example, in large-ion lithophile element ratio diagrams basalts from the CRGN 02 sample collection appear to be the result of differential melting of at least three separate sources or by melting and mixing of two sources. Figure III.10a shows that possible endmembers could be a high Zr/Nb, low La/Sm source and a high La/Sm, low Zr/Nb source. Mixing between two discrete sources would lead to a gradation of $^{87}Sr/^{86}Sr$, the gradation, however, is equivocal. On Figure III.10b alkalic basalts are similar to each other in incompatible element ratios and Pb-isotope values. Tholeiitic and transitional samples are widely different in $^{206}Pb/^{204}Pb$ requiring mixing of more than two homogeneous sources. Therefore, if tholeiitic and transitional lavas are the result of melting only two mantle source compositions, at least one of the sources must be isotopically heterogeneous.

The variations in trace elements may be summarized in a spider diagram which shows trace elements organized by increasing compatibility (Figure III.11). Tholeiitic and alkalic basalts from the same location, for example from Ua Pou or DH 19, cannot be related isotopically or in their trace element patterns [Duncan et al., 1986; Liotard et al., 1986]. Trace element concentrations and ratios of Marquesan basalts cannot be explained by variable degrees of partial melting of a homogeneous source. Differences

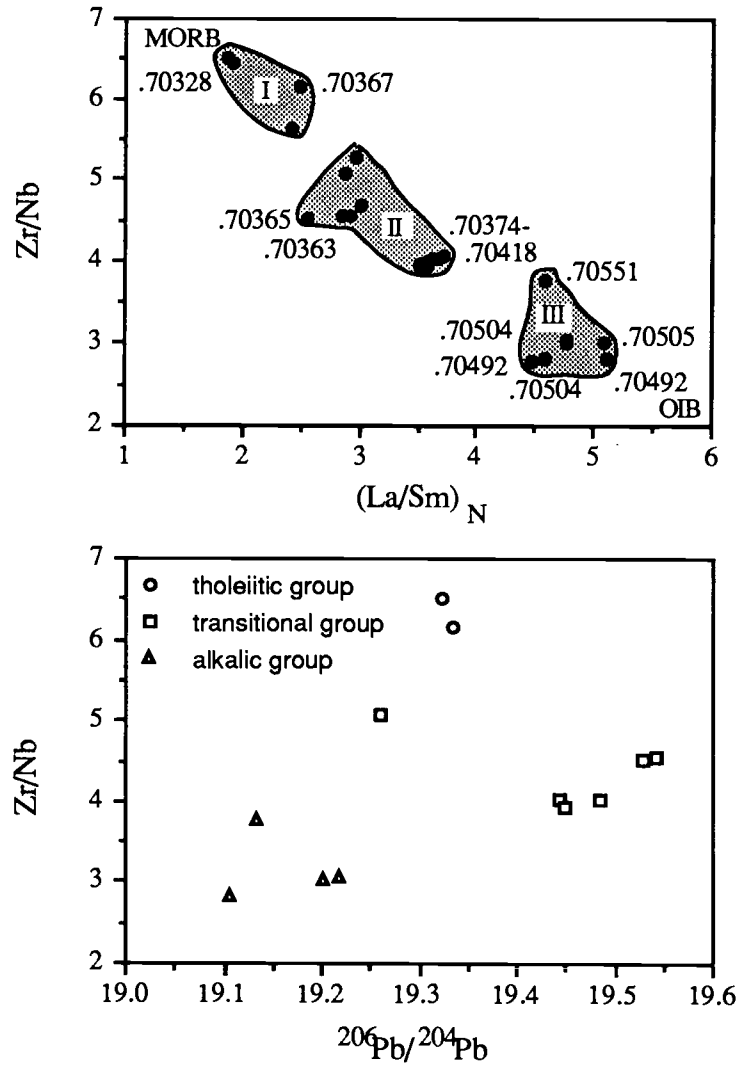

Figure III.10. Zr/Nb versus $(La/Sm)_N$ and $^{206}Pb/^{204}Pb$ for CRGN lavas. Diagram (a) Zr/Nb versus $(La/Sm)_N$ with $^{87}Sr/^{86}Sr$ indicated. Basalts of the different trends cluster between OIB and MORB: I = basalts of the tholeiitic trend, II = basalts of the transitional trend, III = basalts of the alkalic trend. Melting and mixing of a high Zr/Nb, low $(La/Sm)_N$ source (MORB-like) and a low Zr/Nb, high $(La/Sm)_N$ source (OIB-like) cannot explain the trend seen. At least one of the sources must be heterogeneous. Diagram (b) Zr/Nb versus $^{206}Pb/^{204}Pb$ for tholeiitic, transitional, and alkalic lavas of CRGN 02. Mixing of two homogeneous sources cannot explain the pattern seen.

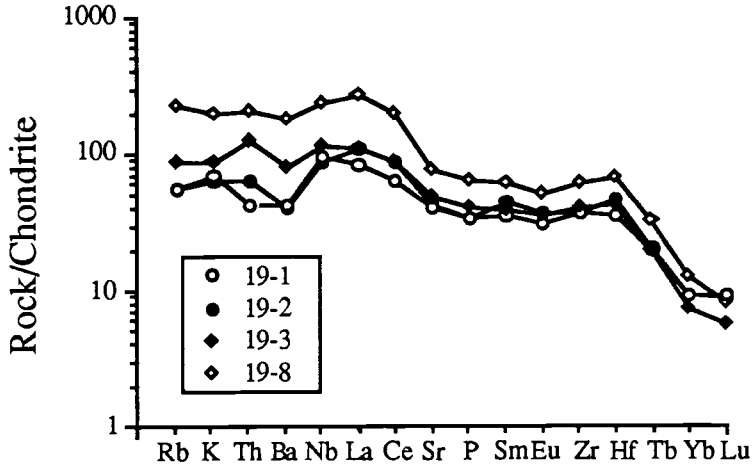

Figure III.11. Spider diagram for samples from DH 19. Geochemical analyses normalized to chondrite [after Nakamura, 1974] for samples from DH 19 for which all geochemical data are available. Incompatibility of an element in normal MORB decreases to the right.

in trace elements in tholeiitic/transitional lavas may be caused by mixing of at least two separate sources or by melting of a heterogeneous source.

Trace element relationships in CRGN basalts require the existence of at least two separate sources. One source, which gives rise to highly radiogenic alkalic lavas, is the high La/Sm endmember on Figure III.12. Primitive samples from DH 22 are the closest representatives of melts of this endmember. DH 24 and 19-8 samples with higher La concentrations appear to be differentiates of primitive melts from that source. The high La/Sm lavas may be representative of a lower degree partial melt or a different source composition than the tholeiitic/transitional lavas. Tholeiitic and transitional lavas partially melted from a component heterogeneous in La/Sm. The most enriched La/Sm seen in the tholeiitic/transitional group are the differentiated DH 12 lavas. DH 21 lavas are the least enriched in La/Sm; compositions parental to these lavas are not represented in the CRGN 02 suite (Figure III.12).

Rare earth elements

Chondrite-normalized REE are enriched relative to MORB in all Marquesan basalts; however, no sample from the dredged suite has as flat a REE pattern as the Ua Pou tholeiites [Ua Pou $(La/Yb)_N$=9, CRGN 02 $(La/Yb)_N$=11] (Figure III.13) [Liotard et al., 1986]. Within the CRGN basalts, enrichment of normalized light (L) REE range from 77 for La in tholeiitic basalts to 247 in basanites and 289 in mugearites. Heavy (H) REEs are less enriched, from only 7x chondritic in tholeiites to 14x in basanites and 17x in mugearites.

The lack of any significant Eu anomaly either suggests that plagioclase addition or removal was not a major factor in the petrogenesis of these suites (Figure III.13). Crossing REE patterns within the Marquesas samples indicate that the basalts must have

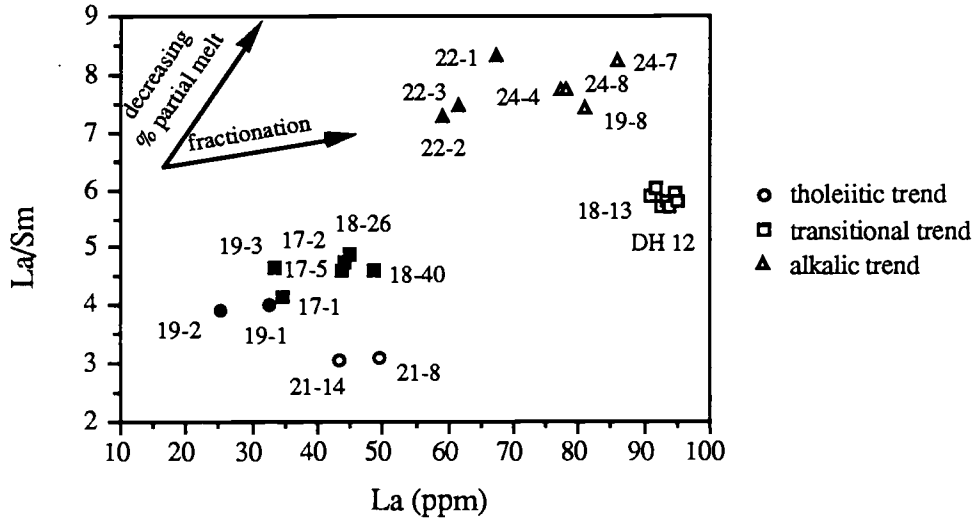

Figure III.12. La/Sm versus La (ppm) for CRGN 02 samples. Increasing La/Sm) results from decreasing degrees of partial melting or increasing LREE enrichment of the source. Increased La results from increased differentiation or increased LREE enrichment of the source. Filled symbols represent compositions with Mg-number > 60.

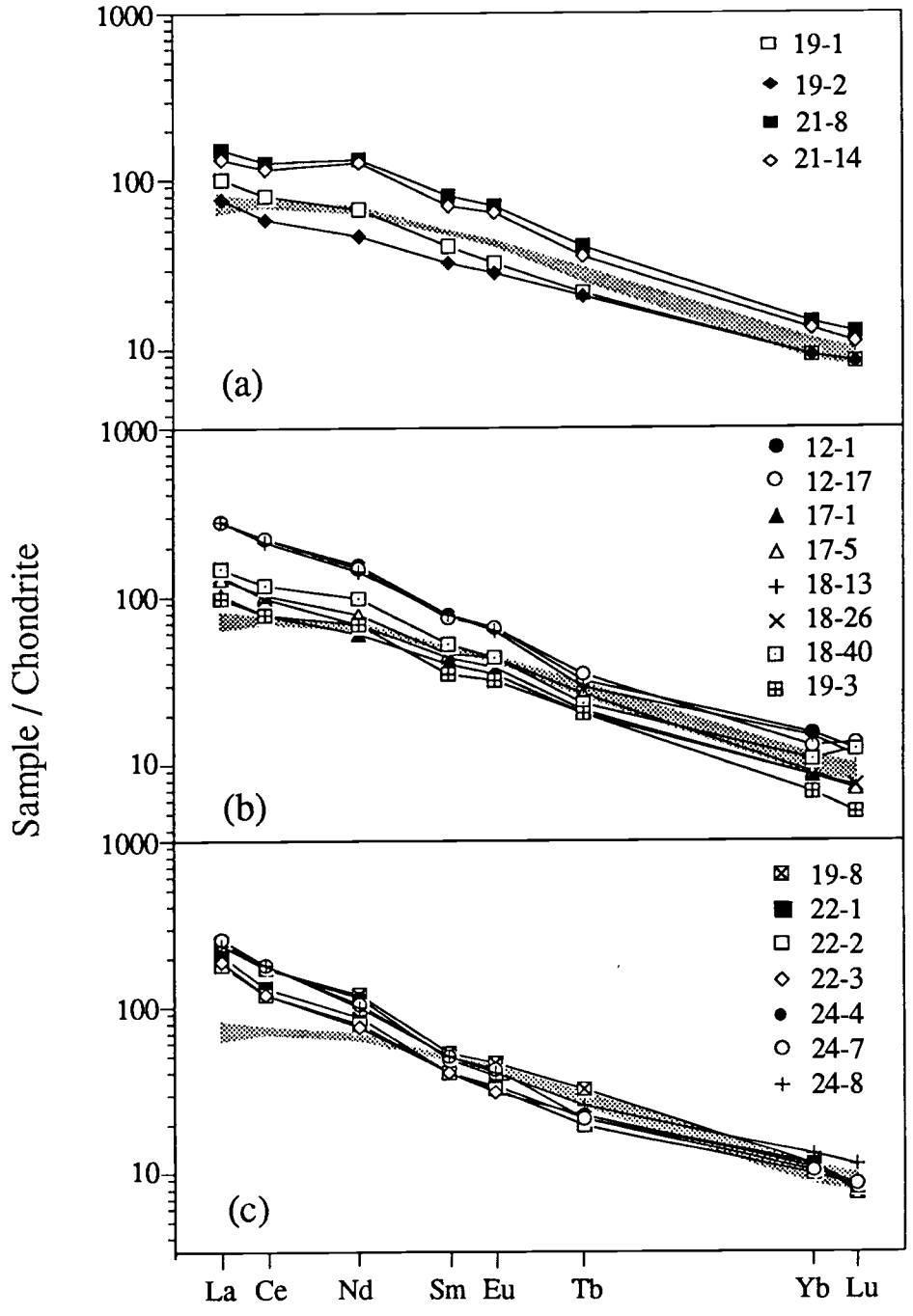

Figure III.13. REE patterns for all Marquesas dredged samples. Diagram (a) pattern for tholeiitic trend lavas, diagram (b) pattern for transitional trend lavas, diagram (c) pattern for alkalic trend lavas. Chondrite normalized [after Nakamura, 1974]. Tholeiitic basalts from the island of Ua Pou are shown as a dotted field.

originated within a heterogeneous mantle source region or from more than one source region. Steepness of the pattern is not so extreme that residual garnet is required in the source.

Isotopic ratios

Isotopic compositions for all basalts analyzed from CRGN 02 are given in Table III.6. The compositions of basalts from the Marquesas volcanic lineament, including the islands and samples from CRGN 02, can be explained in the terminology of Zindler and Hart [1986] by the mixing of three mantle components: a relatively depleted component, the same as, or related to MORB-source mantle (DMM), a component with high $^{206}Pb/^{204}Pb$ but with low $^{87}Sr/^{86}Sr$ and intermediate εNd (HIMU), and a component with generally high radiogenic isotopic ratios (EM II) [Dupuy et al., 1987].

A plot of εNd vs. $^{87}Sr/^{86}Sr$ (Figure III.14a) demonstrates that tholeiitic basalts have less radiogenic Sr than the transitional and alkalic basalts. Although tholeiitic and alkalic sources are somewhat separated, mixing between the sources is prevalent . At Ua Pou and DH 19, for example, tholeiitic/transitional and alkalic basalts are found in different fields on the diagram, further emphasizing the close physical proximity of the sources for the two magma types. Closer inspection of the diagram reveals a significant geographic compositional pattern. At constant εNd, the $^{87}Sr/^{86}Sr$ becomes more radiogenic across the Marquesas lineament, from west to east (Figure III.14b). The presence of tholeiitic samples across the lineament shows that this isotopic gradient is not a function of the major element composition of the samples.

The same separation in isotopic composition for Ua Pou and DH 19 samples can be seen in $^{87}Sr/^{86}Sr$ vs. $^{206}Pb/^{204}Pb$ (Figure III.15a). In this case, tholeiitic and some transitional samples plot near a mixing line between MORB and HIMU while more alkalic compositions exhibit more EM II component. Thus, the EM II component is more thoroughly sampled at lower degrees of partial melting. This component either

Table III.6. Sr, Nd and Pb Isotopic Compositions For CRGN 02 Basalts.

	$^{87}Sr/^{86}Sr$	$^{143}Nd/^{144}Nd$	εNd	$^{206}Pb/^{204}Pb$	$^{207}Pb/^{204}Pb$	$^{208}Pb/^{204}Pb$
12-1	0.703737	0.512835	3.8	19.448	15.590	39.119
12-17	0.703753	0.512680	0.8	19.444	15.554	
14-1	0.703490	0.512886	4.8	19.522	15.592	39.163
16-1	0.703909	0.512842	3.9	19.651	15.621	39.283
16-3	0.703473	0.512869	4.5	19.677	15.598	39.331
17-1	0.703650	0.512864	4.4	19.530	15.602	39.158
17-5	0.703628	0.512860	4.3	19.542	15.615	39.202
18-13	0.703759	0.512840	3.9	19.485	15.605	39.193
19-1	0.703673	0.512875	4.6	19.334	15.535	38.867
19-3	0.704180	0.512818	3.5	19.260	15.571	39.257
19-8	0.705506	0.512690	1.0	19.133	15.632	39.183
19-11	0.705198	0.512744	2.0	19.286	15.614	39.294
21-14	0.703276	0.512895	5.0	19.323	15.562	38.977
22-1	0.704920	0.512700	1.2	19.146	15.620	39.086
22-2	0.704915	0.512727	1.7			
24-4	0.705042	0.512790	2.9	19.203	15.606	39.175
24-7	0.704955			19.167	15.558	39.015
24-8	0.705052	0.512714	1.5	19.218	15.624	39.240

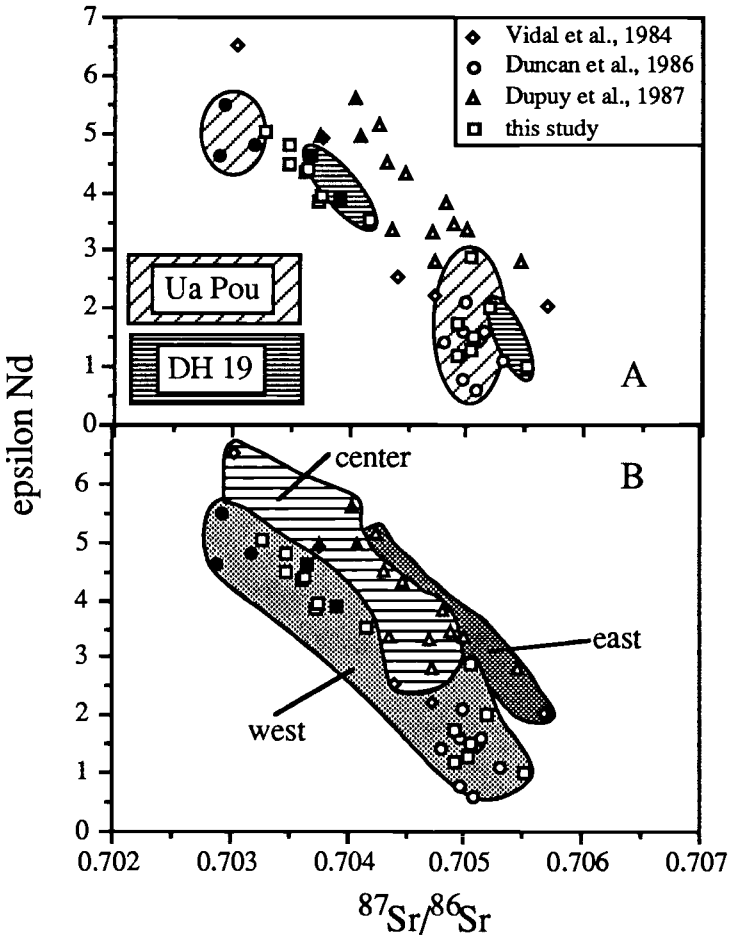

Figure III.14. εNd versus $^{87}Sr/^{86}Sr$ for Marquesan basalts. Diagram (a) with compositional fields for Ua Pou and DH 19, diagram (b) with geographic trends. Filled symbols indicate tholeiitic basalt. Major element data were not available for analyses of Vidal et al., [1984] so normative compositions could not be determined for these samples.

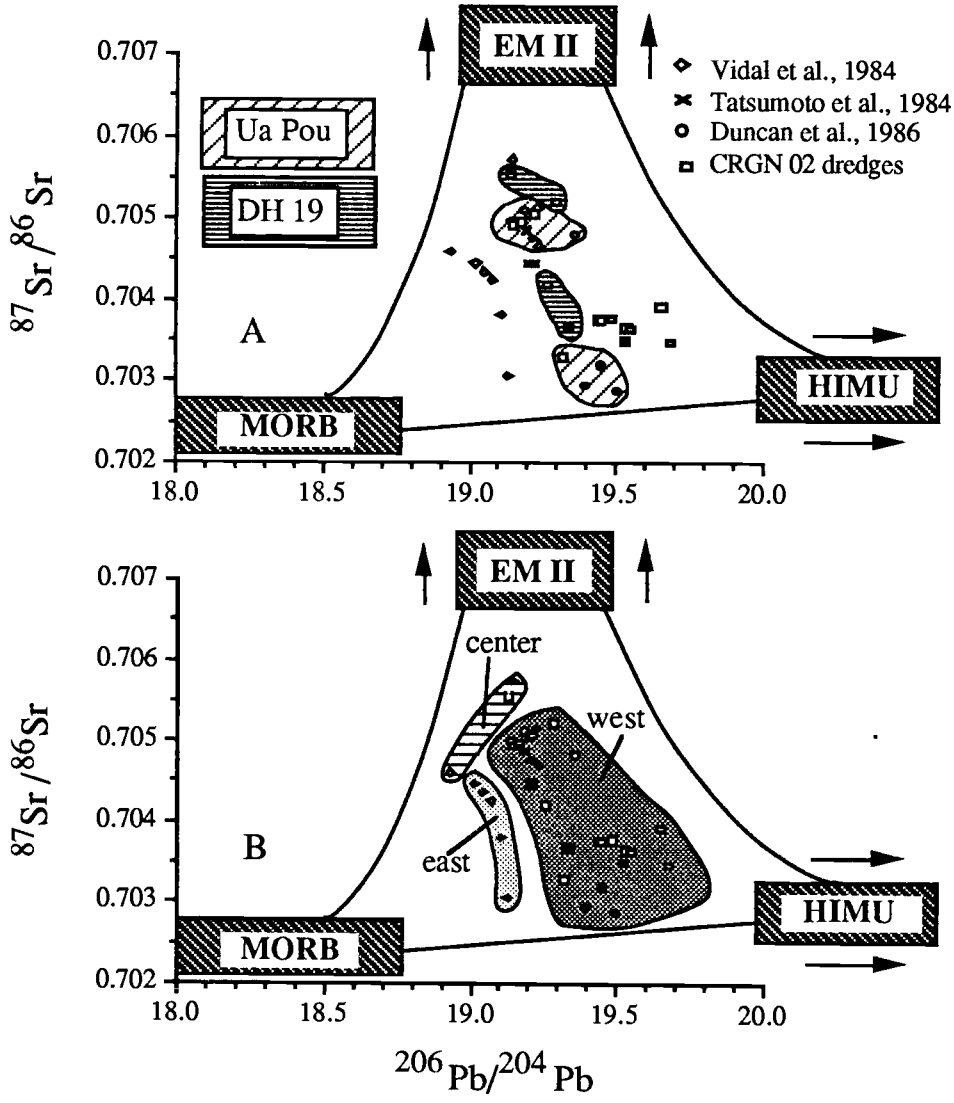

Figure III.15 $^{87}Sr/^{86}Sr$ versus $^{206}Pb/^{204}Pb$ for Marquesan basalts. Diagram (a) with compositional trends for Ua Pou and DH 19, diagram (b) with geographic trends. Proposed compositions of mantle components from Zindler and Hart [1986] are shown in cross-hatched boxes. Tholeiitic basalts are represented by filled symbols.

becomes diluted by the higher degrees of melting necessary to produce the tholeiitic basalts, or it is derived from a part of the plume that is tapped during a later volcanic stage. A geographic trend to the isotopic variation can also be recognized in Figure III.15b. Samples from the western side of the Marquesas lineament show a greater amount of HIMU component while the central samples are more MORB-like and the eastern samples show more of an EM II component.

Pb-isotopic analyses of the CRGN 02 samples has greatly increased the number of such analyses of Marquesan lavas. Mantle components that are distinguishable in $^{87}Sr/^{86}Sr$ and $^{143}Nd/^{144}Nd$ or $^{87}Sr/^{86}Sr$ and $^{206}Pb/^{204}Pb$ are also clear on $^{208}Pb/^{204}Pb$ versus $^{206}Pb/^{204}Pb$ plots (Figure III.16). Samples with relatively high $^{87}Sr/^{86}Sr$ (filled symbols) plot close to the value proposed for enriched mantle composition (EM). HIMU component is seen most strongly in samples from DH 16 (Figure III.16). Products of South Pacific volcanism show mixing of the discrete mantle components proposed by Zindler and Hart [1986].

Generation of Marquesan magmas

Major and trace element compositions from the CRGN 02 collection consistently show that the tholeiitic/transitional lavas that form the shields all along the Marquesas lineament are compositionally similar but the later-stage alkalic lava suite originated from a quite different parental composition. One explanation for this, consistent with both trace element and isotopic compositions for all lavas, is that the tholeiitic and transitional lavas result from variable degrees of partial melting of a heterogeneous source. Alkalic lavas are partial melts of a different, potentially heterogeneous, source.

In diagrams of Sr, Nd, and Pb isotopic compositions of both submerged and subaerial samples, basalts from the Marquesas region consistently lie on mixing curves

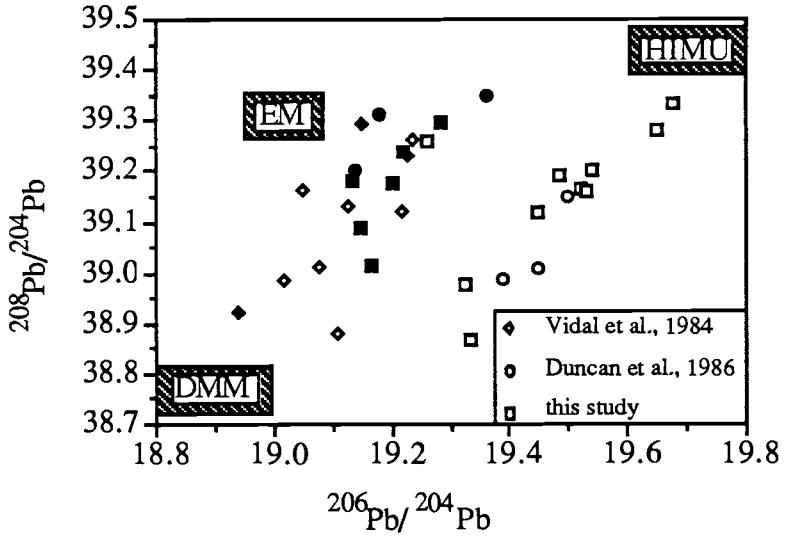

Figure III.16. $^{208}Pb/^{204}Pb$ versus $^{206}Pb/^{204}Pb$ for Marquesan lavas. Filled symbols indicate samples with $^{87}Sr/^{86}Sr > 0.7045$. Mantle components of Zindler and Hart [1986] shown in hatchured boxes.

between three mantle components, DMM, HIMU, and EM II, defined by Zindler and Hart [1986] (Figure III.15a). Phase relationships, depth and degree of melting, and trace element patterns in rocks that result from melting of these components give clues as to the location and type of material being melted. The simplest component to locate is the depleted mantle component (DMM) from which spreading ridge lavas rise. Because melting at spreading centers is thought to take place at a shallow level, the DMM component must reside in the uppermost upper mantle. It may also make up much of the rest of the upper mantle [Hart and Zindler, 1989]. The HIMU component, with high $^{206}Pb/^{204}Pb$ and $^{208}Pb/^{204}Pb$ but without a corresponding elevation in $^{87}Sr/^{86}Sr$ or $^{207}Pb/^{204}Pb$ is thought have undergone enrichment in U/Pb 1.5-2.0 billion years ago [Zindler and Hart, 1986]. Such selective enrichment may have occured in ancient altered oceanic crust to which U was added by seawater during alteration that was stripped of some phases, including Pb and Rb, during subduction [Hart and Zindler, 1989] or in oceanic crust that was metasomatized [Zindler and Hart, 1986]. The ubiquitous presence of the HIMU component in spreading ridge and many hotspot lavas suggests that it is a dispersed component within another widespread mantle component, such as DMM or PREMA [Hart and Zindler, 1989].

Geographic variation from west to east across the Marquesas lineament may be due to different amounts of mantle with EM II and HIMU signatures within different regions of the plume. Also, different degrees of partial melting due to variations in thermal regime across the hotspot would cause different degrees of partial melting and incorporation of variable proportions of HIMU and EM II isotopic components within the melts. Further investigation into this and the more pronounced isotopic variation across the Society Islands hotspot [Devey et al., 1990] is necessary.

The trace element and isotopic composition of the EM II component relates it to continental material such as subcontinental lithosphere or sediments; high $^{207}Pb/^{204}Pb$

requires that the component is sedimentary and probably ancient [Hart and Zindler, 1989]. Conversely, Dupuy et al. [1989] suggest recycled oceanic lithosphere from which island arc basalts have been removed as the source of the alkalic lavas in the French Polynesian lineaments. Whatever its composition, this component must be supplied to the Marquesas lineament by deep mantle upwelling through plume activity.

Models of plume-upper mantle/lithosphere interaction

Two models of dynamic interaction of a mantle plume and upper mantle/lower lithosphere interaction can be developed to explain the age and chemical data from the Marquesas lineament.

(1) *Compositionally buoyant plume and a heterogeneous lithosphere:*

Compositional buoyancy occurs when plume flow is driven by intrinsic density differences between the diapir and its surroundings [Griffiths, 1986a]. Chemical diffusion coefficients within the solid state mantle and lithosphere are 10^{-7} to 10^{-9} times that for heat diffusion so compositional diapirs maintain their chemical identity relative to the upper mantle through which the plume rises [Griffiths, 1986a]. This chemically distinct plume rises to the base of the oceanic lithosphere where it causes melting of the lower lithosphere (Figure 17a). The pronounced lithospheric thinning beneath the Marquesas swell [Fischer et al., 1986] suggests partial melting of at least a small amount of the lithosphere by the plume and incorporation of lithospheric material into it.

In this model, tholeiitic and transitional basalts with depleted radiogenic isotope ratios result from melts of the lower lithosphere (DMM + HIMU) with a small proportion of incorporated enriched plume component (EM II). These shield lavas are formed by large volumes of lithosphere that melt above the thermal upwelling at the center of the hotspot. As the lithosphere moves away from the center of the plume, the

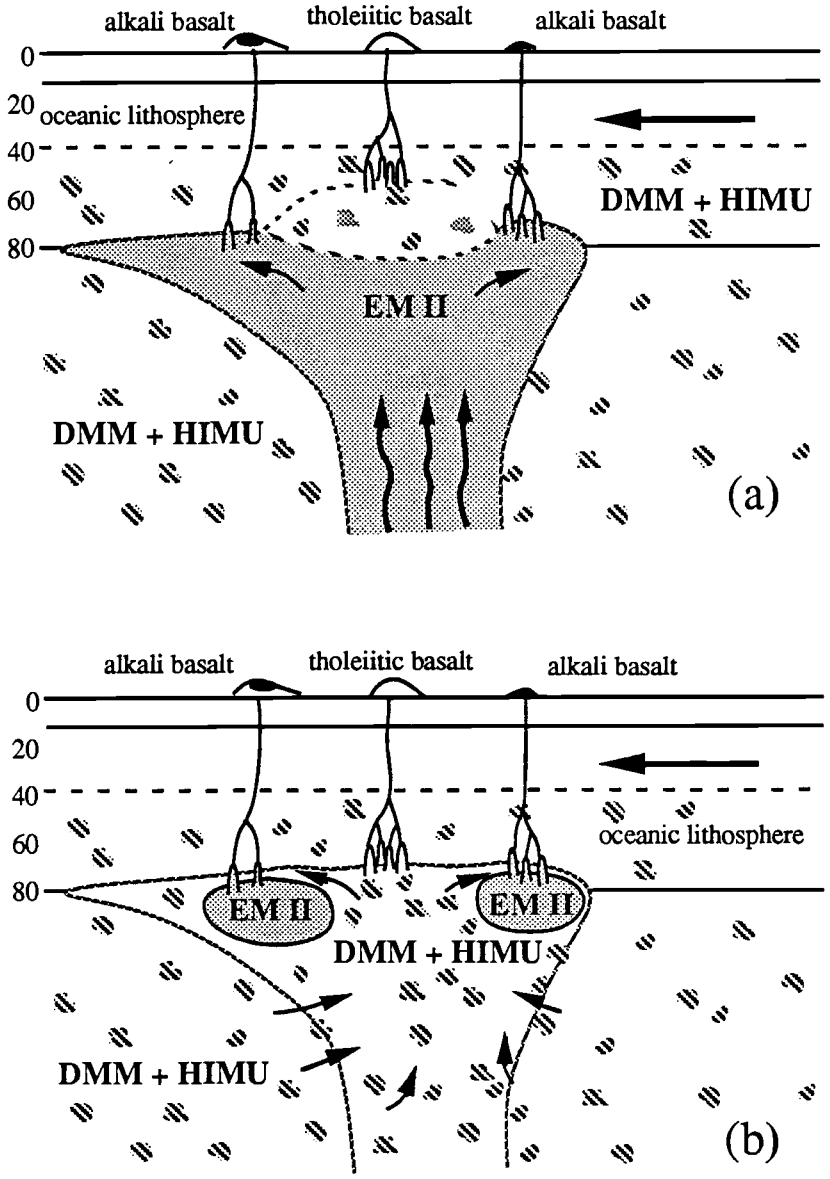

Figure III.17. Plume and lithosphere interaction models for formation of the Marquesas archipelago. (a) Compositional plume. Diapir of EM II rises to the base of the oceanic lithosphere of HIMU + DMM. Melts from the center of the plume are lithosphere, melts from the cooler edge of the plume are EM II. (b) Toroidal plume. During ascent from the lower mantle the thermally active diapir entrains surrounding upper mantle material so that the reslting hotspot is a torus of EM II with a central region of entrained upper mantle material. Melts from the center are DMM + HIMU; melts from the outside are EM II. Both figures are a cross-section perpendicular to the trend of the Marquesas Islands; after Duncan et al. [1986].

reduced thermal regime at the edge of the plume is less able to melt overlying lithosphere and alkalic basalts are erupted. Therefore, the later alkalic basalts at each volcano are a more direct sample of the plume material. Because the hotspot is stationary, we believe that the plume is deeply rooted beneath the asthenosphere, which must be the location of the EM II source. In this scenario, the lower lithosphere is composed of DMM and HIMU that have frozen into place as the lithosphere has moved away from the spreading ridge.

Chen and Frey [1983, 1985] used small degrees of melting of oceanic lithosphere to explain the LREE-enriched but isotopically depleted alkalic lavas of the Hawaiian hotspot. In the Marquesas, however, the isotopically depleted lavas are less enriched in LREE. Generation of the large volumes of tholeiitic and transitional lavas found on a Marquesan shield by the same mechanism would require much larger degrees of melting of huge volumes of oceanic lithosphere. However, upper mantle material that contributed to oceanic lithosphere by underplating would be difficult to distinguish from asthenospheric material, therefore, upper mantle MORB-source material may melt directly to produce the Marquesan shields. Lithospheric thinning above the Marquesas hotspot suggests that at least some lithosphere is contributing materially to Marquesan volcanism.

(2) *Thermally buoyant plume and a heterogeneous upper mantle:*

Thermally buoyant plumes are driven entirely by viscosity and density differences created by a temperature gradient across a thermal boundary layer [Griffiths, 1986a]. Diffusion of heat from such thermal diapirs warms the surrounding mantle and lowers its density sufficiently for the plume to entrain its initially cooler surrounding mantle but conserve its total heat content, buoyancy and driving force. The thermal plume will be a mixture of the diapiric material and surrounding material entrained towards its center [Griffiths, 1986a]. In this case, magmas resulting from melts of upper mantle material

originate in the center of the plume, melts of deeper mantle OIB components will appear along the edges.

Duncan et al. [1986] suggested that one possible explanation for the distribution of tholeiitic and alkalic lavas on Ua Pou was melting above a hotspot that had undergone thermal entrainment of upper mantle. The tholeiitic/transitional, less radiogenic basalts erupted when the volcano passed directly over the center of the plume; the alkalic lavas erupted over the plume edge and represent the initial plume composition from deeper in the mantle. As suggested in the last model, the plume rises from deep in the mantle as a diapir of EM II component. HIMU is dotted through the DMM upper mantle and both are entrained as the plume rises (Figure III.17b).

South Pacific volcanism

Volcanic products of seafloor spreading at the East Pacific Rise are extremely uniform in Sr and Nd isotopic compositions but in Pb isotope ratios they show as large a diversity as seen in MORBs from all oceans [White et al., 1987]. Variations in Pb isotopic ratios are well correlated in EPR lavas [White et al., 1987] (Figure III.18). Mantle upwelling in this region [Dziewonski and Woodhouse, 1987], perhaps associated with the origin of the South Pacific Superswell, may cause a relatively large proportion of HIMU component to be incorporated into the South Pacific asthenosphere and upper mantle. Some of this heterogeneous upper mantle may freeze in place to become incorporated into the lower oceanic lithosphere and some will remain in the upper mantle. Volcanism at Easter hotspot results from mixing of this heterogeneous material and a very small amount of an enriched mantle component (HIMU, Figures III.2 and III.18). The Marquesas hotspot results from a plume of EM II material that originates in the lower mantle and entrains this DMM plus HIMU upper mantle as it

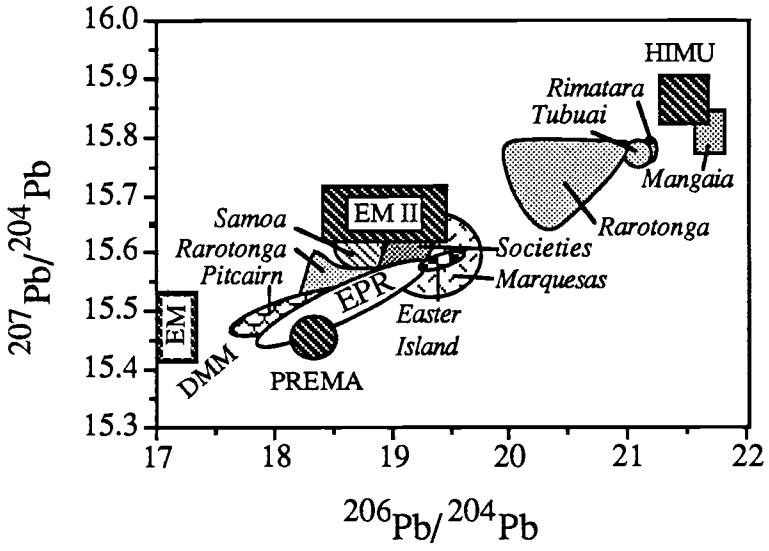

Figure III.18. $^{207}Pb/^{204}Pb$ versus $^{206}Pb/^{204}Pb$ for South Pacific basalts. Dotted pattern represents selected islands from the Cook-Austral lineament. Mantle components of Zindler and Hart [1986] are in hatchured boxes.

rises. Alternatively, EM II diapir arrives at the base of the oceanic lithosphere and melts and assimilates underplated material (Figures III.2 and III.18).

Although the Marquesas lineament sits within the proposed Dupal anomaly belt [Hart, 1984], only some of the alkali basalts have the appropriate radiogenic isotope compositions [Duncan et al., 1986]. Many of the alkalic rocks and all of the tholeiitic samples are isotopically unradiogenic and do not show enrichment in $^{207}Pb/^{204}Pb$ at a given $^{206}Pb/^{204}Pb$ as would be expected for basalts with the Dupal signature (Figure III.17). Because tholeiitic rocks have not yet been discovered elsewhere in Dupal-rich French Polynesia, we must consider that Dupal enrichments are found only in the source for the alkalic samples [Duncan et al., 1986]. The enriched mantle components in the South Pacific hotspot chains, which are supplied by a mantle plume are likely to be the source of the Dupal geochemical signature. In the region of French Polynesia, the Dupal signature appears to be a lower mantle phenomenon.

No systematic variations in isotopic composition with volcanic phase apply to all the hotspots of the South Pacific (Figure III.18). The Samoan Islands, like the Marquesas, are built of transitional or mildly alkalic basaltic shields with relatively less radiogenic isotope ratios that may resemble the composition of the upper mantle or lower oceanic lithosphere in this region [Wright and White, 1986]. A Samoan volcano is capped by highly alkalic lavas with elevated radiogenic isotope ratios that may more closely resemble the plume composition (EM II). The much larger volume of alkalic lavas in this province suggests a more vigorous plume, perhaps aided by lithospheric tearing at the Tonga trench juncture [Wright, 1986]. However, at Pitcairn Island, alkalic shield lavas, built of high $^{87}Sr/^{86}Sr$ EM I-derived volcanics, are capped by low isotopic ratio alkalic rocks. A pronounced mixing trend between the two sources can be traced with time [Woodhead and McCulloch, 1989]. In the young members of the Society Islands

and in the Cook-Austral lineament, isotopic composition is more related to the location of the island than to the age of volcanism at a given location. These two cases may reflect a more complicated scenario involving a heterogeneous plume and lithosphere mixing to varying degrees.

CONCLUSIONS

This thesis is a study of the geochemical expression of hotspot volcanism occurring in two different tectonic environments, on a spreading ridge and intraplate, within the Pacific Ocean basin. A hotspot of each type was characterized: the Cobb, which is currently beneath the Juan de Fuca ridge axis, and the Marquesas, which lies within the Pacific plate. Chapter I, the introduction, laid out the geophysical and geochemical framework of hotspot volcanism, with emphasis on the Pacific Ocean basin. In Chapter II of this thesis, age determinations and geochemical analyses were used to characterize volcanism at the Cobb-Eickelberg seamount chain, a near-ridge hotspot lineament. Chapter III presented similar data for samples dredged from the intraplate Marquesas lineament. This chapter, Chapter IV, summarizes the results of Chapters II and III and places the Cobb and Marquesas hotspots in a plate tectonic and geochemical framework for volcanism in the Pacific basin.

MAJOR RESULTS OF CHAPTER II

1. Cobb hotspot has the temporal characteristics usually attributed to a mantle plume. The earlier volcanic products of the hotspot show a westward progression in age away from the hotspot and a westward increase in the age difference between the seamounts and the crust on which they formed. For at least the last 9 m.y., the Pacific plate moved over a fixed Cobb hotspot which was eventually overtaken by the westwardly migrating Juan de Fuca Ridge.
2. Lavas from the older of the Cobb-Eickelberg seamount chain (CES) are slightly enriched in alkalies and incompatible elements relative to those of the Juan de Fuca

ridge. Seamounts that lie close to or on the spreading ridge have compositions more variable than but similar to the ridge.

3. In isotopic compositions, basalts of the CES are virtually identical to those of the Juan de Fuca ridge, although CES basalts are very slightly enriched in $^{206}Pb/^{204}Pb$ and $^{208}Pb/^{204}Pb$ over Juan de Fuca ridge lavas. CES basalts can be explained by partial melting of depleted upper mantle MORB-source material (DMM) that includes some mantle enriched in some Pb-isotopes (HIMU).
4. A model of entrainment of heterogeneous upper mantle MORB-source material by a thermally-driven lower mantle diapir, possibly also with a MORB-like composition, is consistent with the above observations.

MAJOR RESULTS OF CHAPTER III

1. Samples dredged from the Marquesas lineament show an age progression from northwest to southeast with the youngest Marquesan volcanism at a group of seamounts southeast of the island of Fatu Hiva (0.76 ± 0.10 Ma).
2. The shield of a Marquesan volcano is composed of tholeiitic and transitional basalts; later stage volcanism is alkalic in composition. Differentiation models can relate tholeiitic and transitional lavas to a single, heterogeneous parental composition; alkalic basalts can be related to a single, perhaps heterogeneous, parent that was melted at somewhat greater depth.
3. Sr, Nd, and Pb isotopic compositions are as variable as any found in a single hotspot volcanic lineament. Tholeiitic and transitional lavas result from variable degrees of melting of DMM with pods of incorporated HIMU and a variable amount of enriched mantle (EM). Alkalic lavas result from more direct melting of the enriched mantle source (EM II).

4. A thermally buoyant diapir of EM II composition may have entrained upper mantle MORB-source material, composed of DMM + HIMU as it rose. At each volcanic center tholeiitic melts formed over the entrained material at the center of the hotspot, while alkali basalts subsequently resulted from melting of EM II at the edges of the hotspot.

DISCUSSION

Since hotspots were first described by Wilson [1963] and linked to convective mantle plumes by Morgan [1972] both temporal and chemical characteristics of these features have been recognized. In general, age progressive volcanism and trace element and isotopically enriched lavas are found in oceanic volcanoes thought to originate at a mantle plumes. Since the identification of the age progressive pattern of volcanism [Duncan and McDougall, 1974] and the radiogenic-Sr enrichment of the lavas [Duncan and Compston, 1976] in the Marquesas lineament, the plume origin of the chain has not been questioned. By contrast, many recent studies have not considered Cobb hotspot to have originated above a mantle plume but have considered it to be an upper mantle melting anomaly. However, Cobb-Eickelberg seamount age relationships documented in this study are consistent with volcanism above a fixed mantle plume. Also, the isotopically depleted nature of all basaltic lavas from the northeastern Pacific is evidence that, although hotspot volcanism exists in the area, it is fundamentally different from hotspot volcanism elsewhere. A thermally buoyant diapir that entrains upper mantle MORB-source material, composed of DMM and pods of incorporated HIMU component, can explain the chemical compostions of basalts in the CES. This diapir is not isotopically distinct from MORB and may reflect a fundamental difference in lower mantle character in the north and south Pacific. A thermally buoyant diapir that entrains

upper mantle MORB-source material can also explain the compositions seen in the Marquesas lineament. However, the diapir must have originated in an enriched mantle source (EM II) and must entrain MORB-source material composed of DMM + HIMU.

The ubiquitous presence of HIMU component in spreading ridge lavas throughout the Pacific and the incorporation of this component into volcanoes that form near spreading ridges (e.g. Easter Island) and in some volcanic phases of intraplate hotspots (e.g. the tholeiitic phase at Ua Pou), suggest that HIMU is scattered throughout the otherwise depleted mantle that serves as the MORB-source. The presence of larger amounts of HIMU in the south-central Pacific may reflect the relationship of HIMU to mantle upwelling and to an origin in the lower mantle. Because the most isotopically depleted basalts from this region are enriched relative to north Pacific volcanoes and because the south-central Pacific is a zone of upwelling, it seems possible that enriched mantle components (EM I and EM II) may be incorporated by upwelling into the ambient south-central Pacific upper mantle as well.

Volcanoes with the Dupal geochemical signature correlate with the region of mantle upwelling that is the South Pacific Superswell. This region can be traced to anomalous seismic velocities and lower viscosities within the lower mantle, evidence that Dupal plumes originate in the lower mantle, most likely at the core-mantle boundary. As plumes rise, they incorporate the heterogeneous upper mantle to varying degrees. Lateral variations in temperature within the plume may determine the extent to which pods of different material are melted and incorporated into the basaltic products of the hotspot. Melting of oceanic lithosphere, an important contributor to the alkalic basalt phase of the Hawaiian volcanoes [Chen and Frey, 1983; 1985], must play a role in generation of magmas at hotspots other than Hawaii, but in many cases it may be a small role.

Lithospheric material continuously added to the lower mantle from subduction zones surrounding the south Pacific will, for reasons of mass balance, eventually return to the upper mantle. Large scale return flow can be achieved by mantle plumes [Castillo, 1988]. Lithospheric material that long ago subducted into the lower mantle may remain at the CMB long enough for radioactive decay to create the highly radiogenic Dupal chemical signature. Continued accumulation of material and thermal diffusion into the region from the core will lead to gravitational instability which causes some of the material to rise. Evidence for a superswell-like region in the South Pacific in the past, e.g. at the Darwin Rise [McNutt and Judge, 1990] and at the mid-Pacific Mountains [Smith et al., 1989], may reflect the accumulation and release of material buildup at the CMB.

Differences within the volcanoes of individual hotspots are pronounced. For example, at Pitcairn Island, early shield volcanism is composed of transitional basalts that reflect origin at an EM I source. Later stage alkalic lavas are more depleted in radiogenic isotope ratios, and reflect an origin in south-central Pacific ambient mantle (DMM + HIMU + EM) [Woodhouse and McCulloch, 1989]. Volcanism at a Marquesan shield begins with tholeiitic basalts representative of melting of ambient mantle (DMM + HIMU $\pm$ EM) but later alkalic basalts reflect melting of an EM II source composition. Differences in the composition of enriched mantle may reflect differences in the subducted lithospheric material that later gives rise to a mantle source region. The material may differ for example, in the age of the slab at the time it was subducted, in the amount of alteration it had undergone at the seafloor or during subduction, and in the amount of sediment that went down with it. Differences of the timing of events within a volcanic edifice over a hotspot, i.e. if the basaltic products get more or less enriched in radiogenic isotopes with time, may reflect differences in the type of mantle plume and its interactions with asthenosphere and lithosphere as it rises and melts.

Some remaining questions

Early studies of hotspot volcanism concentrated mostly on the Hawaiian hotspot, which has proved to be the most unusual hotspot on Earth. The increase in data from hotspot regions around the world has led to the realization that not only are all other hotspots different from Hawaii, they are different from each other. "Big picture" views of mantle heterogeneity and plume dynamics will stem from integration of studies of individual hotspots and hotspot regions around the world.

He-isotope ratios can give information as to the "primitiveness" of a mantle source and are useful to determine how long a region within the mantle has isolated. Much of the He-isotope work on oceanic basalts has concentrated on products of the Hawaiian hotspot and only scattered basaltic samples from other hotspots have been analysed thus far. Systematic study of chemical and isotopic compositions at many hotspots must begin to include $^{3}He/^{4}He$ analyses. Characterization of the mantle components of Zindler and Hart [1986] in He-isotope ratios will be necessary to determine their history. The diverse chemistry of French Polynesian basalts, which includes extreme examples of the HIMU, EM II, and EM I components, make this region an excellent location for $^{3}He/^{4}He$ analyses. He-isotope ratios of basalts from the Marquesas, Pitcairn, Society and Cook-Austral chains would give insight into the long-term history of the mantle components in that area.

The changes in chemical composition with evolution of a volcanic edifice is a poorly understood phenomenon. Although the evolution of a Hawaiian volcano from isotopically-enriched tholeiitic basalts to isotopically-depleted alkalic basalts has been explained with some success by the model of plume-lithosphere interaction by Chen and Frey [1983; 1985] and a model of upper mantle entrainment by a thermally buoyant diapir of enriched composition may explain geochemical evolution of volcanism at a Marquesan edifice [Duncan et al., 1986; Chapter III], no unifying concept of mantle

plume volcanism has yet evolved. The intitial composition of a plume and the amount of interaction it has with the upper mantle and lithosphere seems to vary with each hotspot. General characteristics of different plume types and the extent to which they interact with asthenosphere and lithosphere as they rise need to be determined.

The mechanism for the longevity of volcanism at a particular edifice, e.g. 18 m.y. of volcanism at Rimatara, cannot be explained easily by volcanism over a single mantle plume beneath a rapidly moving plate. Also the intermittent nature of some hotspots (e.g., the Marquesas hotspot which turned on or became reactivated to form the northern island of Eiao) is poorly understood. Experiments in plume dynamics may help resolve questions of the continuity of and initiation of volcanism.

Hotspot volcanism, although a volumetrically minor class of basaltic volcanism within the ocean basins, affords a unique view of mantle chemistry and mantle convection. The dynamics of mantle plumes and their interactions with the asthenosphere and lithosphere through which they rise are unique methods of sampling composition of the Earth beneath the oceans. Detailed studies of individual hotspot lineaments and the edifices within them, and integration of the resulting information, will continue to place hotspot volcanism in the larger context of plate tectonics and mantle heterogeneity.

REFERENCES

Allan, J. F., B. L. Cousens, R. L. Chase, M. P. Gorton, and P. J. Michael, Alkaline lavas from the Tuzo Wilson seamounts, NE Pacific: Volcanism at a complex spreading ridge-transform fault intersection, *Eos Trans. AGU, 69*, 1503, 1988.

Anderson, D. L., Hotspots, polar waunder, Mesozoic convection and the geoid, *Nature, 297*, 391-393, 1982.

Bargar, K. E., and E. D. Jackson, Calculated volumes of individual shield volcanoes along the Hawaii-Emporer seamount chain, *J. Res. U. S. Geol. Surv., 2*, 545-550, 1974.

Batiza, R., and D. Vanko, Volcanic development of small oceanic central volcanoes on the flanks of the East Pacific Rise inferred from narrow-beam echo-sounder surveys, *Mar. Geol., 54*, 53-90, 1983.

Batiza, R., and D. Vanko, Petrology of young Pacific seamounts, *J. Geophys. Res., 89*, 11,235-11,260, 1984.

Bishop, A. C. and A. R. Woolley, A basalt-trachyte-phonolite series from Ua Pu, Marquesas Islands, Pacific Ocean, *Contrib. Mineral. Petrol., 39*, 309-326, 1973.

Calmant, S. and A. Cazenave, Worldwide estimates of the oceanic lithosphere elastic thickness under volcanoes, *Nature, 328*, 236-238, 1987.

Castillo, P., The Dupal anomaly as a trace of the upwelling lower mantle, *Nature, 336*, 667-670, 1988.

Chase, C. G., Subduction, the geoid, and lower mantle convection, *Nature, 282*, 464-468, 1979.

Chase, R. L., J. Tuzo Wilson Knolls: Canadian hotspot, *Nature, 266*, 344-346, 1977.

Chase, T. E., H. W. Menard, and J. Mammerickx, *Bathymetry of the North Pacific*, charts 3 and 4, Institute of Marine Resources, Scripps Institute of Oceanography, La Jolla, Calif., 1970.

Cheminee, J. L., R. Hekinian, J. Talandier, F. Albarede, C. W. Devey, J. Francheteau, and Y. Lancelot, Geology of an active hot spot: Teahitia-Mehetia region in the south central Pacific, *Marine Geophys. Res., 11*, 27-50, 1989.

Chen, C. -Y. and F. A. Frey, Origin of Hawaiian tholeiite and alkalic basalt, *Nature, 302*, 785-789, 1983.

Chen, C. -Y., and F. A. Frey, Trace element and isotopic geochemistry of lavas from Haleakala volcano, East Maui, Hawaii: Implications for the origin of Hawaiian basalts, *J. Geophys. Res., 90*, 8743-8768, 1985.

Cheng, Q., J. D. MacDougall, G. W. Lugmair, and J. Natland, Temporal variation in isotopic composition at Tahiti, Society Islands, *EOS Trans. AGU, 68*, 1521, 1987a.

Cheng, Q., K.-H. Park, J. D. Macdougall, A. Zindler, G. W. Lugmair, H. Staudigal, J. Hawkins, and P. Lonsdale, Isotopic evidence for a hotspot origin of the Louisville seamount chain, in B. H. Keating et al. [eds.], *Seamounts, Islands and Atolls*, Geophysical Monograph 43, American Geophysical Union, 283-296, 1987b.

Church, S. E., and M. Tatsumoto, Lead isotope relations in oceanic ridge basalts from the Juan de Fuca-Gorda Ridge area, N. E. Pacific Ocean, *Contrib. Mineral. Petrol., 53*, 253-279, 1975.

Cousens, B. L., Isotopically depleted, alkalic lavas from Bowie Seamount, Northeast Pacific Ocean, *Can. J. Earth Sci., 25*, 1708-1716, 1988.

Cousens, B. L., R. L. Chase, and J. -G. Schilling, Basalt geochemistry of the Explorer Ridge area, northeast Pacific Ocean, *Can. J. Earth Sci., 21*, 157-170, 1984.

Cousens, B. L., R. L. Chase, and J. -G. Schilling, Geochemistry and origin of volcanic rocks from Tuzo Wilson and Bowie seamounts, northeast Pacific Ocean, *Can. J. Earth Sci., 22*, 1609-1617, 1985.

Craeger, K. C., and T. H. Jordan, Slab penetration into the lower mantle beneath the Mariana and other island arcs of the Northwest Pacific, *J. Geophys. Res., 91*, 3573-3589, 1986.

Crough, S. T. and R. D. Jarrard, The Marquesas-Line Swell, *J. Geophys. Res., 86*, 11763-11771, 1981.

Dalrymple, G. B., D. A. Clague, and T. L. Vallier, $^{40}Ar/^{39}Ar$ age, petrology, and tectonic significance of some seamounts in the Gulf of Alaska, in *Seamounts, Islands, and Atolls, Geophys. Monogr. Ser.*, vol. 43, edited by B.H. Keating et al., pp. 297-315, AGU, Washington, D. C., 1987.

Dalrymple, G. B., R. D. Jarrard, and D. A. Clague, K-Ar ages of some volcanic rocks from the Cook and Austral islands, *Geol. Soc. Amer. Bull., 86*, 1463-1467, 1975.

Dalrymple, G. B. and M. A. Lanphere, *Potassium-Argon Dating: Principles, Techniques and Applications to Geocrhonology*, Freeman and Co., San Francisco, 258 pp., 1969.

Davis, E. E., and J. L. Karsten, On the cause of the asymmetric distribution of seamounts about the Juan de Fuca Ridge: Ridge-crest migration over a heterogeneous asthenosphere, *Earth Planet. Sci. Lett., 79*, 385-396, 1986.

Defant, M. J. and R. L. Nielsen, Interpretation of open system petrogenetic processes: Phase equilibria constraints on magma evolution, *Geochim. Cosmochim. Acta, 54*, 87-102, 1990.

Delaney, J. R., H. P. Johnson, and J. L. Karsten, The Juan de Fuca ridge-hotspot-propogating rift system: New tectonic, geochemical, and magnetic data, *J. Geophys. Res.*, *86*, 11,747-11,750, 1981.

Desonie, D. L., and R. A. Duncan, Spreading ridge and hotspot contributions to seamounts near the Juan de Fuca Ridge, *Eos Trans. AGU*, *67*, 1231, 1986.

Desonie, D. L. and R. A. Duncan, The Cobb-Eickelberg seamount chain: Hotspot volcanism with MORB affinity, *J. Geophys. Res.*, *95*, 12,697-12,711,1990.

Devey, C. W., F. Albarede, J. -L. Cheminee, A. Michard, R. Muhe, and P. Stoffers, Active submarine volcanism on the Society hotspot swell (West Pacific): A geochemical study, *J. Geophys. Res.*, *95*, 5049-5066, 1990.

Dixon, J. E., E. Stolper, and J. R. Delaney, Infrared spectroscopic measurements of CO_2 and H_2O in Juan de Fuca Ridge basaltic glasses, *Earth Planet. Sci. Letts.*, *90*, 87-104, 1988.

Duncan, R. A., Linear volcanism in French Polynesia, Ph.D. thesis, Australia National University, Canberra, 150 pp., 1975.

Duncan, R. A., Hotspots in the southern oceans - an absolute frame of reference for motion of the Gondwana continents, *Tectonophysics, 74*, 29-42, 1981.

Duncan, R. A. and D. A. Clague, Pacific Plate motion recorded by linear volcanic chains, in A. E. Nairn et al., [eds.], *The Ocean Basins and Margins, vol. 7A*, Plenum Publishing Corp., 89-121, 1985.

Duncan, R. A. and W. Compston, Sr isotopic evidence for an old mantle source region for French Polynesian volcanism, *Geology*, *4*, 728-732, 1976.

Duncan, R. A. and R. B. Hargraves, ^{40}Ar-^{39}Ar geochronology of basement rocks from the Mascarene Plateau, Chagos Bank, and Maldive Ridge, in R. A. Duncan, J. Backman et al., *Proc. ODP, Sci. Results*, *115*, College Station, TX (Ocean Drilling Program), 43-51, 1990.

Duncan, R. A., M. T. McCulloch, H.G. Barsczus, and D.R. Nelson, Plume versus lithospheric sources for melts at Ua Pou, Marquesas Islands, *Nature* , *322*, 534-538, 1986.

Duncan, R. A. and I. McDougall, Migration of volcanism with time in the Marquesas Islands, French Polynesia, *Earth Planet. Sci. Letts.*, *21*, 414-420, 1974.

Duncan, R. A. and I. McDougall, Linear volcanism in French Polynesia, *J. Volc. Geotherm. Res.*, *1*, 197-227, 1976.

Duncan, R. A. and M. A. Richards, Hotspots, mantle plumes, flood basalts, and true polar wander, *Revs. Geophys.*, in press.

Dupre, B. and C. J. Allegre, Pb-Sr isotope variation in Indian Ocean basalts and mixing phenomena, *Nature, 303*, 142-145, 1983.

Dupuy, C., H. G. Barsczus, J. Dostal, P. Vidal, and J. -M. Liotard, Subducted and recycled lithosphere as the mantle source of ocean island basalts from southern Polynesia, central Pacific, *Chemical Geology, 77,* 1-18, 1989.

Dupuy, C., P. Vidal, H. G. Barsczus, and C. Chauvel, Origin of basalts from the Marquesas Archipelago (south central Pacific Ocean): isotope and trace element constraints, *Earth Planet. Scl. Letts., 82,* 145-152, 1987.

Dymond, J. R., N. D. Watkins, and V. R. Naydu, Age of the Cobb Seamount, *J. Geophys. Res., 73,* 3977-3979, 1968.

Dziewonski, A. M. and J. H. Woodhouse, Global images of the Earth's interior, *Science, 236,* 37-48, 1987.

Eaby, J., D. A. Clague, and J. R. Delaney, Sr isotopic variations along the Juan de Fuca Ridge, *J. Geophys. Res., 89,* 7883-7890, 1984.

Fischer, K. M., M. K. McNutt, and L. Shure, Thermal and mechanical constraints on the lithosphere beneath the Marquesas swell, *Nature, 322,* 733-736, 1986.

Fornari, D. J., M. R. Perfit, J. F. Allen, R. Batiza, R. Haymon, A. Barone, W. B. F. Ryan, T. Smith, T. Simkin, and M. A. Luckman, Geochemical and structural studies of the Lamont seamounts: Seamounts as indicators of mantle processes, *Earth Planet. Sci. Lett., 89,* 63-83, 1988*a*.

Fornari, D. J., M. R. Perfit, J. F. Allan, and R. Batiza, Small-scale heterogeneities in depleted mantle sources: Near-ridge seamount lava geochemistry and implications for mid-ocean-ridge magmatic processes, *Nature, 331,* 511-513, 1988*b*.

Geist, D. J., W. M. White, and A. R. McBirney, Plume-asthenosphere mixing beneath the Galapagos archipelago, *Nature, 333,* 657-660, 1988.

Griffiths, R. W., The differing effects of compositional and thermal buoyancies on the evolution of mantle diapirs, *Phys. Earth Planet. Inter., 43,* 261-273, 1986a.

Griffiths, R. W., Thermals in extremely viscous fluids, including the effects of temperature-dependent viscosity, *Jour. Fluid Mechs., 166,* 115-138, 1986b.

Gurnis, M., and G. Davies, Numerical study of high Rayleigh number convection in a medium with depth-dependent viscosity, *Geophys. J. Roy. Astr. Soc., 85,* 523-541, 1986.

Hart, S. R., A large-scale isotope anomaly in the Southern Hemisphere mantle, *Nature, 309,* 753-757, 1984.

Hart, S. R., Heterogeneous mantle domains: signatures, genesis, and mixing chronologies, *Earth Planet. Sci. Lett., 90,* 273-296, 1988.

Hart, S. and A. Zindler, Constraints on the nature and development of chemical heterogeneities in the mantle, in W. R. Peltier, ed., *Mantle Convection: Plate Tectonics and Global Dynamics,* Gordon and Breach Science Publishers, Montreux Switzerland, pp. 261-387, 1989.

Haxby, W. F. and J. K. Weissel, Evidence for small scale mantle convection from Seasat altimeter data, *J. Geophys. Res., 91*, 3507-3520, 1986.

Hegner, E., and M. Tatsumoto, Pb, Sr, and Nd isotopes in seamount basalts from the Juan de Fuca Ridge and Kodiak-Bowie Seamount Chain, Northeast Pacific, *J. Geophys. Res., 94,* 17,839-17,846, 1989.

Hegner, E., and M. Tatsumoto, Pb, Sr, and Nd isotopes in basalts and sulfides from the Juan de Fuca ridge, *J. Geophys. Res., 92*, 11,380-11,386, 1987.

Hess, H. H., History of ocean basins, in *Petrological Studies: A volume in honor of A. F. Buddington*, edited by A. E. J. Engel, et al., pp. 599-620, Geological Society of America, 1962.

Hooper, P. R., The role of magnetic polarity and chemical analysis in establishing the stratigraphy, tectonic evolution, and petrogenesis of the Columbia River Basalts, *Mem. Geol. Soc. India, 3*, 362-376, 1981.

Jackson, E. S., E. A. Silver, and G. B. Dalrymple, Hawaiian-Emporer chain and its relation to Cenozoic circum-Pacific tectonics, *Geol. Soc. Amer. Bull., 83*, 601-617, 1972.

Karsten, J. L., Spatial and temporal variations in the petrology, morphology and tectonics of a migrating spreading center: the Endeavour segment, Juan de Fuca Ridge, Ph.D. thesis, 329 pp., Univ. of Washington, Seattle, 1988.

Karsten, J. L., and J. R. Delaney, Hot spot-ridge crest convergence in the northeast Pacific, *J. Geophys. Res., 94,* 700-712, 1989.

Kruse, S. E., Magnetic lineations on the flanks of the Marquesas swell: Implications for the age of the seafloor, *Geophys. Res. Letts., 15*, 573-576, 1988.

Langmuir, C. H., Geochemical consequences of in situ crystallization, *Nature, 340,* 199-205, 1989.

Langmuir, C. H., J. F. Bender, and R. Batiza, Petrologic and tectonic segmentation of the East Pacific Rise, 5°30'N-14°30'N, *Nature, 322*, 422-429, 1986.

Langmuir, C. H., J. F. Bender, A. E. Bence, and G.N. Hanson, Petrogenesis of basalts from the FAMOUS area: Mid-Atlantic Ridge, *Earth Planet. Sci. Lett., 36*, 133-156, 1977.

Langmuir, C. H., R. D. Vocke, G. N. Hanson, and S. R. Hart, A general mixing equation with applications to Icelandic basalts, *Earth Planet. Sci. Lett., 37*, 380-392, 1978.

Laul, J. C., Neutron activation analysis of geological materials, *Atomic Energy Review, 17*, 603-695, 1979.

Liias, R. A., Geochemistry and petrogenesis of basalts erupted along the Juan de Fuca Ridge, Ph.D. thesis, 264 pp., Univ. of Mass., Amherst, 1986.

Liotard, J. M., H. G. Barsczus, C. Dupuy, and J. Dostal, Geochemistry and origin of basaltic lavas from Marquesas Archipelago, French Polynesia, *Contrib. Mineral. Petrol., 92*, 260-268, 1986.

Lonsdale, P., Geography and history of the Louisville Hotspot Chain in the Southwest Pacific, *J. Geophys. Res., 93*, 3078-3104, 1988.

Lupton, J. E., Helium isotope variations in Juan de Fuca Ridge basalts, *Eos Trans. AGU, 63*, 1147, 1982.

Macdonald, G. A., and T. Katsura, Chemical composition of Hawaiian lavas, *J. Petrol., 5*, 82-133, 1964.

McDougall, I., Age and evolution of Tutuila, America Samoa, *Pac. Sci., 39* , 311-320, 1985.

McDougall, I. and R. A. Duncan, Linear volcanic chains - recording plate motions? *Tectonophys., 63*, 275-295, 1980.

McDougall, I. and T. M. Harrison, *Geochronology and Thermochronology by the ^{40}Ar-^{39}Ar Method*, Monographs on Geology and Geophysics: No. 9, Oxford Univ. Press, 272 pp., 1988.

McNutt, M. K. and K. M. Fischer, The South Pacific superswell, in B. H. Keating et al. [eds.], *Seamounts, Islands, and Atolls*, Geophysical Monograph 43, American Geophysical Union, 25-34, 1987.

McNutt, M. K. Fischer, S. Kruse, and J. Natland, The origin of the Marquesas fracture zone ridge and its implication for the nature of hot spots, *Earth Planet. Sci. Letts., 91*, 381-393, 1989.

McNutt, M. K. and A. V. Judge, The superswell and mantle dynamics beneath the South Pacific, *Science, 248*, 969-975, 1990.

McNutt, M. K. and H. W. Menard, Lithospheric flexure and uplifted atolls, *J. Geophys. Res., 83*, 1206-1212, 1978.

Menard, H. W., Darwin reprise, *J. Geophys. Res., 89*, 9960-9968, 1984.

Menzies, M. A., and V. R. Murthy, Nd and Sr isotope geochemistry of hydrous mantle nodules and their host alkali basalts: implications for local heterogeneities in metasomatically veined mantle, *Earth Planet. Sci. Lett., 46*, 323-334, 1980.

Morgan, C., Geochemistry of basalts from the Cobb hotspot astride the Juan de Fuca ridge, M.S. thesis, 138 pp., Univ. of Mass., Amherst, 1985.

Morgan, W. J., Deep mantle convective plumes and plate motions, *Am. Assoc. Pet. Geol. Bull., 56*, 201-213, 1972.

Morgan, W. J., Hotspot tracks and the opening of the Atlantic and Indian oceans, in *The Sea: The Oceanic Lithosphere*, vol. 7, edited by C. Emiliani, pp. 443-487, 1981.

Nakamura, N., Determination of REE, Ba, Mg, Na and K in carbonaceous and ordinary chondrites, *Geochim. Cosmochim. Acta, 38*, 757-775, 1974.

Nakamura, Y. and M. Tatsumoto, Pb, Nd, and Sr isotopic evidence for a multi-component source for rocks of Cook-Austral Islands and heterogeneities of mantle plumes, *Geochim. Cosmochim. Acta, 52*, 2909-2924, 1988.

Nielsen, R. L., A model for the simulation of combined major and trace element liquid lines of descent, *Geochim. Cosmochim. Acta, 52*, 27-38, 1988.

Nishimura, C. E. and D. W. Forsyth, Anomalous Love-wave phase velocities in the Pacific: sequential pure-path and spherical harmonic inversion, *Geophys. J. R. Astr. Soc., 81*, 389-407, 1985.

Norris, R. A. and R. H. Johnson, Submarine volcanic eruptions recently located in the Pacific by SOFAR hydrophones, *J. Geophys. Res., 74*, 650-654, 1969.

Okal, E. A. and R. Batiza, Hotspots: the first 25 years, in *Seamounts, Islands, and Atolls, Geophys. Monogr. Ser.*, vol. 43, edited by B.H. Keating et al., pp. 1-11, AGU, Washington, D. C., 1987.

Palacz, Z. A. and A. D. Saunders, Coupled trace element and isotope enrichment in the Cook-Austra-Samoa islands, southwest Pacific, *Earth Planet. Sci. Lett., 79*, 270-280, 1986.

Pollitz, F. F., Episodic North America and Pacific plate motions, *Tectonics, 7*, 711-726, 1988.

Parsons, B. and J. G. Sclater, Depth and age in the North Pacific, *J. Geophys. Res., 93*, 6715-6736, 1977.

Rhodes, J. M., C. Morgan, and R. A. Liias, Geochemistry and axial seamount lavas: Magmatic relationship between the Cobb hotspot and the Juan de Fuca ridge, *J. Geophys. Res., 95*, 12,713-12,733, 1990.

Richards, M. A., Hotspots, plates, and plumes: Toward an integrated theory, *Eos Trans. AGU, 69* , 1413, 1988.

Richards, M. A., Hotspots and the case against a uniform viscosity compositional mantle, in *Glacial Isostasy, Sea Level and Mantle Rheology*, edited by R. Sabadini and K. Lambeck, Kluwer Academic Publishers, Dordrech, in press.

Riddihough, R., Recent movements of the Juan de Fuca Plate system, *J. Geophys. Res., 89*, 6980-6994, 1984.

Schlanger, S. O., M. O. Garcia, B. H. Keating, J. J. Naughton, W. W. Sager, J. A. Haggerty, J. A. Philpotts, and R. A. Duncan, Geology and geochronology of the Line Islands, *J. Geophys Res., 89*, 11,261-11,272, 1984.

Silver, E. A., R. von Huene, and J. K. Crough, Tectonic significance of the Kodiak-Bowie seamount chain, northeastern Pacfic, *Geology, 2*, 147-150, 1974.

Sleep, N. H., Hotspots and mantle plumes: some phenomenology, *J. Geophys. Res., 95*, 6715-6736, 1990.

Smith, W. H. F., H. Staudigel, A. B. Watts, and M. S. Pringle, The Magellan seamounts, Early Cretaceous record of the South Pacific Isotopic and Thermal Anomaly, *J. Geophys. Res., 94*, 10,501-10,523, 1989.

Smoot, N. C., Observations on Gulf of Alaska seamount chains by multi-beam sonar, *Tectonophysics, 115*, 235-246, 1985.

Stefanick, M. and D. M. Jurdy, The distribution of hotspots, *J. Geophys. Res., 89*, 9919-9926, 1984.

Stein, C. A. and D. H. Abbott, Heat flow constraints on the South Pacific Superswell, *J. Geophys. Res.*, submitted.

Sun, S.-S., and R. W. Nesbitt, Chemical heterogeneity of the Archaean mantle, composition of the Earth and mantle evolution, *Earth Planet. Sci. Lett., 35*, 429-448, 1977.

Talandier, J. and E. A. Okal, The volcanoseismic swarms of 1981-1983 in the Tahiti-Mehetia area, French Polynesia, *J. Geophys. Res., 89B,* 11,216-11,234, 1984.

Tatsumoto, M., Isotopic composition of lead in oceanic basalts and its implication to mantle evolution, *Earth Planet. Sci. Letts., 38*, 63-87, 1978.

Turner, D. L. and R. D. Jarrard, K-Ar dating of the Cook-Austral Island chain: A test of the hot-spot hypothesis, *J. Volc. Geotherm. Res., 12*, 187-220, 1982.

Turner, D. L., R. D. Jarrard, and R. B. Forbes, Geochronology and origin of the Pratt-Welker Seamount chain, Gulf of Alaska: A new pole of rotation for the Pacific plate, *J. Geophys. Res., 85*, 6547-6556, 1980.

Vidal, Ph., C. Chauvel, and R. Brousse, Large mantle heterogeneity beneath French Polynesia, *Nature, 307,* 536-538, 1984.

Von Herzen, R. P., J. J. Cordery, R. S. Detrick, and C. Fang, Heat flow and the thermal origin of the hotspot swells: The Hawaiian swell revisited, *J. Geophys. Res., 94*, 13,783-13,799, 1989.

Wakeham, S. E., Petrochemical patterns in young pillow basalts dredged from the Juan de Fuca and Gorda ridges, M.S. thesis, 95 pp., Oreg. State Univ., Corvallis, 1978.

Watts, A. B., J. K. Weissel, R. A. Duncan, and R. L. Larson, Origin of the Louisville ridge and its relationship to the Eltanin fracture zone system, *J. Geophys. Res.*, *93*, 3051-3077, 1988.

White, W. M., M. M. Cheatham, and R. A. Duncan, Isotope geochemistry of Leg 115 basalts and inferences on the history of the Reunion mantle plume, in R.A. Duncan, J. Backman et al., *Proc. ODP, Sci. Results*, 115, College Station, TX (Ocean Drilling Program), 53-61, 1990.

White, W. M. and A. W. Hofmann, Sr and Nd isotope geochemistry of oceanic basalts and mantle evolution, *Nature, 296*, 821-825, 1982.

White, W. M., A. W. Hofmann, and H. Puchelt, Isotope geochemistry of Pacific mid-ocean ridge basalt, *J. Geophys. Res., 92,* 4881-4893, 1987.

Wilson, D. S., R. N. Hey, and C. Nishimura, Propogation as a mechanism of reorientation of the Juan de Fuca Ridge, *J. Geophys. Res.*, *89*, 9215-9225, 1984.

Wilson, J. T., A possible origin of the Hawaiian Islands, *Can. J. Phys.*, *41*, 863-870, 1963.

Wilson, J. T., A new class of faults and their bearing on continental drift, *Nature, 207*, 343-347, 1965.

Woods, M. T., J. J. Leveque, E. A. Okal, Surface wave investigations of the Hawaiian-Emperor seamount chain, *EOS, 71*, 555, 1990.

Woodhead, J. D. and M. T. McCulloch, Ancient seafloor signals in Pitcairn Island lavas and evidence for large amplitude, small length-scale mantle heterogeneities, *Earth Planet. Sci. Lett., 94,* 257-273, 1989.

Wright, E., Petrology and geochemistry of shield-building and post-erosional lava series of Samoa: implications for mantle heterogeneity and magmagenesis, Ph.D. dissertation, Univ. Calif. San Diego, 291 pp., 1986.

Wright, E. and W. M. White, The origin of Samoa: New evidence from Sr, Nd, and Pb isotopes, *Earth Planet. Sci. Lett., 81,* 151-162, 1986.

Wysession, M. E., E. A. Okal, and K. L. Miller, Intraplate seismicity of the Pacific basin, 1913-1988, *Pure Appl. Geophys.*, in press.

Zindler, A. and S. Hart, Chemical geodynamics, *Ann. Rev. Earth Planet. Sci.*, *14*, 493-571, 1986.

Zindler, A., H. Staudigel, and R. Batiza, Isotope and trace element geochemistry of young Pacific seamounts: implications for the scale of upper mantle heterogeneity, *Earth Planet. Sci. Lett.*, *70*, 175-195, 1984.

APPENDIX

^{40}Ar-^{39}Ar AGE SPECTRA AND CORRELATION DIAGRAMS FOR SELECTED SAMPLES FROM CRGN 02

^{40}Ar-^{39}Ar incremental heating experiments were performed on selected samples from the CRGN 02 suite to determine if radiogenic argon was lost after initial cooling of the basalt and to attain plateau ages for the samples. ^{40}Ar-^{39}Ar release patterns show spectra of ages calculated from ^{40}Ar-^{39}Ar ratios of gas fractions released by incremental heating of neutron-irradiated whole rock basaltic samples. Calculated ages from successive steps are plotted against the proportion of total ^{39}Ar released in these steps. Argon-isotope correlation-diagrams (also called inverse isochron diagrams) plot ^{36}Ar-^{40}Ar released against $^{39}Ar/^{40}Ar$ compositions for the step as released during stepwise heating of the irradiated sample. The age is given by the inverse x-intercept and the composition of the atmospheric component at time zero by the inverse y-intercept [e.g., McDougall and Harrison, 1988].

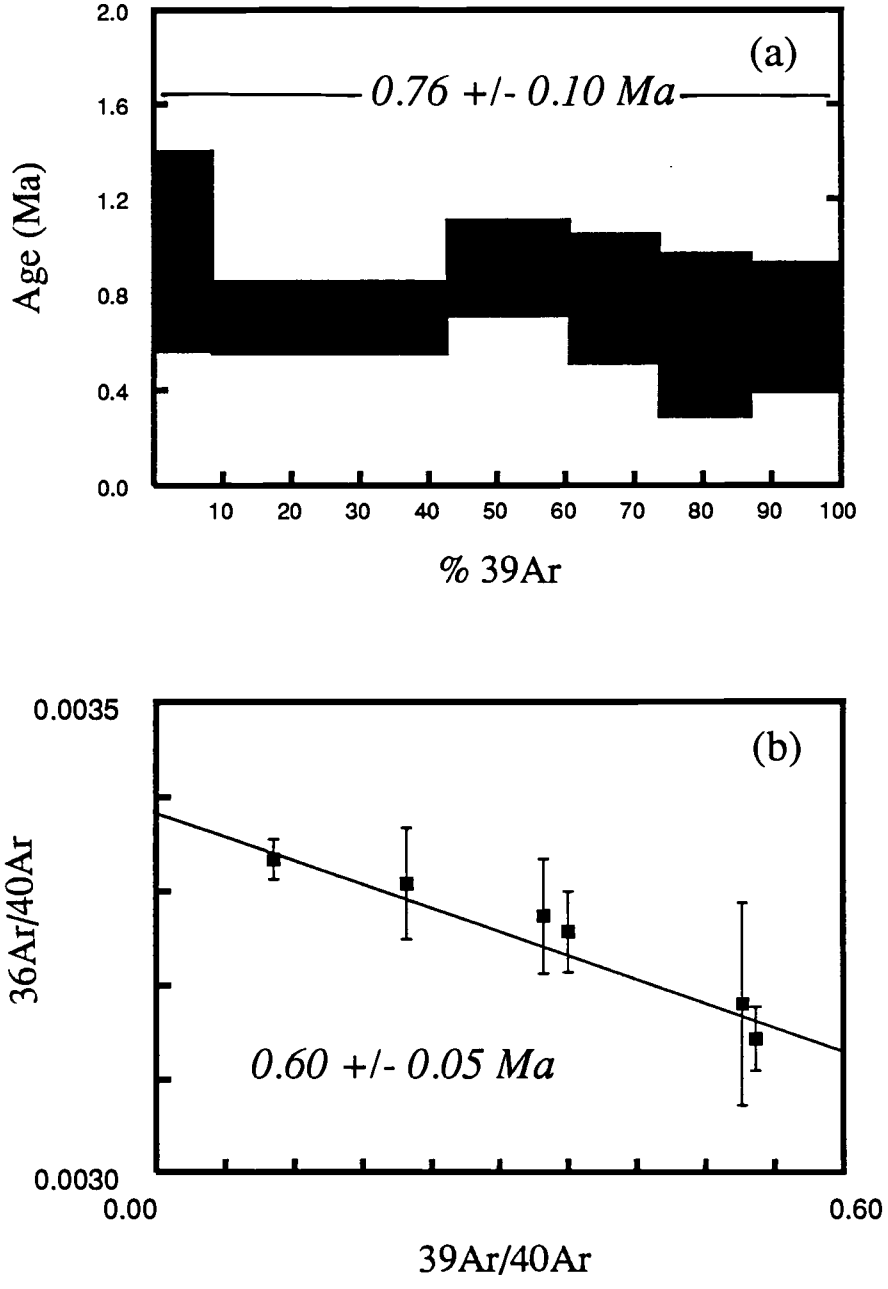

Figure A.1. ^{40}Ar-^{39}Ar age experiments for mugearitic basalt sample DH 12-17. (a) Age spectra diagram with calculated ages and the estimated standard deviation of precision about the calculated ages for each gas increment. Plateau age calculated by weighting each step based on the percentage of ^{39}Ar released appears in figure. A line appears above the steps that were used to calculate the plateau age. (b) Inverse isochron correlation diagram for argon isotope compositions of gas increments from ^{40}Ar-^{39}Ar experiment on sample DH 12-17. Squares for incremental heating steps used to calculate the age listed within the figure are filled.

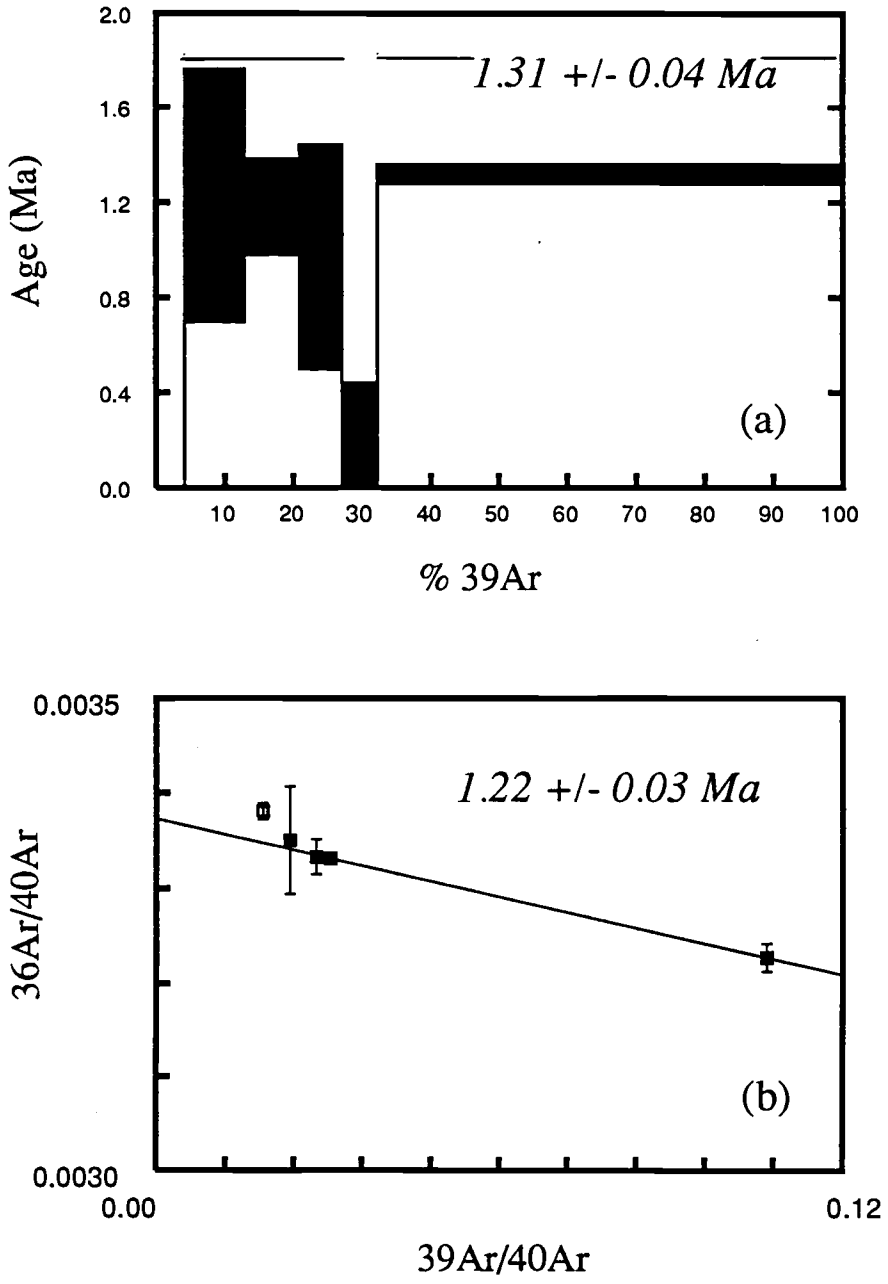

Figure A.2. ^{40}Ar-^{39}Ar age experiments for tholeiitic basalt sample DH 16-1 (a) Age spectra and (b) inverse isochron diagram. Details as in Figure A.1.

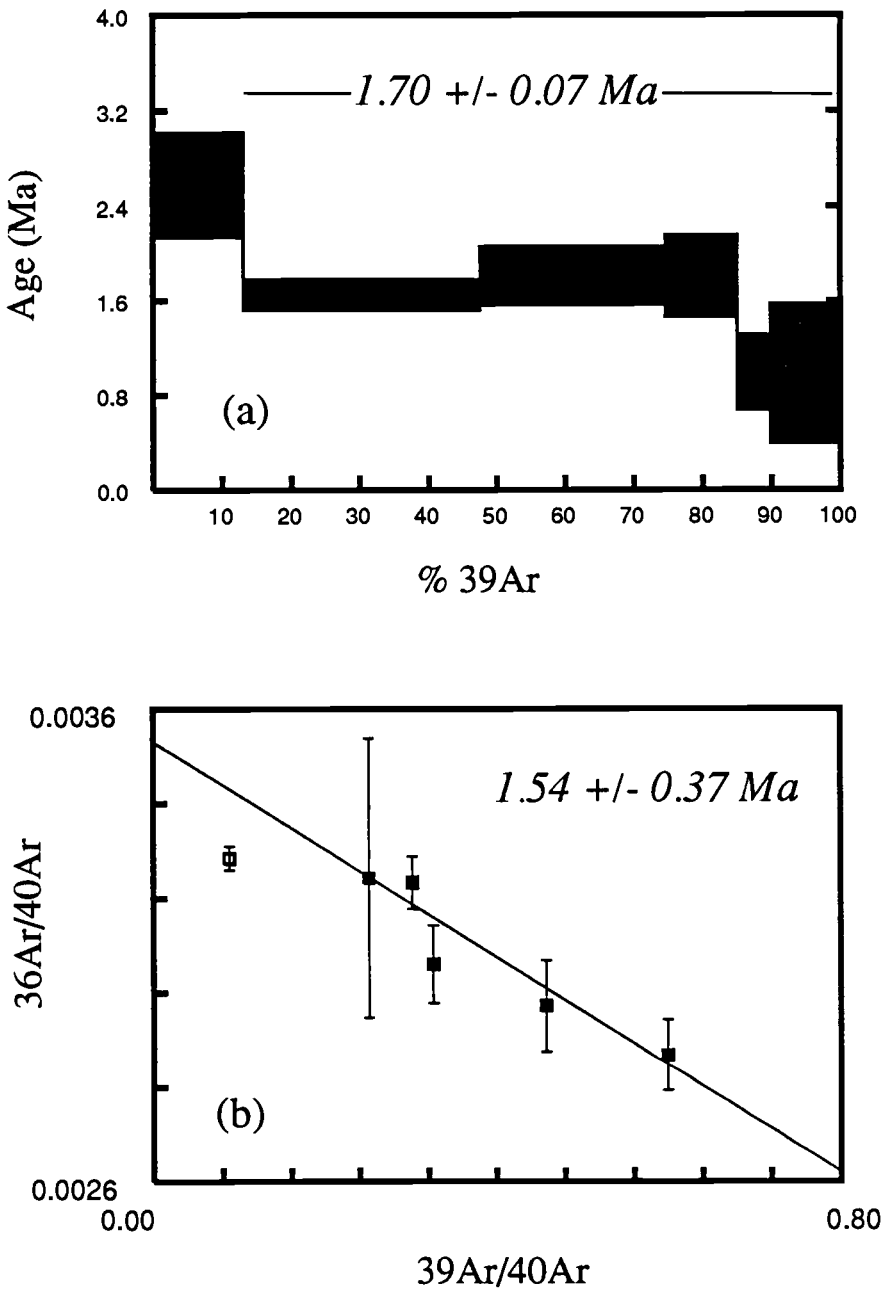

Figure A.3. ^{40}Ar-^{39}Ar age experiments for alkali basalt sample DH 17-1 (a) Age spectra and (b) inverse isochron diagram. Details as in Figure A.1.

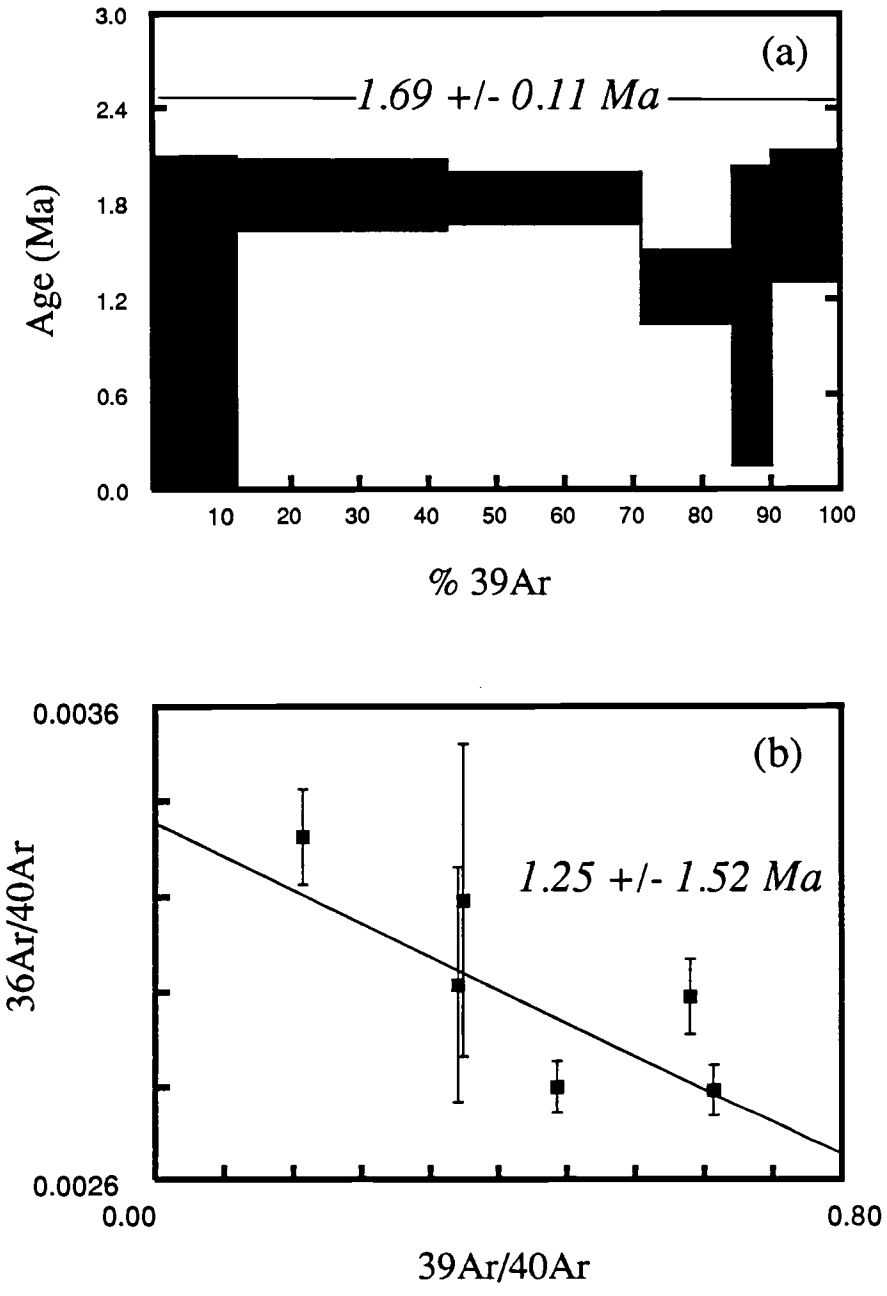

Figure A.4. ^{40}Ar-^{39}Ar age experiments for alkali basalt sample DH 17-5 (a) Age spectra and (b) inverse isochron diagram. Details as in Figure A.1.

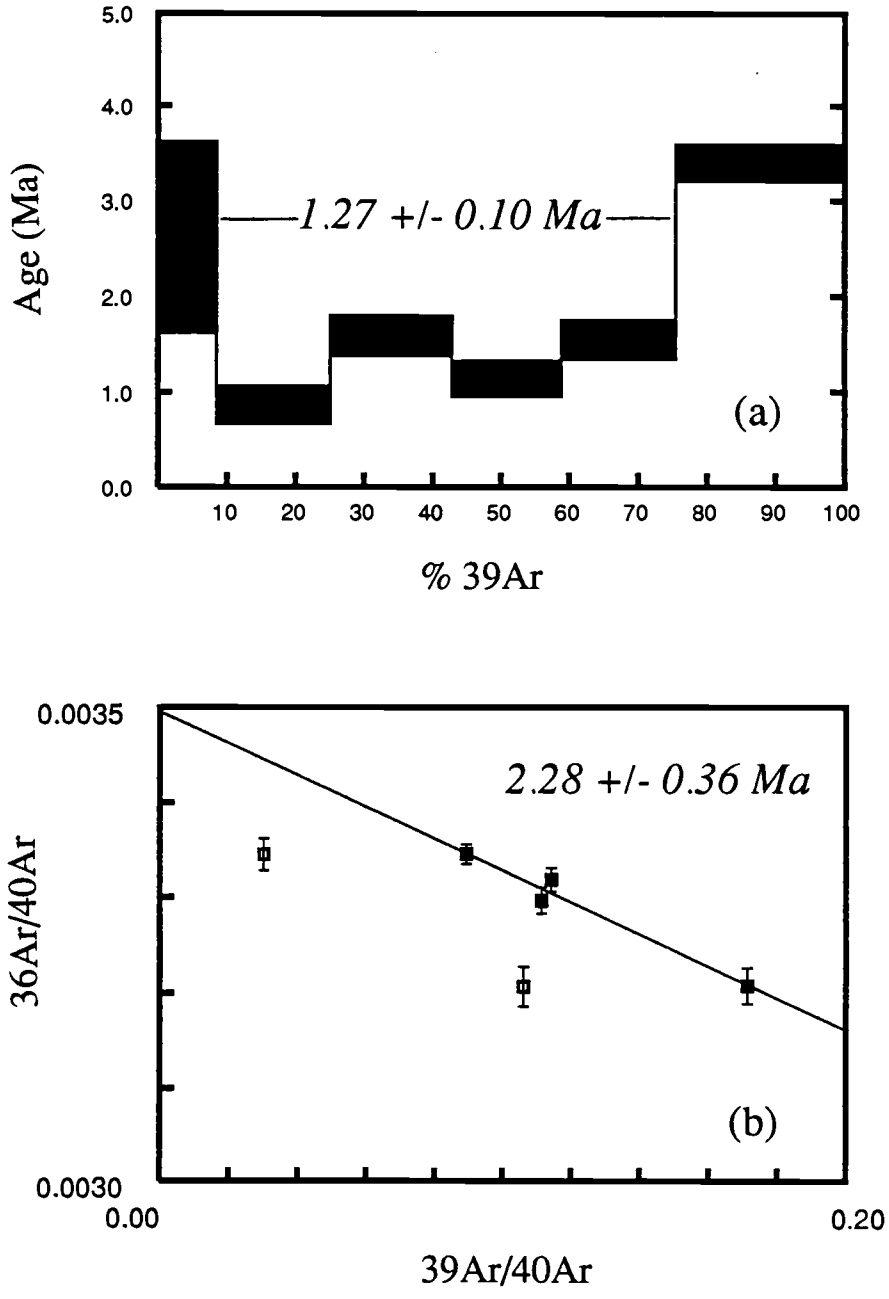

Figure A.5 ^{40}Ar-^{39}Ar age experiments for mugearitic basalt sample DH 18-13 (a) Age spectra and (b) inverse isochron diagram. Details as in Figure A.1.

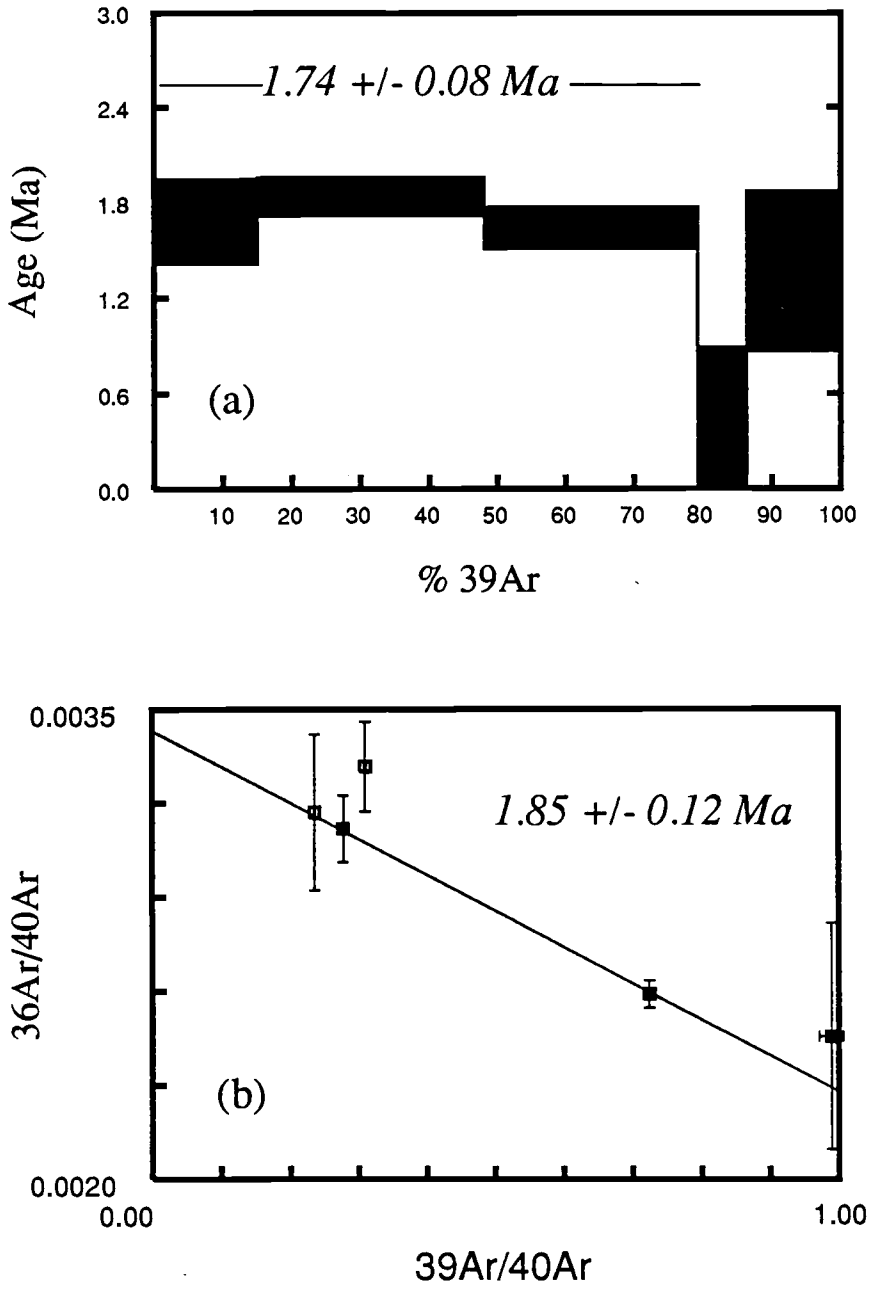

Figure A.6. ^{40}Ar-^{39}Ar age experiments for tholeiitic basalt sample DH 19-2 (a) Age spectra and (b) inverse isochron diagram. Details as in Figure A.1.

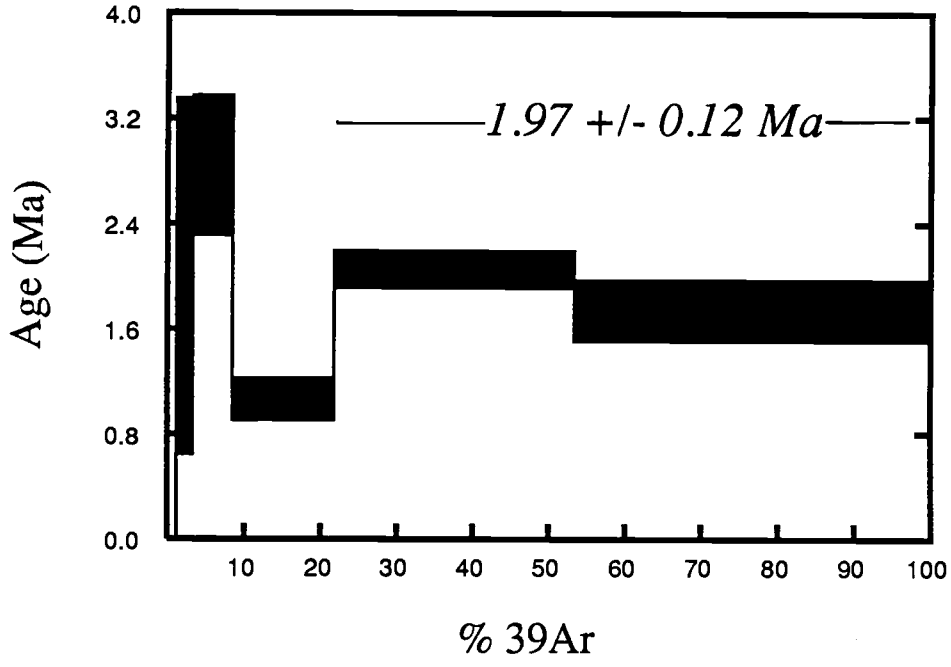

Figure A.7. ^{40}Ar-^{39}Ar age spectra for transitional basalt sample DH 19-3. Details as in Figure A.1.

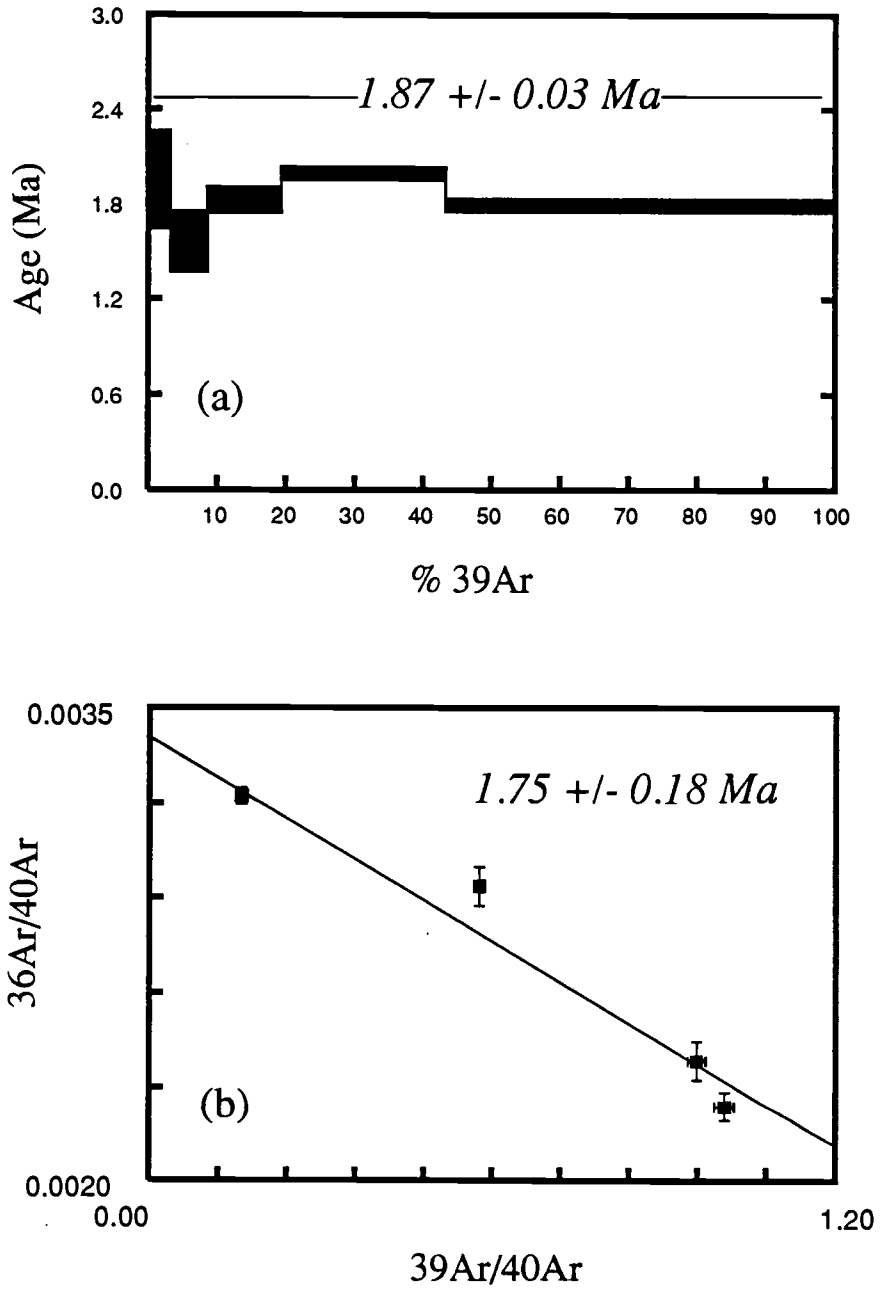

Figure A.8. ^{40}Ar-^{39}Ar age experiments for basanitic basalt sample DH 19-8 (a) Age spectra and (b) inverse isochron diagram. Details as in Figure A.1.

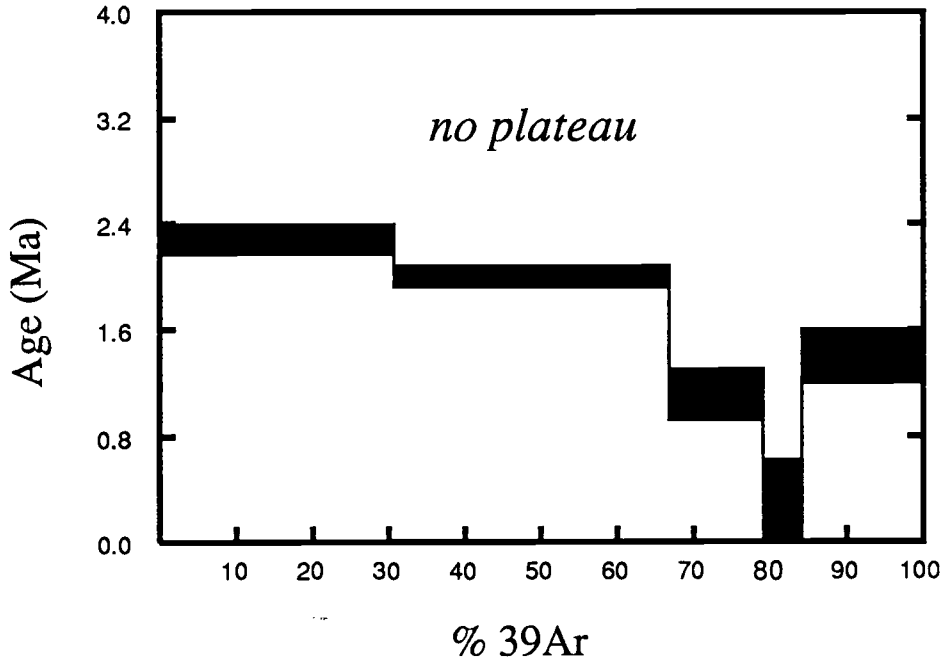

Figure A.9. ^{40}Ar-^{39}Ar age spectra for transitional basalt sample DH 19-11. No plateau was achieved in this set of experiments. Details as in Figure A.1.

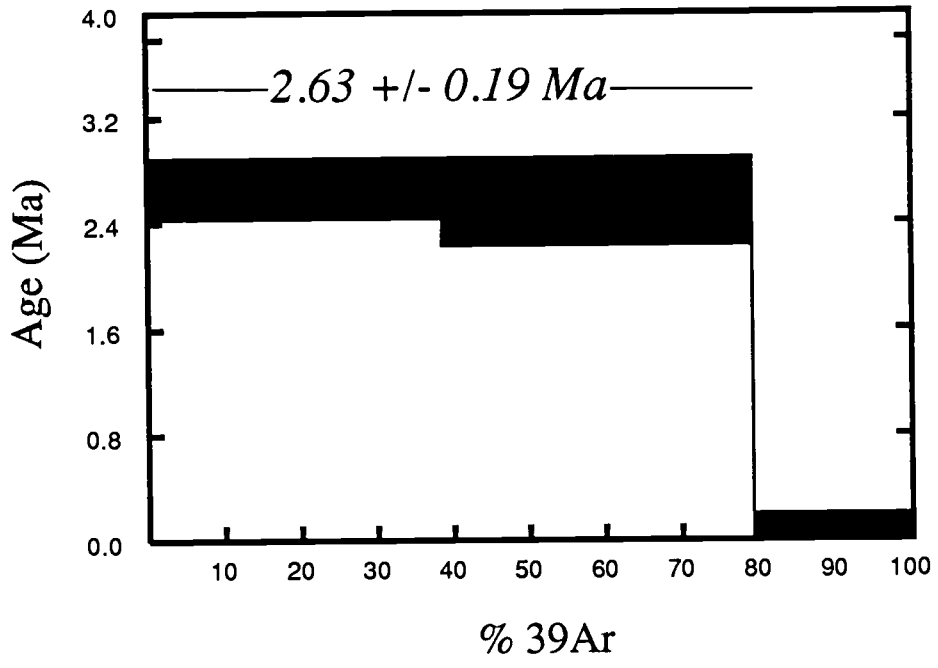

Figure A.10. ^{40}Ar-^{39}Ar age spectra for alkali basalt sample DH 21-14. Details as in Figure A.1.

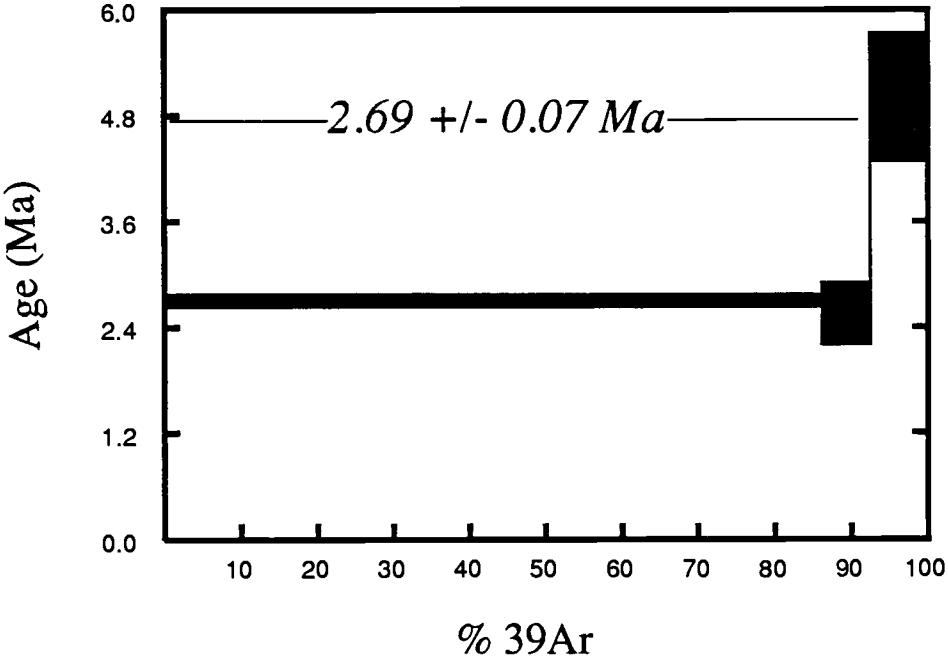

Figure A.11. ^{40}Ar-^{39}Ar age spectra for basanitic basalt sample DH 22-1. Details as in Figure A.1.

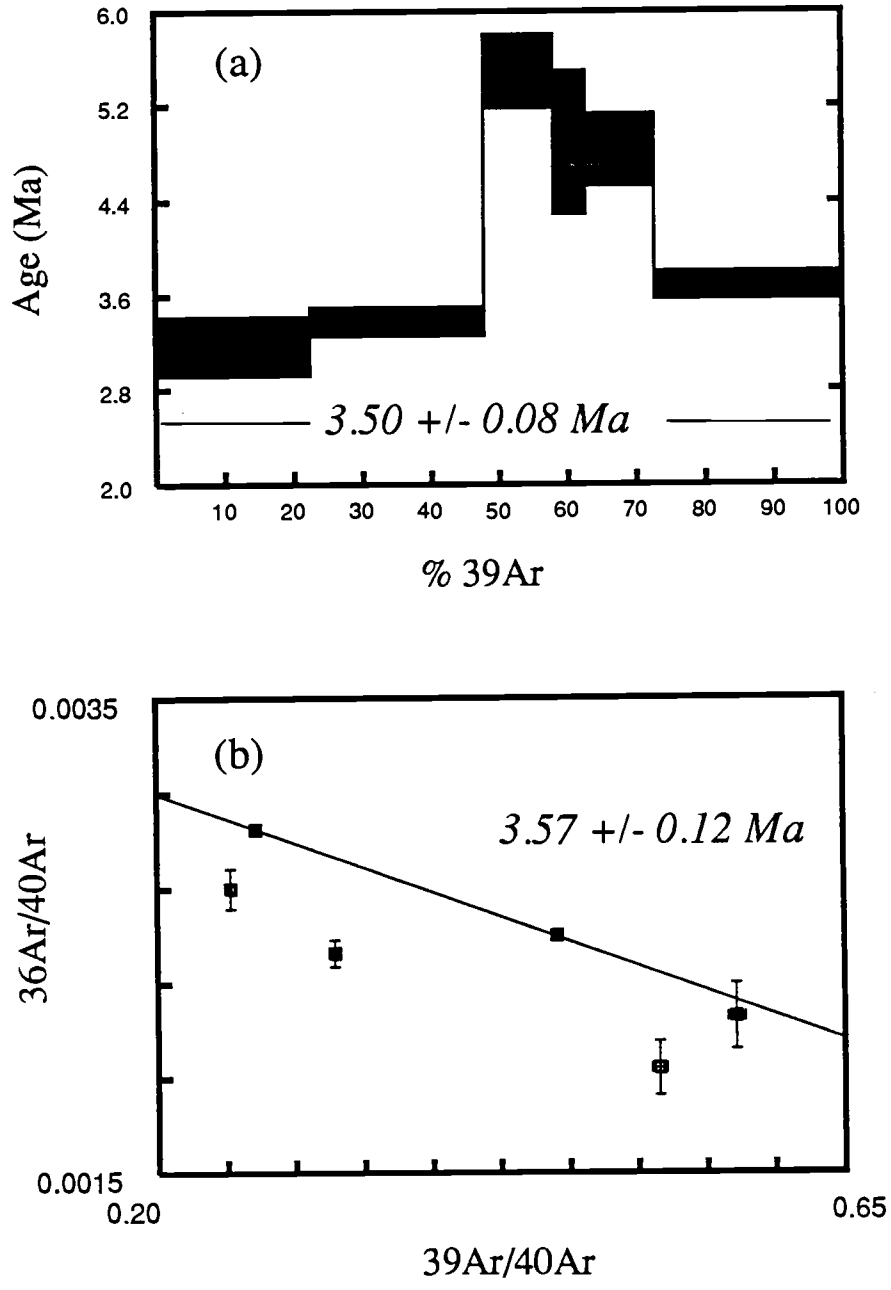

Figure A.12. ^{40}Ar-^{39}Ar age experiments for basanitic basalt sample DH 22-2 (a) Age spectra and (b) inverse isochron diagram. Details as in Figure A.1.

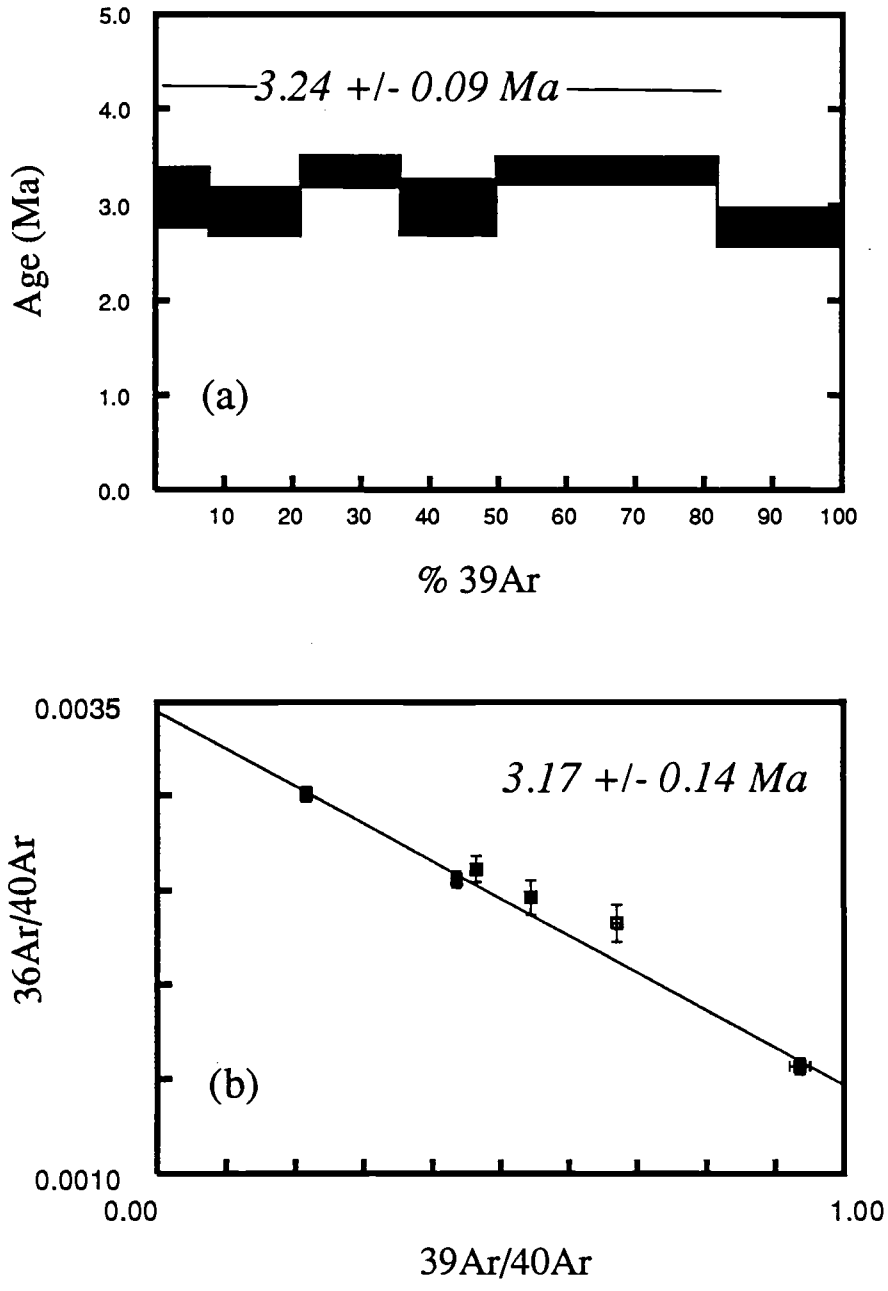

Figure A.13. ^{40}Ar-^{39}Ar age experiments for basanitic basalt sample DH 24-4 (a) Age spectra and (b) inverse isochron diagram. Details as in Figure A.1.

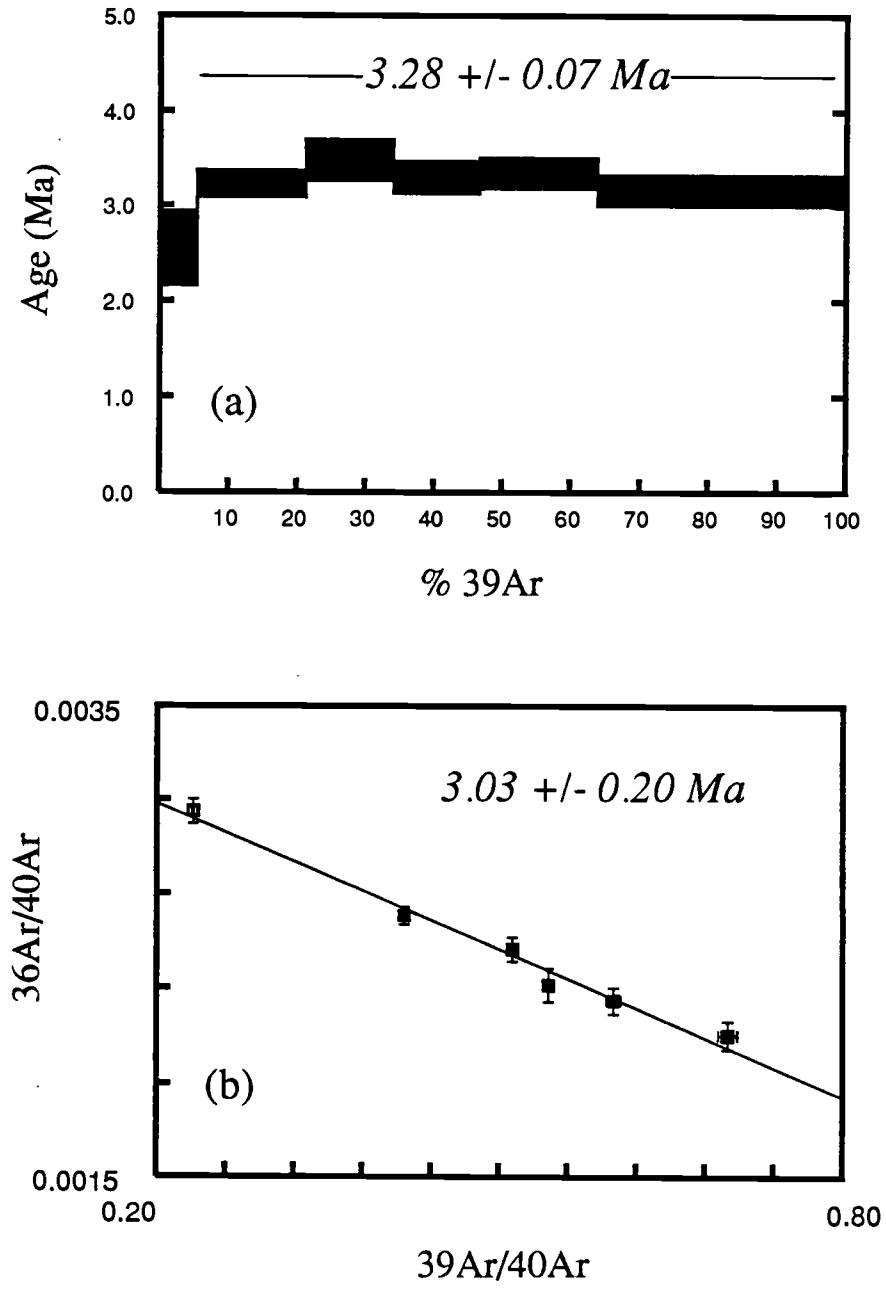

Figure A.14. ^{40}Ar-^{39}Ar age experiments for basanitic basalt sample DH 24-7 (a) Age spectra and (b) inverse isochron diagram. Details as in Figure A.1.